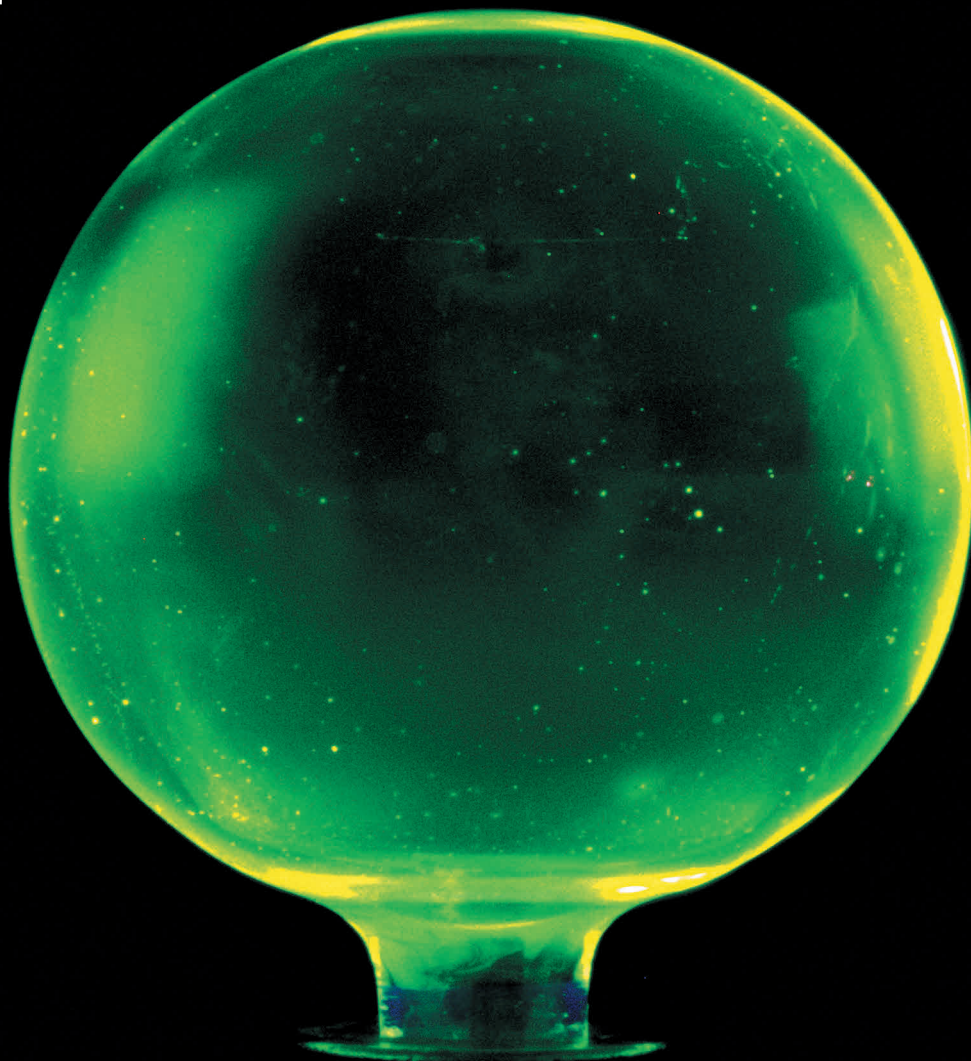




UNIVERSITY
OF TURKU



RADIOSYNTHESIS OF [¹⁸F]F-DPA WITH VARIOUS MOLAR ACTIVITIES FOR THE IMAGING OF NEUROINFLAMMATION

Thomas Keller



UNIVERSITY
OF TURKU

RADIOSYNTHESIS OF [^{18}F]F-DPA WITH VARIOUS MOLAR ACTIVITIES FOR THE IMAGING OF NEUROINFLAMMATION

Thomas Keller

University of Turku

Faculty of Science and Engineering
Department of Chemistry
Turku PET Centre
Department of Radiochemistry
Doctoral Programme in Physical and Chemical Sciences

Supervised by

Professor Olof Solin, PhD
Turku PET Centre
University of Turku
Turku, Finland

Adjunct Professor Merja Haaparanta-Solin, PhD
Turku PET Centre
University of Turku
Turku, Finland

Adjunct Professor Sarita Forsback, PhD
Turku PET Centre
University of Turku
Turku, Finland

Reviewed by

Professor Anthony Gee, PhD
Imaging Chemistry & Biology
King's College London
London, England

Doctor Victor Pike, PhD
Molecular Imaging Branch
National Institute of Mental Health
National Institutes of Health
Bethesda, United States of America

Opponent

Assistant Professor Alex Poot, PhD
Department of Radiology & Nuclear Medicine
VU University Medical Center,
Amsterdam, The Netherlands

The originality of this publication has been checked in accordance with the University of Turku quality assurance system using the Turnitin OriginalityCheck service.

Cover Image: Thomas Keller

ISBN 978-951-29-7672-0 (PRINT)
ISBN 978-951-29-7673-7 (PDF)
ISSN 0082-7002 (Print)
ISSN 2343-3175 (Online)
Painosalama Oy – Turku, Finland 2019

ABSTRACT

UNIVERSITY OF TURKU

Faculty of Science and Engineering

Department of Chemistry and Turku PET Centre

Thomas Keller: Radiosynthesis of [^{18}F]F-DPA with Various Molar Activities for the Imaging of Neuroinflammation

Doctoral Dissertation, 142 pp.

Doctoral Programme in Physical and Chemical Sciences

The use of radioisotopes as a means to non-invasively look into living subjects influenced both diagnostic and therapeutic medicine in the past century. Nowadays positron emission tomography (PET), employing short-lived radioisotopes such as carbon-11 and fluorine-18, is routinely used in nuclear medicine.

The aims of this thesis were to explore a new route by which radioactive [^{18}F]fluoride could be converted into [^{18}F]F₂. Furthermore an aim was to explore various synthesis routes for the production of [^{18}F]F-DPA, a novel translocator protein (TSPO) specific tracer for activated microglia in neuroinflammation. [^{18}F]F-DPA is an analogue of the routinely used [^{18}F]DPA-714. The efficacy of the new tracer was investigated by small animal PET imaging of both healthy animals and a mouse model of Alzheimer's Disease (APP/PS1-21). Various synthesis routes were developed for the production [^{18}F]F-DPA, these gave the same product but with differing molar activities (A_m), thereby enabling the study of the effect that varying A_m has on the imaging of TSPO.

The new method employing vacuum UV photon illumination was successfully applied to synthesise [^{18}F]F₂, and the resulting fluorine gas could be further used in the production of [^{18}F]F-DPA. The [^{18}F]F-DPA produced by the various synthesis methods differed only in the A_m 's achieved. The nucleophilic labelling route resulted in [^{18}F]F-DPA with a hundred-fold higher A_m . The higher A_m increased the uptake of the tracer to TSPO in the APP/PS1-21 mouse brain. It was found that [^{18}F]F-DPA presented greater metabolic stability *in vivo* than [^{18}F]DPA-714. Furthermore, [^{18}F]F-DPA was able to detect neuroinflammation in mouse brain even when it was produced with a low A_m .

Keywords: Molar Activity, Specific Activity, [^{18}F]F-DPA, [^{18}F]F₂, Electrophilic fluorination, [^{18}F]Selectfluor, Cu-mediated fluorination, TSPO, APP/PS1-21

TIIVISTELMÄ

TURUN YLIOPISTO

Luonnontieteiden ja tekniikan tiedekunta

Kemian laitos ja Turun PET-keskus

Thomas Keller: [^{18}F]F-DPA: radiosynteesi ja molaarisen aktiivisuuden vaikutus neuroinflammation kuvantamiseen

Väitöskirja, 142 s

Fysikaalisten ja kemiallisten tieteiden tohtoriohjelma

Radioisotooppien käyttöönotto lääketieteellisessä kuvantamisessa on vaikuttanut sekä diagnostisiin tutkimuksiin että hoidon seurantaan. Positroniemissiotomografiakuvantamista (PET), joka hyödyntää lyhytikäisillä radionuklideilla, kuten hiili-11 ja fluori-18, leimattuja merkkiaineita, käytetään nykyään rutiininomaisesti isotooppilääketieteessä.

Tämän väitöstyön tavoitteina oli tutkia uutta menetelmää, jonka avulla PET-merkkiaineiden leimausprekursorina käytettävä [^{18}F]fluoridi voidaan liittää fluorikaasuun, F_2 . Lisäksi tutkittiin synteesireittejä aktivoituneen mikroglian ilmentämään translokaattoriproteiiniin (TSPO) sitoutuvalle merkkiaineelle [^{18}F]F-DPA:lle, joka kuvastaa neuroinflammation määrää. [^{18}F]F-DPA on yleisesti käytössä olevan [^{18}F]DPA-714 merkkiaineen analogi. [^{18}F]F-DPA:n toimivuutta TSPO-kuvantamiseen tutkittiin sekä terveiden että Alzheimer-tautimallin hiirten (APP/PS1-21) aivoissa pieneläinPET-kameralla. Työssä selvitettiin myös miten merkkiaineen molaarisen aktiivisuuden vaihtelu vaikutti TSPO-kuvantamiseen.

Uusi UV-fotoniavusteinen menetelmä fluori-18 leimatun fluorikaasun tuottamiseksi osoitettiin toimivaksi. Lisäksi osoitettiin, että tällä menetelmällä tuotettua ^{18}F -leimattua fluorikaasua voitiin käyttää [^{18}F]F-DPA:n leimaussynteesiin. Eri synteesimenetelmillä valmistettu [^{18}F]F-DPA erosi vain [^{18}F]F-DPA:n molaarisen aktiivisuuden suhteen. Nukleofiilisellä synteesimenetelmällä pystyttiin tuottamaan [^{18}F]F-DPA:ta noin sata kertaa suuremmalla molaarisella aktiivisuudella kuin muilla menetelmillä. Suurempi molaarinen aktiivisuus lisäsi merkkiaineen TSPO-sitoutumista APP/PS1-21 -hiirten aivoissa. Lisäksi havaittiin, että [^{18}F]F-DPA oli elimistössä pysyvämpi ja herkempi erottamaan neuroinflammation hiiren aivoissa kuin [^{18}F]DPA-714 myös silloin kun se tuotettiin matalalla molaarisella aktiivisuudella.

Avainsanat: Fluori-18, molaarinen aktiivisuus, spesifinen aktiivisuus, [^{18}F]F-DPA, [^{18}F]F $_2$, elektrofiilinen fluorinaatio, [^{18}F]Selectfluori, Cu-avusteinen fluoraus, TSPO, APP/PS1-21

TABLE OF CONTENTS

ABSTRACT.....	4
TIIVISTELMÄ	5
ABBREVIATIONS	8
LIST OF ORIGINAL PUBLICATIONS.....	11
1 INTRODUCTION.....	12
2 REVIEW OF LITERATURE	14
2.1 Positron Emission Tomography	14
2.2 Chemistry of fluorine and its isotopes.....	16
2.2.1 Photochemical reactions of fluorine	17
Excimer lasers	18
2.2.2 Fluorine – ^{18}F	18
2.2.3 Accelerator production of $^{18}\text{F}^-$ and $^{18}\text{F}_2$	19
2.3 ^{18}F -Fluorination.....	19
2.3.1 Isotope exchange reactions of fluorine	21
2.3.2 Post-target production of $^{18}\text{F}_2$	22
2.3.3 Nucleophilic ^{18}F -fluorination.....	23
2.3.4 Umpolung approach.....	28
2.3.5 Electrophilic ^{18}F -Fluorination.....	30
2.4 Translocator protein 18kDa.....	32
2.4.1 PET tracers for TSPO	33
2.4.2 Mouse model of Alzheimer’s disease	37
2.4.3 ^{18}F F-DPA.....	38
3 AIMS OF THE STUDY.....	40
4 MATERIALS AND METHODS	41
4.1 Production of ^{18}F -fluorination reagents.....	41
4.1.1 Production and drying of ^{18}F fluoride (I – IV)	41
4.1.2 High voltage discharge-promoted production of $^{18}\text{F}_2$ and subsequent synthesis of ^{18}F Selectfluor bis(triflate) (I – III)..	42
4.1.3 Vacuum ultraviolet photon-promoted production of $^{18}\text{F}_2$ (IV).....	42
4.2 HPLC analytical and preparative systems.....	44
4.3 Synthesis of ^{18}F DPA-714 using the nucleophilic ^{18}F -fluorination device (I).....	46
4.4 Synthesis of F-DPA precursors (I, II, III and unpublished).....	46
4.5 Electrophilic syntheses of ^{18}F F-DPA (I, II, III and unpublished)	47
4.5.1 Electrophilic ^{18}F -Fluorination of Compound 1 (I – III & unpublished).....	47

4.5.2	Electrophilic ^{18}F -Fluorination of Compound 2 using [^{18}F]Selectfluor bis(triflate) (Unpublished).....	49
4.6	Nucleophilic syntheses of [^{18}F]F-DPA (III)	49
4.6.1	Copper-mediated ^{18}F -Fluorination of Compound 1 (III)	49
4.6.2	Copper-mediated ^{18}F -Fluorination of Compound 2 (Unpublished)	50
4.6.3	HPLC purification, analysis and formulation for injection.....	50
4.7	Preclinical evaluations of [^{18}F]F-DPA and comparison with [^{18}F]DPA- 714.....	51
4.7.1	In vivo PET imaging and tracer kinetics	51
4.7.2	Ex vivo brain autoradiography (II & III).....	52
4.7.3	Ex vivo biodistribution (I & II)	53
4.7.4	Specificity (II)	53
4.7.5	RadioTLC analysis (I – III)	53
4.7.6	Immunohistochemical staining (II)	54
4.8	Statistical methods (I – IV).....	54
5	RESULTS	55
5.1	Electrophilic Syntheses of [^{18}F]F-DPA (I – III and unpublished).....	55
5.2	Synthesis of [^{18}F]F ₂ by VUV-photon promoted isotopic exchange (IV) 57	
5.2.1	Synthesis of [^{18}F]F-DPA using VUV-photon promoted isotopic exchange produced [^{18}F]F ₂ -derived [^{18}F]Selectfluor bis(triflate) (unpublished results)	59
5.3	Copper-mediated nucleophilic ^{18}F -fluorination (III and unpublished) 59	
5.4	Preclinical evaluation (I – III).....	60
5.4.1	In vivo.....	60
5.4.2	Ex vivo brain autoradiography (II & III).....	63
5.4.3	Ex vivo biodistribution	65
5.4.4	Specificity study in mice	67
5.4.5	RadioTLC analysis of radiometabolites	68
6	DISCUSSION	70
6.1	^{18}F -fluorination reactions for the production of [^{18}F]F-DPA (I – IV and unpublished).....	71
6.2	Metabolism of [^{18}F]F-DPA (I & II)	74
6.3	Preclinical evaluation of [^{18}F]F-DPA	75
7	CONCLUSIONS	80
8	ACKNOWLEDGEMENTS.....	81
9	REFERENCES	83
10	ORIGINAL PUBLICATIONS	95

ABBREVIATIONS

AD	Alzheimer's Disease
A _m	Molar Activity
APP	Amyloid Precursor Protein
β ⁺	Positron
Aβ	Beta-Amyloid
CB	Cerebellar Cortex
CNS	Central Nervous System
Compound 1	2-(5,7-Dimethyl-2-(4-(tributylstannyl)phenyl)pyrazolo[1,5- <i>a</i>]pyrimidin-3-yl)- <i>N,N</i> -diethylacetamide
Compound 2	2-(5,7-Dimethyl-2-(4-(4,4,5,5-tetramethyl-1,3,2-dioxaborolan-2-yl)phenyl)pyrazolo[1,5- <i>a</i>]pyrimidin-3-yl)- <i>N,N</i> -diethylacetamide
18-crown-6	1,4,7,10,13,16-Hexaoxacyclooctadecane
CT	Computed Tomography
CTX	Neocortex
DCM	Dichloromethane
DMA	Dimethylformamide
L-DOPA	(<i>S</i>)-2-Amino-3-(3,4-dihydroxyphenyl)propanoic acid
DPA-714	<i>N,N</i> -Diethyl-2-[4-(2-fluoroethoxy)phenyl]-5,7-dimethylpyrazolo[1,5- <i>a</i>]pyrimidine-3-acetamide
EC	Electron Capture
EOB	End of Bombardment
EOS	End of Synthesis
EWG	Electron Withdrawing Group
FC	Frontal Cortex
FDG	2-Deoxy-2-fluoro-D-glucose
F-DPA	<i>N,N</i> -Diethyl-2-[4-fluorophenyl]-5,7-dimethylpyrazolo[1,5- <i>a</i>]pyrimidine-3-acetamide

Freon-11	Trichlorofluoromethane
HIPP	Hippocampus
HPLC	High-Performance Liquid Chromatography
HV	High Voltage
HYP	Hypothalamus
Iba1	Ionised Calcium Binding Adaptor Molecule 1
ID	Injected Dose
K ₂₂₂	4,7,13,16,21,24-Hexaoxa-1,10-diazabicyclo[8.8.8]hexacosane
LV	Lateral Ventricle
MS	Mass Spectroscopy
NFSi	<i>N</i> -Fluoro- <i>N</i> -(phenylsulfonyl)benzenesulfonamide
PET	Positron Emission Tomography
PK11195	<i>N</i> -Butan-2-yl-1-(2-chlorophenyl)- <i>N</i> -methylisoquinoline-3-carboxamide
PSEN-1	Presenilin-1
PTC	Parietotemporal Cortex
RCY	Radiochemical Yield
ROI	Region of Interest
SD	Sprague Dawley
Selectfluor	1-Chloromethyl-4-fluoro-1,4-diazoniabicyclo[2.2.2]octane
S _N 2	Bimolecular Nucleophilic Substitution
S _N Ar	Nucleophilic Aromatic Substitution
SPECT	Single Photon Emission Computed Tomography
STR	Striatum
SUV	Standardised Uptake Value
t _½	Half-life
TAC	Time-Activity Curve
TG	Transgenic

THA	Thalamus
TLC	Thin Layer Chromatography
Ts	Toluenesulfonyl
TSPO	18 kDa Translocator Protein
UV	Ultra Violet
VOI	Volume of Interest
VUV	Vacuum Ultra Violet
WB	Whole Brain
WT	Wild type

LIST OF ORIGINAL PUBLICATIONS

The following original publications form the basis of this thesis, they have been reproduced with the permission of the copyright holders and are referred to in the text by their assigned Roman numerals.

- I Keller T, Krzyczmonik A, Forsback S, López-Picón FR, Kirjavainen AK, Takkinen J, Rajander J, Cacheux F, Damont A, Dollé F, Rinne JO, Haaparanta-Solin M, Solin O. *Radiosynthesis and Preclinical Evaluation of [¹⁸F]F-DPA, A Novel Pyrazolo[1,5a]pyrimidine Acetamide TSPO Radioligand, in Healthy Sprague Dawley Rats*. Mol Imaging Biol. 2017; 19: 736-745
- II Keller T, López-Picón FR, Krzyczmonik A, Forsback S, Kirjavainen AK, Takkinen JS, Alzghool O, Rajander J, Teperi S, Cacheux F, Damont A, Dollé F, Rinne JO, Solin O, Haaparanta-Solin M. *¹⁸F-F-DPA for the Detection of Activated Microglia in a Mouse Model of Alzheimer's Disease*. Nucl Med Biol. 2018; 67: 1-9
- III Keller T, López-Picón FR, Krzyczmonik A, Forsback S, Takkinen J, Rajander J, Teperi S, Dollé F, Rinne JO, Haaparanta-Solin M, Solin O. High Molar Activity [¹⁸F]F-DPA: preclinical comparison with Low Molar Activity [¹⁸F]F-DPA. J Cereb Blood Flow Metab. In Press
- IV Krzyczmonik A*, Keller T*, Kirjavainen AK, Forsback S, Solin O. *Vacuum ultraviolet photon-mediated production of [¹⁸F]F₂*. J Label Compd Radiopharm. 2017; 60: 186–193

*equal contribution

1 INTRODUCTION

Positron Emission Tomography (PET) is a valuable imaging technique that allows us to visualise dynamic biological processes in a living body. This is achieved by monitoring the distribution of biologically active molecules that have been labelled with one of many possible positron-emitting radionuclides. This thesis is based on 4 studies (I – IV) that encompass various radiochemical and preclinical stages in the development of a new tracer molecule. These studies have resulted in 4 original publications, which are accordingly referred to by the same Roman numerals. Some main topics of these studies (I-IV) and well as their relation to one another are outlined in Figure 1.

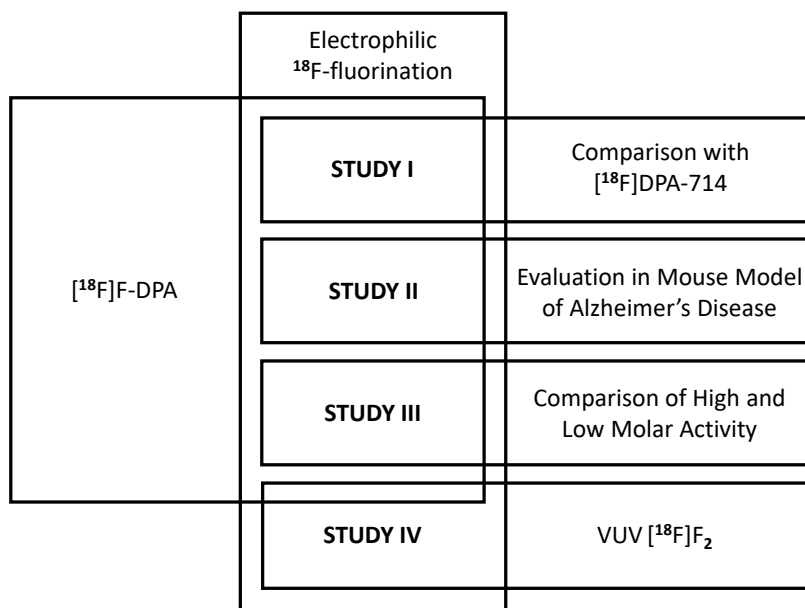


Figure 1: Interrelation of the various studies included in this thesis.

Radiochemistry, or the chemistry of radioisotopes, is a crucial part of PET, since positron-emitting radioisotopes need to be incorporated into biologically active molecules to make tracers. Radiochemistry is distinctly different from the corresponding non-radioactive chemistry since several considerations need to be made when working with radioisotopes. These include but are not limited to; time-constraints which are dependent on the half-life of the radioisotope and need to be met to ensure enough radioactivity at the end of the synthesis, as well as minimising sources of contamination by the naturally occurring, non-radioactive, isotope of the element used for labelling.

The work presented herein focusses on the use of fluorine-18, the most commonly employed PET-radionuclide, in the synthesis of tracer molecules. In standard organic chemistry, electrophilic and nucleophilic fluorination reactions are complementary reactions that are employed indiscriminately. In the case of fluorine-18 chemistry, due to numerous factors, nucleophilic reactions are often used for labelling in preference to electrophilic reactions. Nevertheless the electrophilic fluorine-18 labelling approach still represents a valuable route for the production of radiotracers, namely due to the simplicity and ease of reactions employing F_2 , given the necessary equipment.

This thesis explores the use of both nucleophilic as well as electrophilic fluorine-18 labelling routes for the synthesis of $[^{18}F]F$ -DPA (Figure 2). This molecule is a promising new tracer for the imaging of the translocator protein (TSPO), a mitochondrial membrane protein that is involved in the transport of cholesterol and is over-expressed in conditions of neuroinflammation. Despite the existence of many radioligands for TSPO imaging there are numerous limitations associated with various TSPO radiotracers. One such shortcoming is the metabolic instability of the radiolabel in some radiotracers, such as $[^{18}F]DPA$ -714. This results in the formation of small non-specifically binding radiometabolites which decrease the quality of PET images. $[^{18}F]F$ -DPA was developed to address this issue of metabolic instability by introducing the ^{18}F -label a metabolically stable position.

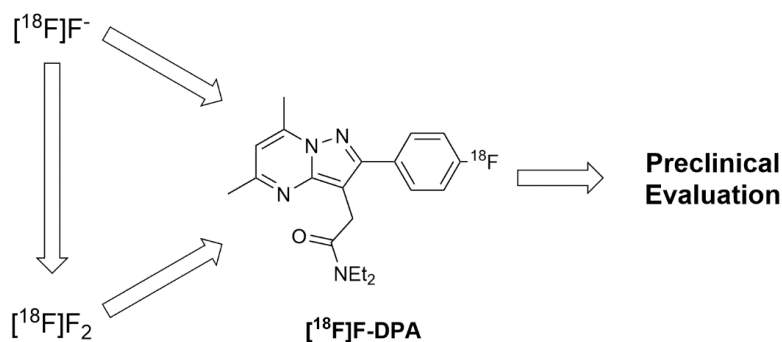


Figure 2: Outline of various stages of $[^{18}F]F$ -DPA syntheses and preclinical evaluation discussed within this work.

Preclinical evaluation is a vital aspect in the development of any new radiotracer because it provides an idea of how the radiotracer behaves in a living being. This is crucial for shedding light on key characteristics, such as the metabolic stability and the specificity of the tracer for the target of interest, which can be pivotal in the acceptance or rejection of a potential new radiotracer for clinical use.

2 REVIEW OF LITERATURE

2.1 Positron Emission Tomography

The conception and evolution of the imaging modality that we have come to know as Positron Emission Tomography, or PET, has been ongoing for approximately the past 100 years. It started in the 1920s with the invention of the particle accelerator known as a cyclotron. In the late 1920s Dirac postulated the existence of electrons with positive energy (Dirac 1928, 1930). However, it was not until 1932, that the positron itself was discovered by C.D. Anderson (Anderson 1933), an achievement which earned him the Nobel Prize in Physics in 1936. When irradiating samples of boron, magnesium and aluminium with α -particles from polonium, Frederic Joliot and Irene Curie discovered that radiation could be detected from the samples even after the radioactive source had been removed. This led them to the conclusion that a transmutation had occurred and that the resulting compounds were emitters of positrons (Curie and Joliot 1933a, 1933b, 1934a). Curie and Joliot hypothesised that in the case of boron the $^{10}\text{B}(\alpha, n)^{13}\text{N}$ nuclear reaction had occurred and confirmed the presence of an isotope of nitrogen by synthesising ammonia (Curie and Joliot 1934b, Joliot and Curie 1934). This transmutation of elements to form new isotopes of different elements spurred Ernest O. Lawrence, who was developing and working with cyclotrons at the time, to explore the possibility of using cyclotron irradiation to the same end. His deuteron-bombardment of various elements resulted in numerous transmutations and the formation of several radioisotopes (Henderson et al. 1934, Lawrence 1934, 1935, Lawrence et al. 1935a, 1935b, McMillan and Lawrence 1935). The discovery of positrons and man-made, neutron-poor, positron-emitting radionuclides opened the door to a new field of research. In 1953 Sweet and Brownell reported the first use of positron-emitters for the localisation of brain tumours by detecting annihilation radiation (Brownell and Sweet 1953).

As the name suggests PET employs positron-emitting radionuclides to generate a slice-wise image of radioactivity distribution in a living subject. The short-lived positron-emitting radionuclides employed are chemically bound to bioactive molecules of interest. When these, so called, radiopharmaceuticals are administered to the subject of the study they are distributed throughout the entire body and accumulate in certain locations depending on the identity of the molecule in question.

The decay of a positron-emitting radionuclide results in the generation of a positron. However, the emitted positron typically has a low energy and is not very penetrating hence it has a short range of travel within tissue. After emission the

positron scatters in the nearby tissue, losing energy with each collision, until it has decelerated to the extent that it can interact with an electron. Since the positron is the antiparticle of an electron the particles annihilate and create two gamma photons (511 keV) which, to conserve momentum, travel in approximately opposite directions. These emitted gamma photons can be detected by a ring of scintillation detectors and used to generate an image of the radioactivity distribution. When carried out over time, a PET scan provides a dynamic image of how the radioactivity is distributed during the scan. Depending on the identity of the bioactive molecule that has been labelled, this provides insight into functional processes occurring within the living subject.

The ability to see non-invasively into living patients and to quantitatively monitor where certain bioactive molecules accumulate has had a great impact on the diagnosis and monitoring of diseases as well as on the field of drug development. PET is now routinely used for diagnosing and monitoring the progression of diseases such as; many forms of cancer, various neurological conditions including Alzheimer's disease (AD), stroke and Multiple Sclerosis, to name a few, and different cardiac conditions.

Table 1: Some of the most commonly employed radionuclides in PET (Clementi et al. 1967, International Atomic Energy Agency; Nuclear Data Section; A-1400 Vienna; Austria, National Nuclear Data Center; Brookhaven National Laboratory; NY 11973-5000; Upton)

Radionuclide	$t_{1/2}$ (min)	Decay mode	β^+ energy max. (MeV)	Atomic radius (pm)
Carbon - 11	20.4	99.8% β^+ 0.2% EC	0.96	67
Nitrogen - 13	10.0	99.8% β^+ 0.2% EC	1.20	56
Oxygen - 15	2.0	99.9% β^+ 0.1% EC	1.73	48
Fluorine - 18	109.8	96.7% β^+ 3.3% EC	0.63	42
Copper - 64	762.1	17.6% β^+ 43.7% EC 38.5% β^-	0.65	145
Gallium - 68	67.7	88.9% β^+ , 11.1% EC	1.90(87.7%) 0.82(1.2%)	136

Most conditions or diseases that are studied favour different biologically active molecules and these can be labelled with a range of various positron-emitting

isotopes. Like their respective non-radioactive counterparts each different radionuclide brings chemical properties which can impart various characteristics to the labelled tracer molecule. In addition to the various chemical properties the different radionuclides also have varying radiological properties which have to be carefully considered when selecting a radionuclide for the labelling of a biologically active molecule. Some of the most commonly employed radionuclides in PET are listed in Table 1. In addition to the characteristics listed, there are other attributes such as the positron range in tissue and biological half-life of the molecule to be labelled, to consider when selecting a radionuclide for the production of a tracer for PET.

2.2 Chemistry of fluorine and its isotopes

The element fluorine was first isolated in its elemental state by the electrolysis of potassium hydrogen fluoride and dry hydrogen fluoride by Moissan in 1886 (Moissan 1886). This achievement earned Moissan the Nobel Prize in Chemistry in 1906.

Fluorine has several properties that make it a particularly interesting and useful element. It has the highest electronegativity of all the elements and due to this a small atomic radius. This small atomic radius, together with the high electron density, and resulting electron repulsion, in diatomic fluorine gas results in the F₂ molecule having a relatively low bond energy compared to the other halogens (Table 2).

Table 2: Atomic radius, bond length and bond energy of various halogens (Greenwood and Earnshaw 1997, Huheey et al. 1993, Slater 1964, Sutton 1965)

Molecule	Covalent radius (pm)	Bond length (pm)	Bond energy (kJ/mol)
F ₂	71	142	158
Cl ₂	99	199	243
Br ₂	114	228	193
I ₂	133	267	151

Thanks to the high electronegativity of fluorine, its covalent bonds with other elements are highly polar in character. The partial charges of the dipole attract one another and cause these covalent bonds to be very strong. Due to the relatively low bond energy of the F-F bond and very high strengths of the fluorine bond when it is bound to other elements, fluorine is one of the most reactive elements. In fact, the C-F bond is the strongest single bond to carbon that any element can form.

Table 3: Bond length and strength of some C-F bonds (Chambers 2004, O'Hagan 2008)

Molecule	C-F Bond length (pm)	Bond energy (kJ/mol)
MeF	139	459.8
CH ₂ F ₂	136	500
CHF ₃	133	533.5
CF ₄	132	546.0

The strength of the C-F bond increases with each consecutive fluorine that is added to the geminal carbon (Chambers 2004) (Table 3) resulting in a very low reactivity of perfluorinated compounds, such as polytetrafluoroethylene (Teflon).

While fluorine is not native to many naturally occurring bioactive molecules, fluorine can be used to impart certain useful properties including improved metabolic stability and higher lipophilicity to bioactive compounds (Gillis et al. 2015, Shah and Westwell 2007). As a result, its presence has become increasingly more prevalent in pharmaceutical compounds.

Apart from the natural isotope, fluorine-19, fluorine has two radioisotopes with sufficiently long half-lives to allow for practical application. These are the positron-emitting radioisotopes; fluorine-18 ($t_{1/2} = 109.8$ min) and fluorine-17 ($t_{1/2} = 64.5$ s). Even though fluorine radiochemistry is dominated by the longer-lived fluorine-18 radioisotope, the relatively short-lived fluorine-17 has found applications including in the field of PET. Due to the very short half-life of fluorine-17, its use is very limited and it has been employed exclusively as [¹⁷F]fluoromethane for the study of blood flow (Barnhart et al. 2005, Converse et al. 2001, 2004, Dabbs et al. 2001, Ferrarelli et al. 2004, Mulholland et al. 1987, Roberts et al. 2000).

2.2.1 Photochemical reactions of fluorine

Photochemical reactions of fluorine, those in which a part or all the activation energy required for the reaction to proceed is supplied by an incident photon, have been studied since the 1960s. Since fluorine gas usually has a very high reactivity, these reactions, requiring external energy, have been employed for the synthesis of relatively exotic compounds such as XeF₂ (Holloway 1966, Streng and Streng 1965a, Weeks et al. 1962), XeF₄ (Šmalc et al. 1976), XeF₆ (Lutar et al. 1980), KrF₂ (Streng and Streng 1965b) and SF₆ (Armendia and Schumacher 1985).

Excimer lasers

Exotic fluorine-containing species can also be employed for the generation of photons, as in the case of some excimer lasers.

The term “laser” was first used by Gould in 1959 as an acronym for Light Amplification by Stimulated Emission of Radiation (Gould 1959). Numerous types of laser exist nowadays. One of these types are the “excimer” lasers. These employ an electric discharge to produce excited dimers (exci-mers) which can be either heteroatomic or homoatomic in nature. These excimers are molecules that can only exist in the excited state, specifically with one of the 2 atoms being in an excited electron state. When an excimer passes its energy to a photon, via stimulated emission, the bond of the excimer will break giving the two unbound atoms of the ground state.

The first excimer laser to be developed had a wavelength of 172 nm and employed a noble gas dimer (Xe₂). Since then other homo- and hetero-atomic excimer lasers have been developed that employ other noble gases or noble gas halides. Typically, these emit radiation in the ultraviolet or vacuum ultraviolet range and have found use in a range of fields such as high-resolution photo-lithography and medicine where they are used for Lasik eye surgery. The ArF excimer laser (wavelength 193 nm) is used in both applications.

$$E = \frac{hc}{\lambda}$$

Equation 1: Formula for calculating the energy of a photon using the Planck constant (h), speed of light (c), and wavelength (λ)

The energy of light is inversely proportional to the wavelength. The energy of a photon can be calculated from its wavelength, the speed of light and the Planck Constant according to the equation in Equation 1. Hence the energy of light is often referred to simply by the wavelength.

2.2.2 Fluorine – 18

Fluorine-18 has a particularly useful set of radiochemical properties which have made it one of the most commonly used PET radioisotopes. The decay mode of fluorine-18 is quite clean, decaying 96.7% by positron emission. It is the emitter of the lowest energy positrons (β^+ energy max: 0.6335 MeV). Due to this the positrons have an accordingly low range in tissue and tissue-equivalent materials and hence high resolution PET images can be obtained when using fluorine-18 (Alva-Sánchez et al. 2016).

Furthermore the high yield of production of fluorine-18 by a cyclotron via the $^{18}\text{O}(\text{p},\text{n})^{18}\text{F}$ nuclear reaction on an enriched water target, together with the half-life ($t_{1/2} = 109.8$ min) which is sufficiently long to allow for multistep syntheses to be performed as well as for the distribution of labelled products to PET facilities without on-site cyclotrons, makes fluorine-18 the most commonly employed radionuclide for the production of tracers for PET.

2.2.3 Cyclotron production of [^{18}F] F^- and [^{18}F] F_2

Historically, numerous nuclear reactions have been employed for the production of fluorine-18. Nowadays the field of fluorine-18 production is dominated by the $^{18}\text{O}(\text{p},\text{n})^{18}\text{F}$ (Nickles et al. 1984) reaction for the production of [^{18}F]fluoride or fluorine-18 labelled fluorine gas ([^{18}F] F_2) and the much less common $^{20}\text{Ne}(\text{d},\alpha)^{18}\text{F}$ (Casella et al. 1980) reaction, for the generation of [^{18}F] F_2 . The $^{18}\text{O}(\text{p},\text{n})^{18}\text{F}$ reaction reported by Nickles et al. was carried out for the first time using protons accelerated using a tandem Van der Graff accelerator. However, nowadays cyclotrons are much more commonly employed in the synthesis of PET radionuclides due to the much more compact size of medical cyclotrons compared to other particle accelerators.

Most commonly, fluorine-18 is employed for radiolabelling in the form of the [^{18}F]fluoride which is azeotropically dried to increase reactivity. However [^{18}F] F_2 is an invaluable reagent for the labelling of certain compounds. In particular, electrophilic ^{18}F -fluorination with [^{18}F] F_2 or [^{18}F] F_2 -derived radiolabelling reagents can provide a fast and synthetically simple route to label electron rich aromatics, which can be difficult to access using the nucleophilic [^{18}F]fluoride. [^{18}F] F_2 gas can be produced in-target via the nuclear reactions described above and subsequent isotope exchange reaction of the fluorine-18 produced with non-radioactive “carrier” F_2 gas.

2.3 ^{18}F -Fluorination

$$\text{Molar activity } (A_m) = \frac{\text{Activity of Compound (MBq)}}{\text{Amount of Compound (mol)}}$$

Equation 2: Definition of molar activity

Molar activity (A_m) (Equation 2), formerly referred to as specific activity, can be described as the molar concentration of activity for a particular radionuclide. It is defined as the measured radioactivity per mole of compound (Coenen et al. 2017); typically the units are in GBq/ μmol or TBq/ μmol for PET tracers. Since A_m is

calculated from the radioactivity of a compound, which decays with time depending on the half-life of the radionuclide, it is necessary to refer to the time point for which the A_m is calculated. Most often these are key points in the reaction such as the end of bombardment (EOB) or the end of the synthesis (EOS), or in the case of clinical or preclinical work; the time of injection (TOI).

$$\text{Maximum Theoretical } A_m = \frac{N_A \ln 2}{t_{1/2}}$$

Equation 3: Maximum theoretical A_m defined as a function of Avogadro's Constant (N_A) and the $t_{1/2}$

As shown in Equation 3, the maximum theoretical A_m for a particular radionuclide is inversely proportional to its $t_{1/2}$. However, in practice the A_m can be affected by numerous factors depending on the identity of the radioisotope in question as well as on the production route employed.

In the case of carbon-11, one of the main issues affecting the A_m is the high natural abundance carbon-containing molecules and the subsequent possibility of contamination of cyclotron-produced synthons such as $[^{11}\text{C}]\text{CO}_2$ or $[^{11}\text{C}]\text{methane}$ by their non-radioactive counterparts. This presents a much more significant problem in the case of $[^{11}\text{C}]\text{CO}_2$ where the natural abundance of the non-radioactive analogue is 330 ppm compared to $[^{11}\text{C}]\text{methane}$ which has a non-radioactive natural abundance of 1.6 ppm (Elsinga 2002). Oxygen-15 which has the shortest $t_{1/2}$ of all the commonly employed radioisotopes in PET and is hence typically employed as O_2 , CO , CO_2 or water can likewise suffer from contamination by naturally occurring oxygen-16 containing analogues.

In the case of fluorine-18, numerous parameters have been studied with respect to their impact on the resulting A_m . These include; the irradiation time, dose rate and anionic contaminants from the target as described by Solin et al. (Solin et al. 1988) as well as contamination from materials (Berridge et al. 2009, Link et al. 2012, Savisto et al. 2018), reagents (Link et al. 2012) and solid phase extraction resins (Lu et al. 2009).

A_m is an important parameter for PET tracers, because a low A_m will result in a high injected mass of tracer. The portion of this that is not radioactive will compete with the radioactively labelled molecules for the same biological target. While a high A_m is not crucial in all cases, for example when the biological target being studied is very abundant, the high injected mass of non-radioactive "cold" compound when a low A_m tracer is employed can have a marked effect on the kinetics of the tracer uptake and subsequent washout (Delforge et al. 1993, Eberl et al. 2017).

The variation in the A_m 's obtained for syntheses of tracers for PET stems from the labelling methodologies that are employed as well as the prevalence of sources of contamination by the non-radioactive isotope. Hence due to the necessary addition of carrier F_2 gas during the production of $[^{18}F]F_2$ the resulting gas and any subsequently labelled electrophilic ^{18}F -fluorination or PET tracers have accordingly low A_m 's. The post-target, high voltage-promoted production method for $[^{18}F]F_2$ yields the highest A_m of all the electrophilic $[^{18}F]F_2$ production methods. However, at best this has been reported to be 55 GBq/ μ mol (Bergman and Solin 1997). In contrast, the A_m 's achieved during nucleophilic ^{18}F -fluorinations typically range between 10 GBq/ μ mol to 5 TBq/ μ mol, and hence this fluorination methodology is often selected in favour of an electrophilic approach since the resulting PET tracers will be able to provide good data and images even when the biological target is not very abundant.

2.3.1 Isotope exchange reactions of fluorine

The isotope exchange reaction between fluorine-18 and fluorine-19 was first studied by Dodgen and Libby in 1949. Their work explored the thermal and photochemical induced exchange reactions between hydrogen halides and the halogens in the gaseous state. The findings showed that while $^{19}F/^{18}F$ exchange reaction between $[^{18}F]HF$ and F_2 did not proceed under the photochemical conditions (light of a mercury arc) or at room temperature, heating the reaction mixture in a brass vessel at 200 °C for approximately an hour was sufficient to accomplish the isotope exchange (Dodgen and Libby 1949). Since then, fluorine isotope exchange reactions were further studied between HF and halogen fluorides (Rogers and Katz 1952) as well as between fluorine and the halogen fluorides (Bernstein and Katz 1952).

In the late 1970s and 1980s the concept of isotope exchange was applied to the production of $[^{18}F]F_2$. Casella et al. employed the $^{20}Ne(d,\alpha)^{18}F$ nuclear reaction, irradiating a Ne/0.1% F_2 target with a 15- μ A deuteron beam at 14 MeV to successfully produce $[^{18}F]F_2$ (Casella et al. 1980). The 2-shoot method, described by Nickles et al. (Nickles et al. 1984), employed a 2- μ A proton beam at 10 MeV to irradiate an enriched $[^{18}O]O_2$ target. This resulted in the formation of fluorine-18 which adsorbed onto the nickel walls of the target chamber. Subsequently the chamber was evacuated, the remaining $[^{18}O]O_2$ target gas was recovered and the chamber was filled with 3% F_2 in a noble gas. A further irradiation of the chamber with a 2- μ A proton beam at 10 MeV resulted in the $^{19}F/^{18}F$ isotope exchange reaction and the production of $[^{18}F]F_2$. The isotope exchange reaction can also be used for the synthesis of other fluorination reagents such as $[^{18}F]XeF_2$. $[^{18}F]XeF_2$ is a milder electrophilic ^{18}F -fluorination reagent which was first synthesised by

$^{19}\text{F}/^{18}\text{F}$ fluoride exchange between XeF_2 and $[^{18}\text{F}]\text{HF}$, $[^{18}\text{F}]\text{SiF}_4$, and $[^{18}\text{F}]\text{AsF}_5$ in 1981 (Schrobilgen et al. 1981) since then $[^{18}\text{F}]\text{XeF}_2$ can also be synthesised by isotope exchange with the ^{18}F fluoride ion (Constantinou et al. 2001, Lu and Pike 2010, Vasdev et al. 2002).

Alternatively the fluoride isotopic exchange reaction can also be employed for the nucleophilic ^{18}F -labelling of aromatics as described in 1981 by Cacace et al. (Cacace et al. 1981). The aromatic $^{19}\text{F}/^{18}\text{F}$ isotope exchange reaction depends strongly on the substituents present on the aromatic ring (Blom et al. 2009, Cacace et al. 1982). Despite this, aromatic isotope exchange has been used as a synthesis route for the production of several tracers for PET such as 6- $[^{18}\text{F}]$ fluoro-L-DOPA (Al-Labadi et al. 2006, Wagner et al. 2009), *N*-methyl- $[^{18}\text{F}]$ flumazenil (Ryzhikov et al. 2004) and $[^{18}\text{F}]$ 1-benzyl-*N*-(3,4-difluorobenzyl)-2-isopropyl-6-(2-methoxyethoxy)-1H-indole-3-carboxamide (Rokka et al. 2013). However due to the relatively high amount of the fluorine-19 isotope present during these reactions the A_m 's of the final products are quite low, in the order of 100 MBq/ μmol – 1 GBq/ μmol .

2.3.2 Post-target production of $[^{18}\text{F}]\text{F}_2$

Due to the necessary addition of carrier F_2 , the $[^{18}\text{F}]\text{F}_2$ gas synthesised by cyclotron-production methods and any labelling reagents derived from the $[^{18}\text{F}]\text{F}_2$ gas suffer from the downside of relatively low molar activity (A_m).

A post-target synthesis of higher A_m $[^{18}\text{F}]\text{F}_2$ from cyclotron produced $[^{18}\text{F}]$ fluoride was reported by Bergman and Solin in 1997 (Bergman and Solin 1997) (Figure 3). This approach utilises $[^{18}\text{F}]$ fluoride from the cyclotron which is azeotropically dried and reacted with iodomethane to give $[^{18}\text{F}]$ fluoromethane ($[^{18}\text{F}]\text{MeF}$) by a standard nucleophilic ^{18}F -fluorination procedure. After purification by gas chromatography the $[^{18}\text{F}]\text{MeF}$ is mixed with carrier F_2 gas, and the resulting mixture is exposed to a high voltage electrical discharge (approximately 30 kV). The electrical discharge atomises the gases within the reaction chamber and they subsequently rearrange to give various fluorine-18 labelled products.

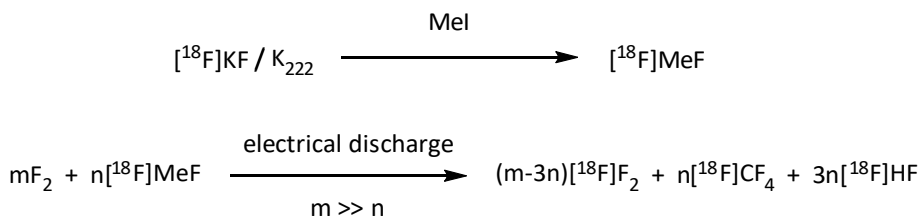


Figure 3: Post-target production of $[^{18}\text{F}]\text{F}_2$

When the quantity of carrier F_2 gas is significantly higher than that of the initial $[^{18}F]MeF$ (i.e. $m \gg n$), the reaction produces an appreciable yield of the $[^{18}F]F_2$ gas. The product of this synthetic approach has a much higher A_m (55 GBq/ μ mol) (Bergman and Solin 1997) than the $[^{18}F]F_2$ from the cyclotron production methods (0.1-1.3 GBq/ μ mol) (Blessing et al. 1986, Hess et al. 2000).

Recently, the post-target production method was studied further by replacing the carrier F_2 gas with SF_6 , a less toxic and easier to handle source of fluorine (Krzyszmonik et al. 2017).

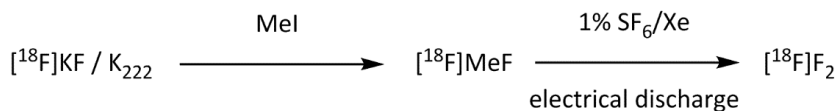


Figure 4: Post-target production of $[^{18}F]F_2$ gas using SF_6

In this proof-of-concept study it was demonstrated that SF_6 can indeed be used as an alternative to carrier- F_2 (Figure 4). The A_m of the resulting F_2 gas was assessed by performing labelling reactions, such as the synthesis of 6- $[^{18}F]$ fluoro-L-DOPA, and determining the A_m of the resulting product. The A_m obtained with the optimal conditions was 2.2 ± 0.5 GBq/ μ mol. This A_m is approximately the same as that which can be attained using the in-target cyclotron production methods.

2.3.3 Nucleophilic ^{18}F -fluorination

Due to the relative ease of production of the $[^{18}F]$ fluoride and the high electronegativity of fluorine, the nucleophilic S_N2 and S_NAr approaches are those most commonly used for the introduction of fluorine-18 into organic molecules. This extensive field of research has been reviewed at length several times (Van Der Born et al. 2017, Coenen and Ermert 2018, Damont et al. 2013, Gouverneur et al. 2019, Gu et al. 2011, Hollingworth and Gouverneur 2012, Jacobson et al. 2014, Petersen et al. 2017, Preshlock et al. 2016a, Schirrmacher et al. 2007, 2017, Tredwell and Gouverneur 2012).

Under some conditions the solvated fluoride ion can act as a good nucleophile (Kim et al. 2008, Vincent and Hillier 2005). However, typically the solvation shell surrounding fluoride along with the resulting partial charge neutralisation hinders nucleophilic reactions under aqueous conditions (Jacobson et al. 2014). The nucleophilic character of the fluoride increases with dryness (Vlasov 1993) and hence the nucleophilic approach is dependent on a sufficiently high level of dryness of the $[^{18}F]$ fluoride. This is achieved by replacing the fluoride's counterion with an alkali metal, usually potassium, and the azeotropic distillation and

complexation of the metal counterion in a cryptand or crown-ether (such as Kryptofix 222 or 18-crown-6) thereby enabling the [^{18}F]fluoride complex to be soluble in dry organic solvents (Jacobson et al. 2014).

While aliphatic fluorination reactions are not so sensitive to trace amounts of water (Block et al. 1986) and occasionally even benefit from the presence of trace amounts of water (Briard and Pike 2004, Kilbourn et al. 1986), aromatic fluorinations require a more meticulous drying procedure and higher level of dryness to adequately decrease the solvation (Vlasov 1993). However, there is a downside that is associated with the more thorough drying procedure, that is; as the dryness of the fluoride increases so does its tendency to stick on the reaction vessel walls (Brodack et al. 1986, Gnade et al. 1981, Nickles et al. 1986). This results in the loss of a portion of [^{18}F]fluoride from the reaction mixture and a subsequent decrease in radiochemical yield (Coenen et al. 1981). Recently, Kwon et al. reported an approach by which the lengthy drying procedure can be avoided (Kwon et al. 2018). This approach employs a mixed organic solvent system which lessens the effect of the water present, and was successfully applied for the synthesis of three model PET radiopharmaceuticals.

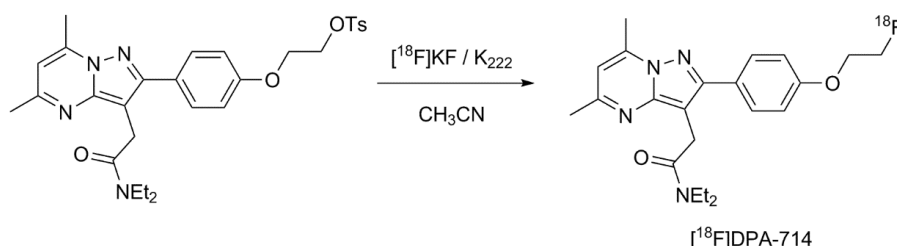


Figure 5: Direct aliphatic fluorination for the synthesis of [^{18}F]DPA-714

Aliphatic fluorination, via the S_N2 mechanism, is a routinely employed methodology for the synthesis of various tracer molecules for PET. This approach is typically a synthetically simple approach that involves the direct substitution of a suitable leaving group with [^{18}F]fluoride. Typically, leaving groups such as various sulfonic esters or halogens are employed, however careful consideration must be made when selecting which specific leaving group to use. Depending on the reaction conditions and the lability of the leaving group, a competing elimination side reaction can occur (Coenen 2007). Because elimination reactions are base-promoted, particular attention must be paid to the basicity of the potassium source as well as the ratio of base to cryptand or crown-ether used in the formation and drying of the [^{18}F]KF complex (Jacobson et al. 2014). Numerous ^{18}F -labelled tracers are produced by this method, including 2-deoxy-2- ^{18}F fluoro-D-glucose ([^{18}F]FDG) (Hamacher et al. 1986), the most commonly used of all PET radiotracers, [^{18}F]fluoroethyl-L-tyrosine (Hamacher and Coenen 2002),

[^{18}F]florbetapir ([^{18}F]AV-45) (Choi et al. 2009, Zhang et al. 2005) and *N,N*-diethyl-2-[4-(2-[^{18}F]fluoroethoxy)phenyl]-5,7-dimethylpyrazolo[1,5-*a*]pyrimidine-3-acetamide ([^{18}F]DPA-714) (James et al. 2008) (Figure 5), to name a few.

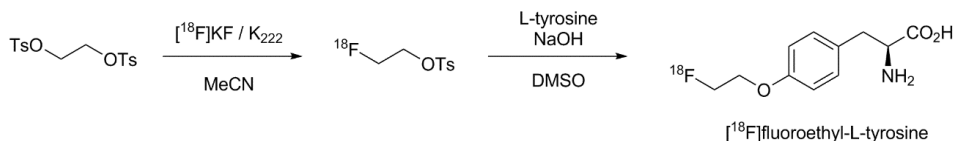


Figure 6: Synthesis and use of [^{18}F]fluoroethyltosylate synthon

Alternatively the radioactive label can be introduced onto a synthon such as [^{18}F]fluoroethyltosylate, [^{18}F]fluoroethylazide or [^{18}F]4-fluoro-1-butyne which can subsequently be further used for synthesis. This method can be applied for the synthesis of relatively small molecules such as [^{18}F]fluoroethyl-L-tyrosine (Wester et al. 1999) (Figure 6) which can also be produced by direct aliphatic fluorination.

The copper (I) catalysed Huisgen cycloaddition of an alkyne and azide (Figure 7) in particular is a valuable method for the fluorine-18-labelling of larger biomolecules such as of proteins (Gill and Marik 2011, Glaser and Årstad 2007, Marik and Sutcliffe 2006), since its can be carried out under quite mild condition that will be tolerated by biomolecules. The downside of employing prosthetic groups as labelling reagents for biomolecules lies in the necessary purification of both the prosthetic group as well as the final molecule (Jacobson et al. 2014, Kiesewetter et al. 2011). Despite these time-consuming purifications, ^{18}F -labelled prosthetic groups have been employed in the synthesis of numerous PET tracers based on biomolecules (Schirmacher et al. 2017).

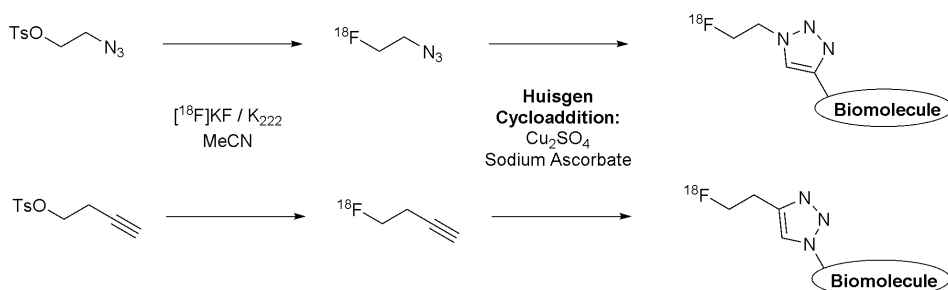


Figure 7: Synthesis and use of [^{18}F]synthons for copper (I) catalysed Huisgen cycloaddition

In some cases the aliphatic ^{18}F -labelling of an organic molecule results in the radioactive label being on a metabolically unstable position, in particular when the

labelling position is on the C-terminal end of an alkoxy chain as in the case of [^{18}F]DPA-714 (Peyronneau et al. 2013). In such cases the nucleophilic ^{18}F -fluorination of an aromatic ring can provide a more robust labelling position with respect to metabolism.

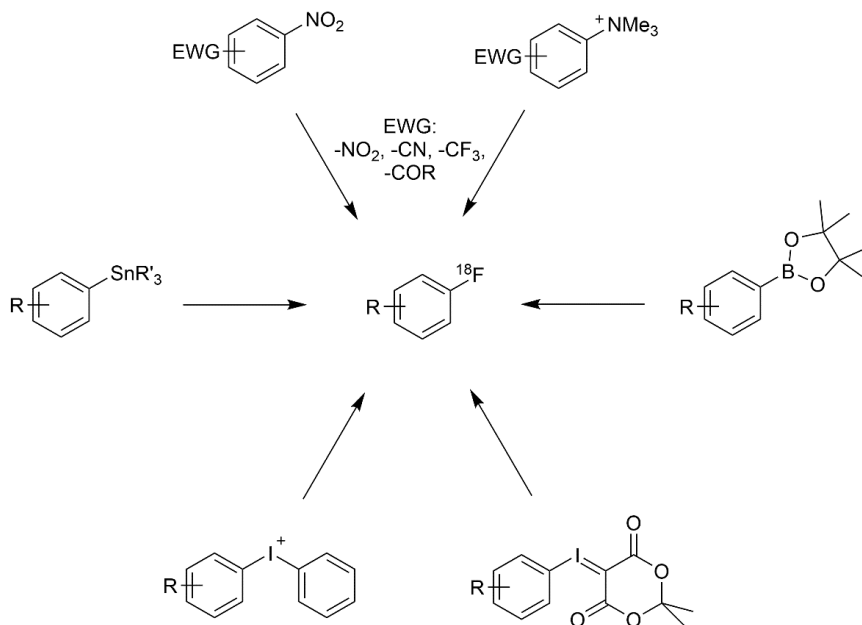


Figure 8: Nucleophilic aromatic ^{18}F -fluorination (EWG: Electron Withdrawing Group)

While the nucleophilic labelling of aromatic rings, via $\text{S}_{\text{N}}\text{Ar}$, can be achieved with high A_{m} , the reaction is critically dependent on the presence of a suitable leaving group, as well as an electron withdrawing substituent on the *ortho* or *para* position relative to the leaving group (Jacobson et al. 2014, Preshlock et al. 2016a). As a result, direct, late stage nucleophilic fluorination of insufficiently activated aromatic rings is far from facile.

Various methodologies have been developed to implement the labelling of aromatic rings and the most common approaches employ, aryl nitro or ammonium compounds (Tredwell and Gouverneur 2012), hypervalent iodine compounds (Pike 2018, Yusubov et al. 2013) such as diaryliodonium salts (Pike and Aigbirhio 1995) and iodonium ylides (Satyamurthy et al. 2010), aryl boronic esters (Tredwell et al. 2014), or aryl stannanes (Gamache et al. 2016, Zarrad et al. 2017)(Figure 8).

The nucleophilic aromatic fluorination of many aryl compounds is highly dependent of the presence of activating electron withdrawing groups on the *ortho* or *para* positions (Jacobson et al. 2014, Preshlock et al. 2016a). In the case of the diaryl iodonium salts, the regioselectivity of the radiofluorination is driven by the

“*ortho* effect” wherein an *ortho* substituent present on the aromatic rings directs the ^{18}F -fluorination to that same ring, despite the steric and electronic contributions (Gail et al. 1997). Recently, reactions for the chemoselective ^{18}F -fluorination of diaryliodonium salts have been developed employing electron-rich spectator aryl rings such as 2,4,6-trimethoxybenzene (Kwon et al. 2019) to minimise the formation of ^{18}F -fluorinated aromatic side products. The ^{18}F -fluorination of diaryliodonium salts has also been applied to the synthesis of functionalised [^{18}F]fluoroarenes which can be used as prosthetic groups for further labelling (Chun and Pike 2013). In the case of iodonium ylides the auxiliary group is not susceptible to radiofluorination as is the case with diaryliodonium salts, hence measures do not need to be taken to ensure chemoselectivity (Hill and Holland 2015, Pike 2018, Rotstein et al. 2016). This lack of side reactions makes this methodology a very attractive approach for the synthesis of tracer molecules (Rotstein et al. 2014, Yusubov et al. 2013). Recently it has been adapted for use in microfluidic reactors (Calderwood et al. 2015), by this approach two molecules of interest were synthesised, the PET tracer [^{18}F]FPEB and 4-[^{18}F]fluorobenzyl azide a prosthetic group that can be used for the click reaction.

Recently many groups have been working on copper-mediated ^{18}F -fluorination as nucleophilic procedures for the introduction of fluorine-18. Gouverneur et al. developed the Cu-mediated ^{18}F -fluorination of aryl boronic esters (Tredwell et al. 2014) and this approach has been shown to be applicable to the synthesis of numerous radiopharmaceutical compounds of interest (Preshlock et al. 2016b, Tredwell et al. 2014). Since then, due to the low efficacy of the reaction in the presence of “high” amounts of carbonate (Zlatopolskiy et al. 2015), numerous research groups have explored alternatives to the potassium carbonate and kryptofix combination typically used for the drying of the [^{18}F]fluoride (Antuganov et al. 2019, Giglio et al. 2017, Mossine et al. 2017, Schäfer et al. 2016, Zischler et al. 2017). These studies have resulted in this versatile methodology being applied to the synthesis of numerous PET tracers as model molecules (Wilson et al. 2018), these include: 4-L-[^{18}F]fluorophenylalanine (Antuganov et al. 2017, 2019), [^{18}F]F-DPA, [^{18}F]DAA1106, 6-[^{18}F]FDA, 6-[^{18}F]fluoro-L-DOPA (Zischler et al. 2017), 6-[^{18}F]fluoro-L-tryptophan (Schäfer et al. 2016) and 5-[^{18}F]fluoro- α -methyl tryptophan (Giglio et al. 2017). Although automation of the Cu-mediated ^{18}F -fluorination of aryl boronic esters methodology for application in clinical production is proceeding, the radiochemical purification of products proves to be somewhat troublesome (Mossine et al. 2018). A slight modification of the reaction conditions also makes the reaction applicable to the fluorination of boronic acids (Mossine et al. 2015).

Cu-mediated nucleophilic fluorination has proven to be quite a versatile methodology that is not limited to aryl boronic esters as precursors. It has been

applied to the fluorination of various diaryliodonium salts (Ichiishi et al. 2014a, 2014c, 2014b, McCammant et al. 2017, Zlatopolskiy et al. 2015) and to the C-H fluorination of arenes (Lee et al. 2019). Recently, the Cu-mediated nucleophilic fluorination of stannyl precursors has also been reported recently both in organic chemistry (Gamache et al. 2016) as well as radiochemistry (Makaravage et al. 2016).

2.3.4 Umpolung approach

Umpolung refers to inverting the polarity of a functional group thereby changing how it reacts. Ritter et al. have worked extensively with transition metal complexes to achieve both aryl as well as fluoride umpolung. The fluoride umpolung reaction reported by Lee et al. (Lee et al. 2011) employs a palladium complex to couple with the [^{18}F]fluoride resulting in a complex which functions as an electrophilic ^{18}F -fluorination reagent. The possibility of reductive elimination from the intermediate ^{18}F -containing complex is minimised by using multi-dentate ligands. A fluorine transfer occurs between the 2 palladium complexes and results in the oxidation of Pd in the aryl containing complex and the formation of an ^{18}F -labelled aryl fluoride (Figure 9).

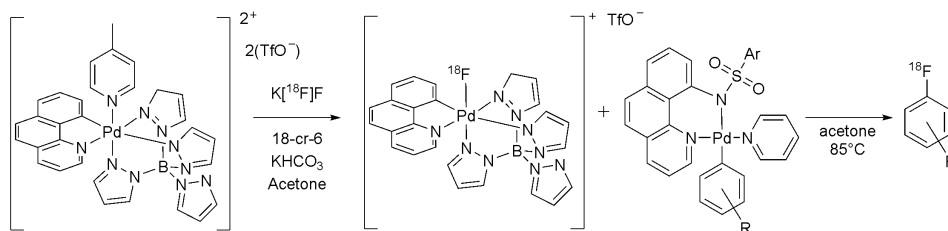


Figure 9: Fluoride umpolung reaction achieved through use of a Pd-complexes

The alternative aryl umpolung was reported also by Lee et al. (Lee et al. 2012). However, this employed an aryl-nickel complex and a hypervalent iodine oxidant to achieve the reaction (Figure 10). The one-step nature of this reaction, together with the ability to use the [^{18}F]fluoride in its aqueous form, rather than azeotropically dried [^{18}F]fluoride makes this procedure more favourable.

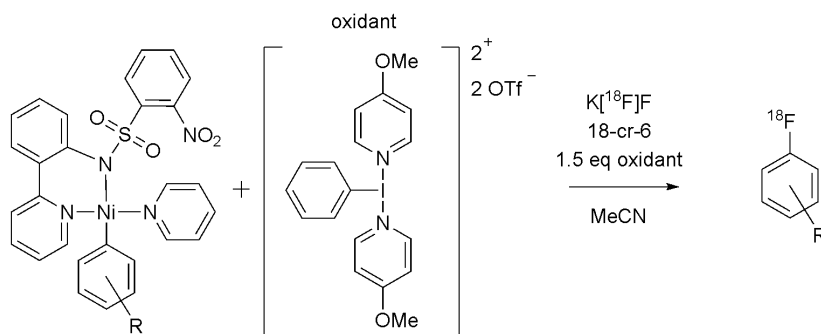


Figure 10: Aryl umpolung reaction achieved through formation of a Ni-complex

Metal-free aryl umpolung reactions for the fluorination of phenols, anilines, *N*-aryl acetamides and *N*-aryl sulphonamides have also been reported by various groups. These employ hypervalent iodine (III) reagents that undergo reduction during the reaction thereby enabling the inversion of polarity.

The oxidative fluorination of phenols was initially described by Bienvenu et al. (Bienvenu et al. 2002) and subsequently inspired the work on the metal-free oxidative ^{18}F -fluorination of phenols (Gao et al. 2012) and *N*-arylsulfonamides (Buckingham et al. 2015) by the Gouverneur group and on the *para*-selective fluorination of anilides by Tian et al. (Tian et al. 2013).

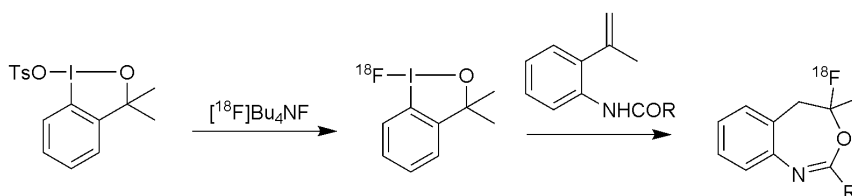


Figure 11: Synthesis of $[^{18}F]$ fluoro-benzoxazepines from *o*-styrylamides using $[^{18}F]$ fluoro-benziodoxole

Recently, $[^{18}F]$ fluoro-benziodoxole was reported as a no-carrier-added electrophilic fluorination reagent (Cortés González et al. 2018). Fluoride umpolung is achieved here by use of a hypervalent iodine compound which is labelled by an initial nucleophilic ^{18}F -fluorination reaction to displace a tosyl group (Figure 11). Subsequently it can be used in the synthesis of $[^{18}F]$ fluoro-benzoxazepines by electrophilic fluorocyclisation of *o*-styrylamides. However, for now, this approach is limited to the synthesis of $[^{18}F]$ fluoro-benzoxazepines.

2.3.5 Electrophilic ^{18}F -Fluorination

During early days of PET tracer production, due to the simplicity and robustness of the chemistry involved, many fluorine-18 labelled tracers, such as ^{18}F FDG (Ido et al. 1978), were synthesised by electrophilic methods (Figure 12).

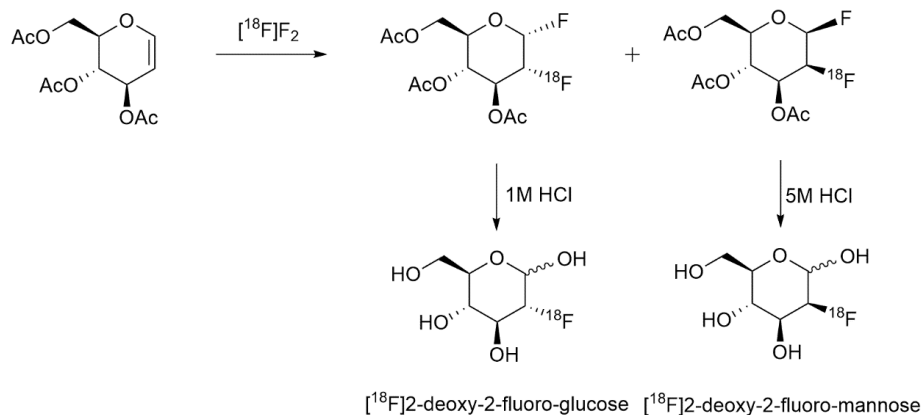


Figure 12: Synthesis of 2-deoxy-2- ^{18}F fluoro-D-glucose and 2-deoxy-2- ^{18}F fluoro-D-mannose by an electrophilic approach using $^{18}\text{F}\text{F}_2$

Since then many of these electrophilic synthesis methods have been abandoned in favour of nucleophilic approaches that were developed with the intention of increasing yields and in particular A_m 's of the final products. Despite the numerous nucleophilic ^{18}F -fluorination methodologies available, electrophilic ^{18}F -fluorination can still provide an alternative, fast and synthetically simple way of introducing fluorine-18 into organic molecules. Hence, numerous electrophilic ^{18}F -fluorination reagents have been developed and studied.

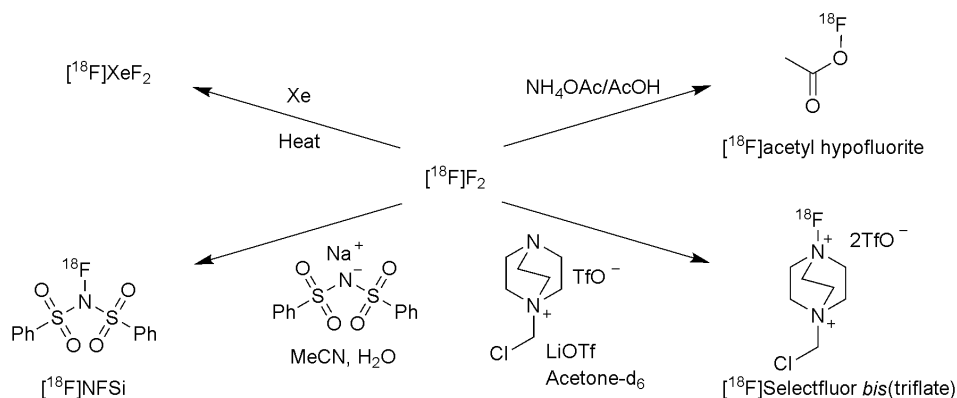


Figure 13: Synthesis of various “mild” ^{18}F -fluorination reagents

The simplest of these reagents is [^{18}F] F_2 gas, the production of which has already been discussed. While being the structurally simplest of the reagents it is also the most reactive and hence can in some cases lead to the production of undesired poly-fluorinated side-products. To tame the reactivity of fluorine gas various milder electrophilic reagents have been developed (Figure 13). These include [^{18}F] XeF_2 (Chirakal et al. 1984, Schrobilgen et al. 1981, Sood et al. 1983), O-F type reagents such as [^{18}F]acetyl hypofluorite (Salvadori et al. 1982), and N-F reagents such as [^{18}F]N-fluorobenzenesulfonimide ([^{18}F]NFSi) (Teare et al. 2007) and [^{18}F]Selectfluor *bis*(triflate) (Teare et al. 2010).

The 1-alkyl-4-fluoro-1,4-diazoniabicyclo[2.2.2]octane (Selectfluor) salts were first reported as electrophilic fluorination reagents by Banks et al. (Banks et al. 1992). The fluorine-18 labelled analogue, [^{18}F]Selectfluor *bis*(triflate), was subsequently developed (Teare et al. 2010) and its worth as fluorination reagent was demonstrated by its use in the synthesis of 6-[^{18}F]fluoro-L-DOPA (Figure 14) (Stenhagen et al. 2013).

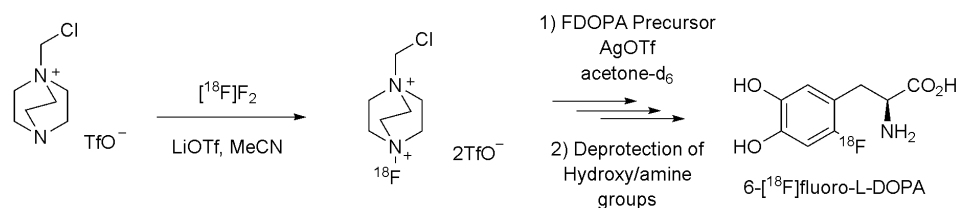


Figure 14: Synthesis of [^{18}F]Selectfluor *bis*(triflate) and its use in the synthesis of 6-[^{18}F]fluoro-L-DOPA from *N*-formyl or *N*-boc protected aryl trimethylstannane FDOPA precursor.

There are numerous beneficial properties that make [^{18}F]Selectfluor *bis*(triflate) a valuable tool for electrophilic ^{18}F -fluorination. It is relatively easy to produce from [^{18}F] F_2 gas and can be used for labelling reactions without the need for prior purification. In contrast to [^{18}F] F_2 gas, [^{18}F]Selectfluor *bis*(triflate) is employed as a solution in acetone and this allows for longer reaction times. Furthermore, the crude [^{18}F]Selectfluor *bis*(triflate) solution from the labelling with [^{18}F] F_2 gas is easily portioned for multiple reactions and the crude stock solution can be stored for a matter of hours.

Electrophilic ^{18}F -fluorination of aromatics without the presence of a suitable leaving group to direct the reaction generally results in formation of ^{18}F -fluorinated isomers as demonstrated by Firnau et al. (Firnau et al. 1986). Various metal or pseudometal-containing leaving groups have been employed to direct the fluorination position. These include; Li and MgBr (Satyamurthy et al. 1990), alkyl and aryl silanes (Coenen and Moerlein 1987, Di Raddo et al. 1984, Speranza et al. 1985), stannanes (Adam et al. 1981, 1984, Coenen and Moerlein 1987, Namavari

et al. 1992) or germanes (Coenen and Moerlein 1987) and most recently boron-containing groups (Stenhagen et al. 2013).

Recently the ^{18}F -fluorination of unactivated C-H bonds has been reported by Nodwell et al. (Nodwell et al. 2017). The reaction employs a photoactivated decatungstate catalyst to effect hydrogen atom abstraction. Subsequently, $^{18}\text{F}]\text{NFSi}$ acts as a source of fluorine-18 to achieve the labelling reaction. This novel synthesis was used to make a number of ^{18}F -labelled amino acids which were successfully employed in the imaging cancers in mice. The milder electrophilic ^{18}F -fluorination reagents are largely produced from $^{18}\text{F}]\text{F}_2$ gas, and hence suffer from some of the same drawbacks associated with the use of $^{18}\text{F}]\text{F}_2$ gas for labelling. Due to the necessary addition of non-radioactive fluorine gas and the reactivity profile of the resulting $^{18}\text{F}]\text{F}_2$, at least half of the radioactivity is lost by this approach. Also this dilution of ^{18}F -fluoride with ^{19}F -fluorine results in relatively low A_m 's compared to nucleophilic labelling approaches. Despite this, electrophilic ^{18}F -fluorination is still employed for the production of some tracers, such as; 6- ^{18}F]fluoro-L-DOPA (Forsback et al. 2008), $^{18}\text{F}]\text{CFT}$ (Forsback et al. 2012) and $^{18}\text{F}]\text{EF5}$ (Eskola et al. 2005).

2.4 Translocator protein 18kDa

The translocator protein 18kDa (TSPO), previously known as the peripheral benzodiazepine receptor, is a mitochondrial protein that is found on the outer mitochondrial membrane. It has numerous roles within the body that depend on the tissue that is being studied. The high levels of TSPO found in steroid-producing organs stem from its key role in the transport of cholesterol into mitochondria (Lacapère and Papadopoulos 2003, Li et al. 2016, Papadopoulos et al. 1997).

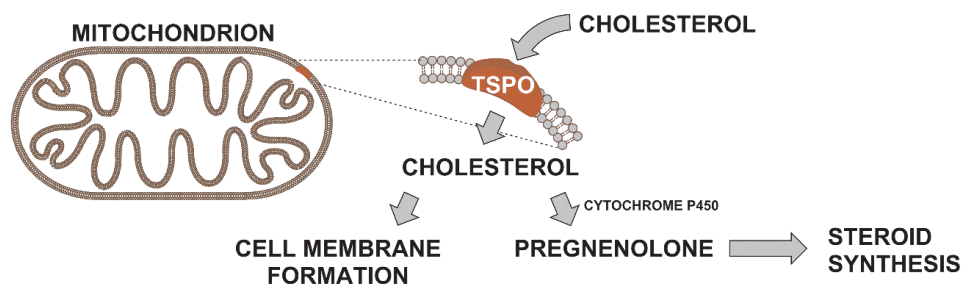


Figure 15: Translocator protein 18 kDa (TSPO) – location and function

Within the mitochondria, cholesterol is converted into pregnenolone by scission of a side chain and the pregnenolone produced can subsequently be further used in the synthesis of various steroids. Alternatively, the cholesterol in mitochondria can

be used in the formation of new mitochondrial membrane when the cells undergo growth or repair (Figure 15).

Increased expression of TSPO has been observed in numerous inflammatory responses. In particular, the brains of individuals that suffer from various neurological conditions, amongst others; stroke, traumatic brain injury, multiple sclerosis and AD, often show an overexpression of TSPO and as a result it has been accepted as a biomarker for neuroinflammation and activation of microglia (Banati 2002).

Microglia are phagocytic cells that are found in the central nervous system (CNS). They account for approximately 10% of the cells in the brain, and under normal conditions they are distributed throughout the brain. In the case of AD and many other neurological conditions, the various associated irregularities and foreign objects cause the microglia to activate and fulfil their main function, to act as the immune defence of the CNS. They phagocytise foreign material as well as plaques and dead or dying cells, to decrease the resulting inflammation.

In AD, neuroinflammation and microglial activation occur primarily in the tissue directly surrounding the amyloid plaques. Hence, rather than imaging the disease pathology directly, using TSPO-specific radioligands provides insight into the extent and progression of the disease by visualising the body's response to the disease pathology.

2.4.1 PET tracers for TSPO

Numerous tracers based on various substructures and labelling methodologies have been used for the PET imaging of TSPO distribution, especially within the brain (Damont et al. 2013). The most commonly used of the first generation TSPO-specific ligands is *N*-butan-2-yl-1-(2-chlorophenyl)-*N*-methyloquinoline-3-carboxamide (PK-11195). It was first developed by Le Fur et al. in 1983 and was shown to potently inhibit binding of other TSPO-ligands of the time (Le Fur et al. 1983a, 1983b). The structure of the ligand lent itself well to the labelling with a [¹¹C]methyl substituent and this was achieved in 1984 by Camsonne et al. (Camsonne et al. 1984) (Figure 16).

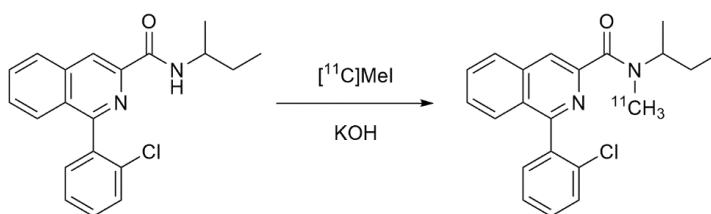
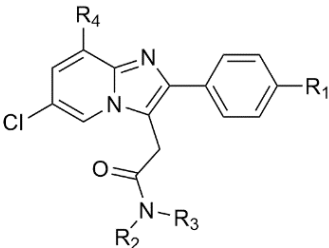
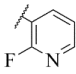


Figure 16: Synthesis of [^{11}C]PK11195

The success of [^{11}C]PK11195 as a TSPO ligand for imaging with PET drove the further development of different motifs that could also be labelled and used to visualise TSPO distribution. These present an extensive list of compounds that have been labelled with either fluorine-18 or carbon-11 for PET or iodine-123 for single-photon emission computer tomography (SPECT). Some of the main motifs that these are based on include; the benzodiazepines ([^{11}C]Ro5-4864 (Coenen et al. 1981)), vinca alkaloids ([^{11}C]Vinpocetine (Gulyás et al. 1999)), dihydro-9H-purinacetamide ([^{11}C]AC-5216 (Zhang et al. 2007) and [^{11}C]DAC (Zhang et al. 2009), indoleacetamides ([^{11}C]SSR180575 (Thominiaux et al. 2010) and [^{18}F]GE-180 (Wadsworth et al. 2012)), the phenoxyarylacetamides; such as [^{18}F]FEDAA1106 and [^{18}F]FMDAA1106 (Zhang et al. 2003), [^{18}F]FEPPA (Wilson et al. 2008), and [^{11}C]PBR28 (Briard et al. 2005, 2008) to name a few, and the imidazopyridines (Table 4) and bioisosteric pyrazolopyrimidines (Table 5).

The lower positron energy, and hence lower positron range, of fluorine-18 compared to that of carbon-11 means that PET images collected with ^{18}F -labelled tracers have superior image quality. This together with the longer half-life of fluorine-18 and the implication this has on the possibility of tracer distribution and the use of one tracer batch for imaging several patients, means that there is much focus devoted to the development of ^{18}F -fluorinated radiotracers (Best et al. 2019, Vivash and O'Brien 2015).

Table 4: Second Generation TSPO-specific PET radiopharmaceuticals based on the imidazopyridine acetamide motif

 <p>Imidazopyridine acetamides</p>	[¹¹ C]CLINME	R ₁ : I, R ₂ : [¹¹ C]Me, R ₃ : Me, R ₄ : Me	K _i = 1.6 nM in rat	(Boutin et al. 2007, Mattner et al. 2015, Thominiaux et al. 2007)
	[¹⁸ F]CB251	R ₁ : [¹⁸ F]OCH ₂ CH ₂ F, R ₂ : Pr, R ₃ : Pr, R ₄ : Cl	K _i = 0.3 nM in rat	(Perrone et al. 2016)
	[¹⁸ F]PBR102	R ₁ : [¹⁸ F]CH ₂ CH ₂ F, R ₂ : Me, R ₃ : Et, R ₄ : H	K _i = 5.8 nM in rat	(Fookes et al. 2008, Katsifis and Fookes 2008)
	[¹⁸ F]PBR111	R ₁ : [¹⁸ F]OCH ₂ CH ₂ F, R ₂ : Et, R ₃ : Et, R ₄ : H	K _i = 3.7 nM in rat	(Fookes et al. 2008, Katsifis and Fookes 2008)
	[¹¹ C]PBR170	R ₁ : OEt, R ₂ : [¹¹ C]Me, R ₃ :  R ₄ : Cl	K _i = 2.4 nM in rat	(Bourdier et al. 2014)

When many of these second generation TSPO-tracers were used for PET imaging or their binding was evaluated by *in vitro* studies, a substantial variability in binding potential between different subjects could be observed (Kreisl et al. 2010, Owen et al. 2010, 2011). It was found that in humans a single nucleotide polymorphism (rs6971) means that subjects can be broadly divided into 3 categories in terms of tracer binding to TSPO (Owen et al. 2012). High-affinity and low-affinity binders, each of which express a single binding site with either high or low affinity, and mixed-affinity binders which express similar numbers of high and low affinity binding sites (Owen et al. 2011). It has been shown that polymorphism sensitive TSPO-tracers such as [^{11}C]PBR28 have the same binding site as the first generation ligand, [^{11}C]PK11195, as demonstrated by their ability to displace one another *in vitro* and *in vivo* (Imaizumi et al. 2008, Kreisl et al. 2010). However, despite this common binding site, [^{11}C]PK11195 does not show such a great sensitivity to the polymorphism (Ikawa et al. 2017). Due to this [^{11}C]PK11195 has not been phased out as TSPO ligand in favour of the newer candidates. On the contrary, development of compounds closely related to [^{11}C]PK11195 structurally, such as [^{11}C]ER176, has been ongoing in recent years (Fujita et al. 2017, Ikawa et al. 2017).

2.4.2 Mouse model of Alzheimer's disease

The APP/PS1-21 mice are transgenic (TG) animals that contain the human transgenes for the amyloid precursor protein (APP) with the KM670/671NL or "Swedish" mutation and for presenilin-1 (PSEN-1) with the L166P mutation.

APP is an integral membrane protein, which, when hydrolysed, forms beta amyloid (A β). The deposition of A β results in the formation of amyloid plaques which is the characteristic pathology associated with AD and plays a central role in neurodegeneration. The Swedish mutation is in fact a double mutation in which 2 amino acids, lysine and methionine, have been replaced by asparagine and leucine and was first discovered in 2 Swedish families that were genealogically linked (Mullan et al. 1992). This double mutation in the APP gene results in an increased production of A β .

The L166P mutation to the PSEN-1 gene was first reported by Moehlmann et al. and is a relatively rare mutation that results in an early onset of AD symptoms (Moehlmann et al. 2002). Presenilin-1 is a core component of the gamma secretase complex which is also an integral membrane protein and has been shown to have a key role in A β regulation, and mice that express mutant Presenelin-1 display increased A β their brains (Duff et al. 1996).

The APP/PS1-21 developed by Radde et al. (Radde et al. 2006) coexpress the amyloid precursor protein Swedish mutation and the very aggressive presenilin-1 mutation under the control of a neuron-specific Thy1 promoter. The resulting cerebral amyloidosis starts at 6 – 8 weeks and there is a threefold increase in the number of neocortical microglia between 1 and 8 months of age.

2.4.3 [^{18}F]F-DPA

All of the pyrazolopyrimidine and related imidazopyridine tracers discussed thus far have a common shortcoming, that is, the relative instability of the labelling position with respect to metabolic cleavage (Peyronneau et al. 2011, 2013). This instability arises from the use of metabolically unstable linker chains for the binding of the labels to the bioactive part of the molecules. The metabolism results in the formation of small radioactively-labelled fragments which add non-specific signal to PET scans and autoradiography images. This limitation has driven the development of new metabolically fortified analogues that are less susceptible to loss of the radiolabel (Banister et al. 2014, Damont et al. 2015a).

N,N-Diethyl-2-(2-(4-fluorophenyl)-5,7-dimethylpyrazolo[1,5-*a*]pyrimidin-3-yl)acetamide (F-DPA) was first synthesised and reported by Selleri et al. (Selleri et al. 2001) as part of a larger study which identified the 2-arylpyrazolo[1,5-*a*]pyrimidin-3-yl acetamides as a potent and selective new class of TSPO (then PBR) specific ligands. In this study, F-DPA was shown to have a binding affinity (K_i TSPO = 9.2 ± 1.0 nM) and selectivity (K_i CBR > 1 μM) similar to those of PK11195 (K_i TSPO = 9.3 ± 0.5 nM, K_i CBR > 1 μM).

Several years later, following the development and successful use of related compounds such as [^{18}F]DPA-714 and [^{11}C]DPA-713, [^{18}F]F-DPA was postulated to be a potential metabolically resistant analogue of [^{18}F]DPA-714 and the synthesis of [^{18}F]F-DPA was reported by Damont et al. (Damont et al. 2015b). The nucleophilic synthesis was achieved using a range of precursors. The leaving groups employed were the fluoride, for $^{19}\text{F}/^{18}\text{F}$ fluoride exchange, nitro, trimethylammonium and hypervalent iodine, in the form of the diaryliodonium salt. However the reactions were found challenging and not sufficiently reliable to merit preclinical evaluation. In parallel to the work described herein, Zischler et al. further explored the possibility of a nucleophilic ^{18}F -fluorination reaction for the synthesis of [^{18}F]F-DPA, this time a boronic ester precursor was employed for a Cu-mediated fluorination reaction (Zischler et al. 2017). This study did not report an A_m for the final product, however two other tracer synthesised by the same approach during the course of the study were obtained in approximately 40 GBq/ μmol . The nucleophilic ^{18}F -fluorination for preclinical evaluation was developed

by Wang et al. wherein a spirocyclic iodonium ylide-precursor was employed (Wang et al. 2017) (Figure 17). This synthetic approach yielded the final product with an A_m of 96 ± 22 GBq/ μ mol, sufficient to perform *in vivo* preclinical evaluation. The [18 F]F-DPA made by this approach was evaluated in a rat model of ischemic stroke and in a mouse model of AD (APP/PS1). This study demonstrated that [18 F]F-DPA can be used for the imaging of neuroinflammation in both of the models employed. The binding affinity (K_i : 2.0 ± 0.8 nM) was found to be consistent with prior reports and a blocking with PK11195 indicated a high *in vivo* specificity.

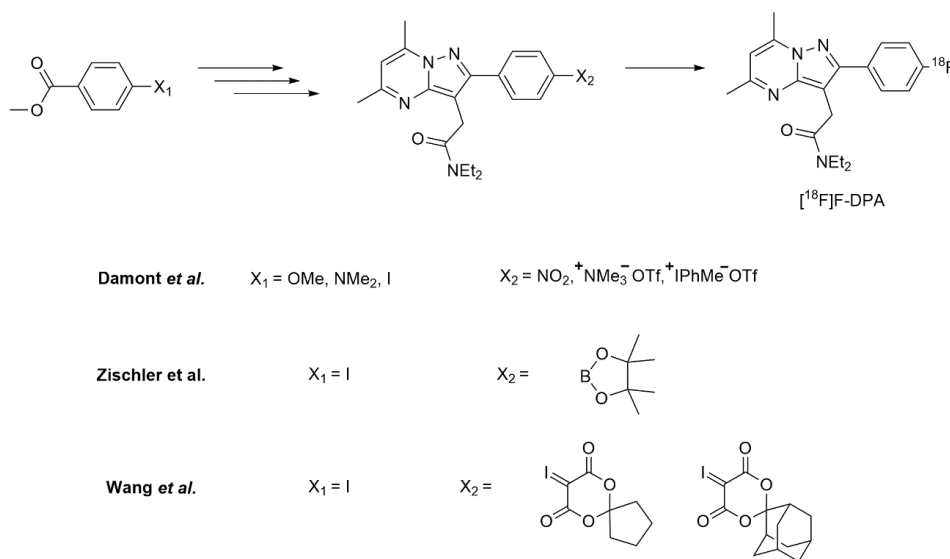


Figure 17 : Syntheses of [18 F]F-DPA from various precursors

3 AIMS OF THE STUDY

The aims of this work were to study various new ^{18}F -fluorination methodologies and to apply these to the synthesis of $[\text{}^{18}\text{F}]\text{F-DPA}$, a novel tracer for TSPO.

The specific aims for each study were:

- Study I To develop a synthesis of $[\text{}^{18}\text{F}]\text{F-DPA}$.
- To investigate whether the new tracer candidate penetrates the blood brain barrier.
- To compare the *in vivo* metabolism with that of $[\text{}^{18}\text{F}]\text{DPA-714}$ in healthy rats.
- Study II To evaluate the efficacy of $[\text{}^{18}\text{F}]\text{F-DPA}$ for visualising neuroinflammation in the transgenic APP/PS1-21 mouse model of Alzheimer's disease.
- To observe the $[\text{}^{18}\text{F}]\text{F-DPA}$ uptake in the Alzheimer's disease model at different ages.
- Study III To explore alternative syntheses for the production of $[\text{}^{18}\text{F}]\text{F-DPA}$, via nucleophilic routes, with the intention of increasing A_m
- To compare the effect that differing A_m 's have on *in vivo* and *ex vivo* imaging of transgenic APP/PS1-21 mice.
- To assess the usefulness of different labelling methodologies for the synthesis of TSPO tracers.
- Study IV To explore an alternative route for the post-target production of $[\text{}^{18}\text{F}]\text{F}_2$, by employing a VUV-laser to promote the isotopic exchange reaction.
- To use the resulting $[\text{}^{18}\text{F}]\text{F}_2$ for the synthesis of $[\text{}^{18}\text{F}]\text{F-DPA}$ via $[\text{}^{18}\text{F}]\text{Selectfluor bis(triflate)}$.

4 MATERIALS AND METHODS

4.1 Production of ^{18}F -fluorination reagents

4.1.1 Production and drying of $[^{18}\text{F}]\text{fluoride}$ (I – IV)

Aqueous $[^{18}\text{F}]\text{fluoride}$ was produced from ^{18}O -enriched water via the $^{18}\text{O}(\text{p},\text{n})^{18}\text{F}$ nuclear reaction. The 17 MeV proton beam was generated by either a CC-18/9 cyclotron (Efremov Scientific Institute of Electrophysical Apparatus, St. Petersburg, Russia) or an MGC-20 cyclotron (Efremov Scientific Institute of Electrophysical Apparatus, Leningrad, USSR) (Table 6).

Table 6: Details of cyclotrons used for the production of $[^{18}\text{F}]\text{fluoride}$

Study	Cyclotron	Target Details	Pre-reaction procedures
I – IV	MGC-20	0.8 mL silver target	None, target contents directly transported to the reaction vessel
II & III	CC-18/9	2.3 mL niobium target	Target contents passed over anion exchange cartridge, eluted aqueous K_{222} and K_2CO_3

The $\text{K}_{222}/\text{K}^+[^{18}\text{F}]\text{F}^-$ complex was formed by drying the cyclotron-produced aqueous $[^{18}\text{F}]\text{fluoride}$ with MeCN at 100 °C under a flow of helium in the presence of K_{222} and a source of potassium (K_2CO_3 or a 9:1 mixture of $\text{K}_2\text{CO}_3/\text{K}_2\text{C}_2\text{O}_4$). Two subsequent additions of MeCN were made, each followed by evaporation of the solvent. In the case of Cu-mediated reactions, to ensure sufficiently high dryness, a more thorough drying procedure was employed. The azeotropic distillations were carried out with an elevated temperature (120 °C) and for a longer time (8 min each) under a flow of He (Figure 18).

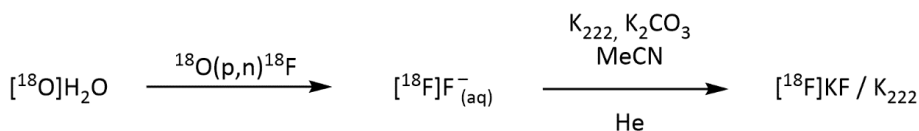


Figure 18: Cyclotron production of fluorine-18 via the (p,n) reaction on an oxygen-18 enriched water target, followed by azeotropic distillation and drying

4.1.2 High voltage discharge-promoted production of [^{18}F] F_2 and subsequent synthesis of [^{18}F]Selectfluor bis(triflate) (I – III)

[^{18}F] F_2 gas was synthesised according to the procedure previously described by Bergman and Solin (Bergman and Solin 1997) (Figure 3). Initially [^{18}F]MeF was synthesised from the dry $\text{K}_{222}/\text{K}^+[\text{F}^-]$ complex by the addition of MeI (1.5 mmol) in MeCN heating of reaction mixture under reflux for 1 min. The [^{18}F]MeF produced was purified by gas chromatography and trapped in a stainless-steel loop submerged in liquid nitrogen.

After trapping, the stainless steel loop was allowed to warm up to room temperature and the [^{18}F]MeF was mixed with carrier F_2 gas, approximately 1 μmol in Ne (0.5% F_2/Ne), in a quartz discharge chamber (Table 7, Figure 19 Chamber A). The $^{19}\text{F}/^{18}\text{F}$ isotopic exchange reaction was promoted by applying a high-voltage electrical discharge (30.5 ± 1.0 kV, 10 s) through the gas mixture.

[^{18}F]Selectfluor bis(triflate) was synthesised from [^{18}F] F_2 following the procedure previously reported by Teare et al. (Figure 14) (Teare et al. 2010). [^{18}F] F_2 , produced by high voltage-promoted isotope exchange, was bubbled through a solution of 1-chloromethyl-4-aza-1-azoniabicyclo[2.2.2]octane triflate and LiOTf in acetone- d_6 . No purification was necessary and the resulting [^{18}F]Selectfluor bis(triflate) could be used “as is” for further electrophilic ^{18}F -labelling, alternatively, the crude solution of [^{18}F]Selectfluor bis(triflate) in acetone- d_6 could be stored as a stock ^{18}F -labelling reagent solution for later experiments.

4.1.3 Vacuum ultraviolet photon-promoted production of [^{18}F] F_2 (IV)

Various chambers and reflective coatings were tested for the illumination-promoted isotopic exchange reaction and these are described in Table 7.

Table 7: Dimensions of the discharge chamber (A) and various illumination chambers (B-E)

Chamber	Volume (cm^3)	Coating(s) tested
A	1.7	none
B	10.3	TiO_2
C	9.8	Al
D		TiO_2
E	4.1	Al

After the trapped [^{18}F]MeF had warmed up to room temperature and expanded into the illumination chamber (Table 7, Figure 19, Chambers B - E), the carrier F_2 (0.1

– 1.7 μmol) in Ne was added to the reaction chamber. The $^{19}\text{F}/^{18}\text{F}$ isotopic exchange reaction was promoted by illumination with 193 nm VUV photons from the laser.

The aluminium coating of chambers C and E was achieved using a vacuum evaporator while the TiO_2 of the end of chamber B and the entire chamber D was applied in the form of TiO_2 -containing reflective paint.

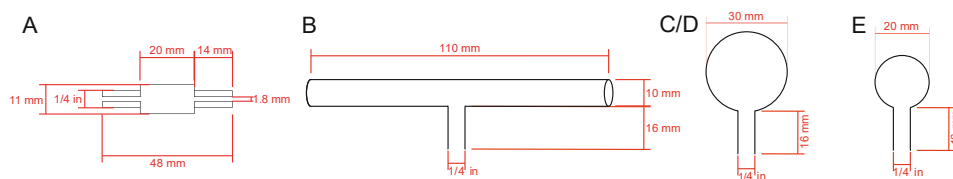


Figure 19: Discharge chamber (A) and Illumination chamber (B-E) designs and dimensions

For the evaluation of the VUV-photon-promoted production of $[^{18}\text{F}]\text{F}_2$, $[^{18}\text{F}]\text{NFSi}$ was selected as a model molecule to assess the electrophilic ^{18}F -fluorination ability of the resulting gas mixture (Figure 20). $[^{18}\text{F}]\text{NFSi}$ was chosen primarily due to the simplicity of the radio-HPLC analysis (Figure 21) and labelling reaction.

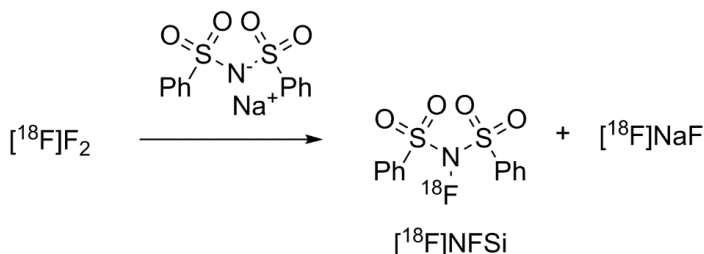


Figure 20: Synthesis of $[^{18}\text{F}]\text{NFSi}$

The gas mixture produced by VUV-photon illumination of the $[^{18}\text{F}]\text{MeF}/\text{F}_2/\text{Ne}$ gas mixture was bubbled through a solution of NFSi precursor in a 9:1 solution of MeCN and H_2O (total volume 1 mL). The resulting crude solution of $[^{18}\text{F}]\text{NFSi}$ was analysed by radio-HPLC (Table 8 Entry 6). The non-isolated radiochemical yields and A_m 's were calculated based on the radio-HPLC analyses of the crude reaction products. The A_m 's were decay corrected to the EOS.

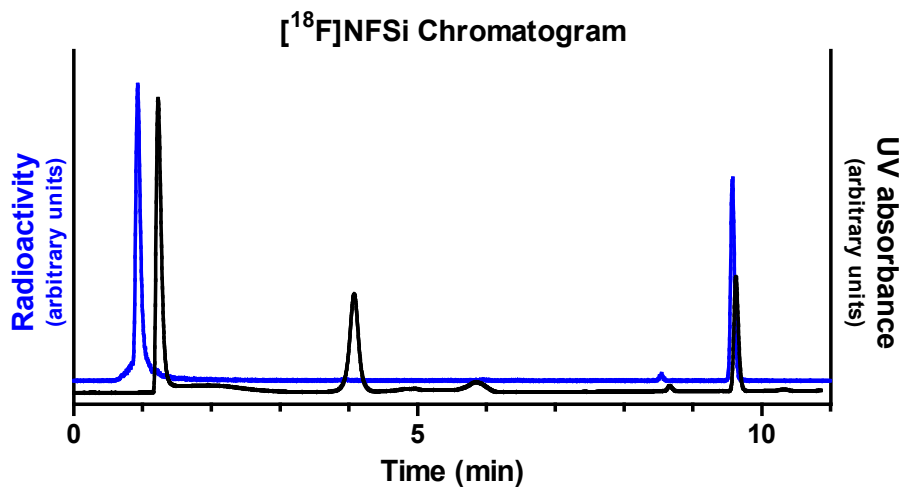


Figure 21: An example analytical chromatogram obtained for [¹⁸F]NFSi produced from VUV-illumination generated [¹⁸F]F₂. The [¹⁸F]NFSi product has an elution time of 9.6 min, the UV active compound with a retention time of 4.1 min corresponds to the unreacted NFSi precursor.

4.2 HPLC analytical and preparative systems

Three different HPLC-columns were employed during Studies I – IV. The details of the employed eluents and retention times are described in Table 8.

Table 8: Details of radioHPLC systems used in the Studies I-IV

Entry	Study	Use	Column	Eluents	Eluent System	Flow (mL/min)	Product	Product elution time (min)
1	I – III	Preparative	Waters X-Terra Prep RP18 (10 μ m, 7.8 x 300 mm)	A: 0.1M AcONH ₄ B: MeCN	65% A 35% B	4	[¹⁸ F]DPA-714	20 - 22
							[¹⁸ F]F-DPA	22 - 23
2	III	III	Waters X-Terra Prep RP18 (7 μ m, 7.8 x 300 mm)	A: 0.1M AcONH ₄ (pH 8.5) B: MeCN	0 - 5 min: 100% A 5 - 55 min: 0 - 22% B 55 min on: 22% B	6	[¹⁸ F]F-DPA _N	115
3	I	Analytical	Merck Chromolith Performance RP-18e (10 μ m, 4.6 x 100 mm)	A: 0.1% HCOOH acid B: MeCN	70% A 30% B	4	Various	Various
4	I – III			A: 0.025M NaH ₂ PO ₄ (pH 3.5) B: MeCN	70% A 30% B	4	[¹⁸ F]DPA-714	4.3
							[¹⁸ F]F-DPA	5.6
5	III				0 - 5 min: 100% A 5 - 55 min: 0 - 22% B 55 min on: 22% B	2	[¹⁸ F]F-DPA _N	64.2
6	IV	IV	Waters Atlantis dC18, (5 μ m, 3.9 \times 150 mm)	A: H ₂ O B: MeCN	0 - 10 min 5 - 20% B	1.5	[¹⁸ F]NFSi	9.6

4.3 Synthesis of [^{18}F]DPA-714 using the nucleophilic ^{18}F -fluorination device (I)

The device employed for the nucleophilic ^{18}F -fluorination reactions is an in-house constructed device, a technical representation of this device is showed in Figure 22.

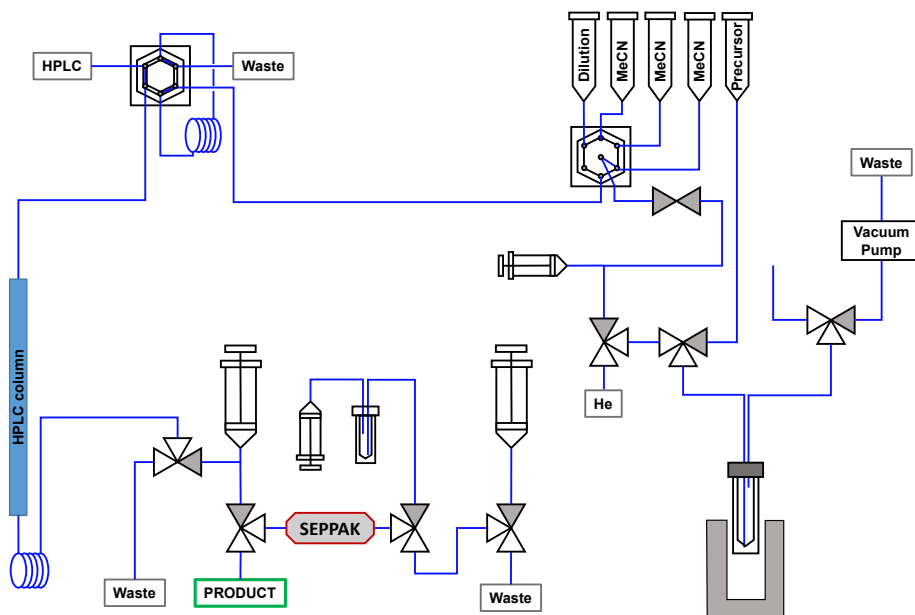


Figure 22: Technical diagram of device used for nucleophilic ^{18}F -fluorination reactions.

Following the formation of the dry $\text{K}_{222}/\text{K}^+[\text{}^{18}\text{F}]\text{F}^-$ complex, the synthesis of [^{18}F]DPA-714 was carried out as previously described in literature (Figure 5) (James et al. 2008), however a longer, 10 min, reaction time was employed. After preparative radioHPLC, (Table 8 Entry 1) the product-containing fraction was collected, concentrated and formulated for injection. This was implemented using a Waters Sep-Pak Light tC18 cartridge to trap radioligand. After washing with water, the [^{18}F]DPA-714 was eluted with ethanol and diluted with saline. The resulting 10% ethanolic solution was suitable for intravenous injection, the final product was analysed by radioHPLC (Table 8 Entry 4).

4.4 Synthesis of F-DPA precursors (I, II, III and unpublished)

The precursors for the syntheses of [^{18}F]F-DPA were synthesised from *para*-iodobenzaldehyde according to previously described procedures (Damont et al. 2015a), which were used to arrive at I-DPA, the iodinated analogue (Figure 17). Subsequently, the two different precursors; 2-(5,7-dimethyl-2-(4-

(tributylstannyl)phenyl)pyrazolo[1,5-*a*]pyrimidin-3-yl)-*N,N*-diethylacetamide (Figure 23, Compound **1**) and 2-(5,7-dimethyl-2-(4-(4,4,5,5-tetramethyl-1,3,2-dioxaborolan-2-yl)phenyl)pyrazolo[1,5-*a*]pyrimidin-3-yl)-*N,N*-diethylacetamide (Figure 23, Compound **2**) were produced from this by applying and modifying previously reported reactions (Landge et al. 2012, Skaff et al. 2005) the conditions of which are outlined in Figure 23.

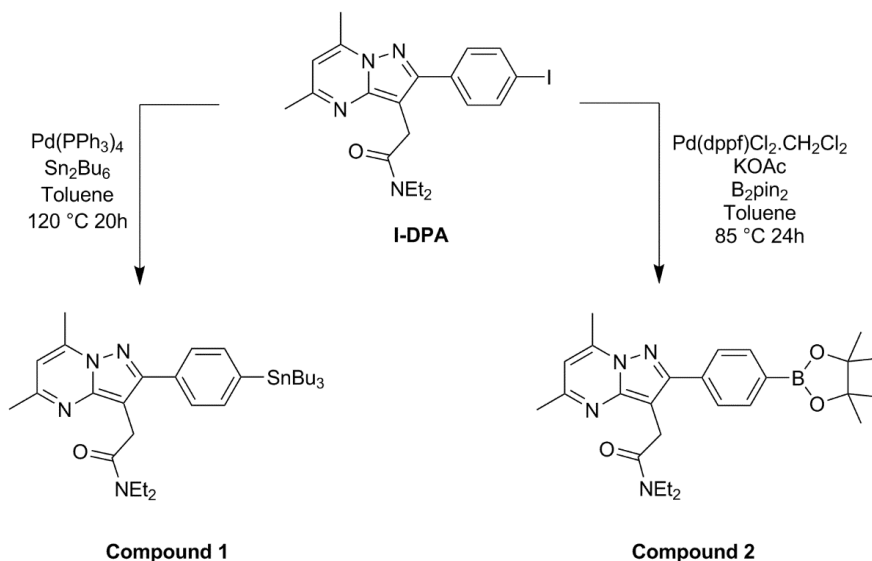


Figure 23: Synthesis of [^{18}F]F-DPA labelling precursors from I-DPA

4.5 Electrophilic syntheses of [^{18}F]F-DPA (I, II, III and unpublished)

4.5.1 Electrophilic ^{18}F -Fluorination of Compound 1 (I – III & unpublished)

The synthesis of [^{18}F]F-DPA was initially attempted using discharge-produced [^{18}F]F $_2$. For this, the [^{18}F]F $_2$ was bubbled through a solution of the Compound **1** in freon-11 or acetone- d_6 containing AgOTf as an additive.

The products of these reaction were analysed using the same analytical HPLC system described for [^{18}F]DPA-714, where the non-radioactive F-DPA was found to have a retention time of 5.6 min (Table 8 Entry 4). Following an unsuccessful identification of even traces of the desired [^{18}F]F-DPA product, a second analytical HPLC method was developed to enable mass spectroscopy to be carried out on the collected fractions (Table 8 Entry 3).

After the unsuccessful initial attempts to synthesise [^{18}F]F-DPA from Compound **1** using [^{18}F]F $_2$, [^{18}F]Selectfluor *bis*(triflate) was selected as an alternative, milder,

electrophilic ^{18}F -fluorination reagent (Figure 24). Initially, to test this hypothesis, reactions were carried out with 1 equivalent of Compound **1** and AgOTf (2 equivalents) that were added to 200 μL of a stock solution of ^{18}F Selectfluor *bis*(triflate) in acetone- d_6 (total radioactivity: approx. 500 MBq). The reaction mixture was stirred at 45 $^{\circ}\text{C}$ and samples were taken for radio-HPLC analysis after 15 and 60 min.

The effect of a higher concentration of reactants in the reaction mixture was also investigated. For this, following the addition of the ^{18}F Selectfluor *bis*(triflate), half of the acetone was evaporated at room temperature under a flow of helium. These reactions were sampled at 15 and 30 min. Radio-HPLC analysis of the crude reaction product was carried out to determine the non-isolated radiochemical yield.

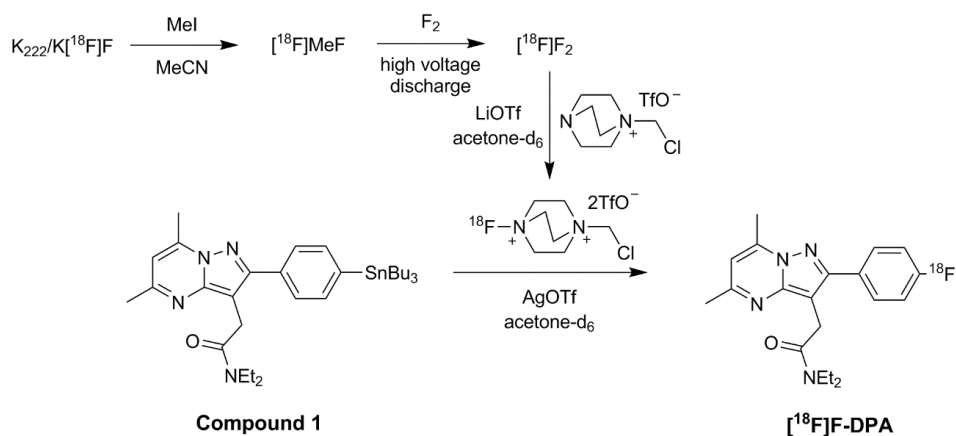


Figure 24: Synthesis of ^{18}F F-DPA using ^{18}F Selectfluor *bis*(triflate)

After the initial test reactions, the final conditions chosen for the synthesis of ^{18}F F-DPA for preclinical evaluation were: 1 eq. F-DPA precursor (Compound **1**), 2 eq. AgOTf, a double concentration of reagents and a reaction time of 15 min. The entire crude stock of the ^{18}F Selectfluor *bis*(triflate) was used in these reactions for the production of ^{18}F F-DPA. Following HPLC purification (Table 8 Entry 1), the same formulation procedure described for ^{18}F DPA-714 was employed for the formulation of ^{18}F F-DPA for injection. For the large scale reactions for preclinical evaluation, radiochemical yields were calculated from the total radioactivity of the final product (decay corrected to EOB) expressed as a percentage of the ^{18}F Selectfluor radioactivity (also decay corrected to EOB). A_m 's were calculated from the radioactivity measured for the product fraction collected from the analytical radio-HPLC of the crude product, decay corrected to EOB.

Post-target VUV-illumination-produced $[^{18}\text{F}]\text{F}_2$ was also used to synthesise $[^{18}\text{F}]\text{Selectfluor bis(triflate)}$ and subsequently $[^{18}\text{F}]\text{F-DPA}$. These reactions employed F_2 (1.7 μmol) for the isotope exchange reaction. The $[^{18}\text{F}]\text{F-DPA}$ labelling reaction was carried out using the optimised conditions described above.

4.5.2 Electrophilic ^{18}F -Fluorination of Compound 2 using $[^{18}\text{F}]\text{Selectfluor bis(triflate)}$ (Unpublished)

Fluorination of Compound 2 (Figure 25) was achieved by following the previously described procedure (Stenhagen et al. 2013). Compound 2 was initially premixed with NaOH in MeOH by stirring the mixture at room temperature for 3 h. After the mixture had been cooled to 0 °C, AgOTf was added and the mixture was stirred at 0 °C for a further 30 min.

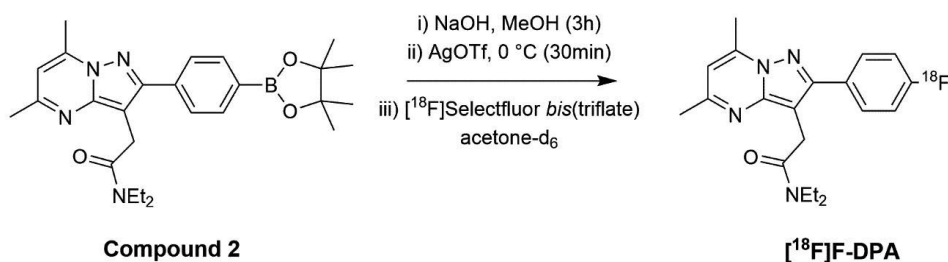


Figure 25: Synthesis of $[^{18}\text{F}]\text{F-DPA}$ from Compound 2 using $[^{18}\text{F}]\text{Selectfluor bis(triflate)}$

The radiolabelling itself was achieved by adding $[^{18}\text{F}]\text{Selectfluor bis(triflate)}$ to the premixed reaction mixture and further stirring the resulting solution for 10 min at room temperature. The crude reaction mixture was analysed by radio-HPLC (Table 8 Entry 4) and non-isolated radiochemical yield and A_m were determined. For A_m calculations the activity was decay corrected to the EOB.

4.6 Nucleophilic syntheses of $[^{18}\text{F}]\text{F-DPA}$ (III)

4.6.1 Copper-mediated ^{18}F -Fluorination of Compound 1 (III)

In the case of Compound 1, the drying procedure was performed with only K_2CO_3 as the potassium source (Figure 26). Upon cooling, the $\text{Cu}(\text{OTf})_2(\text{pyr})_4$ (2.8 eq) in MeCN was added to the $\text{K}_{222}/\text{K}[^{18}\text{F}]\text{F}$ complex and the resulting mixture was stirred at room temperature. After 10 min the solvent was evaporated and the labelling precursor (Compound 1) in DMA was added and the resulting reaction mixture heated under reflux for 10 min.

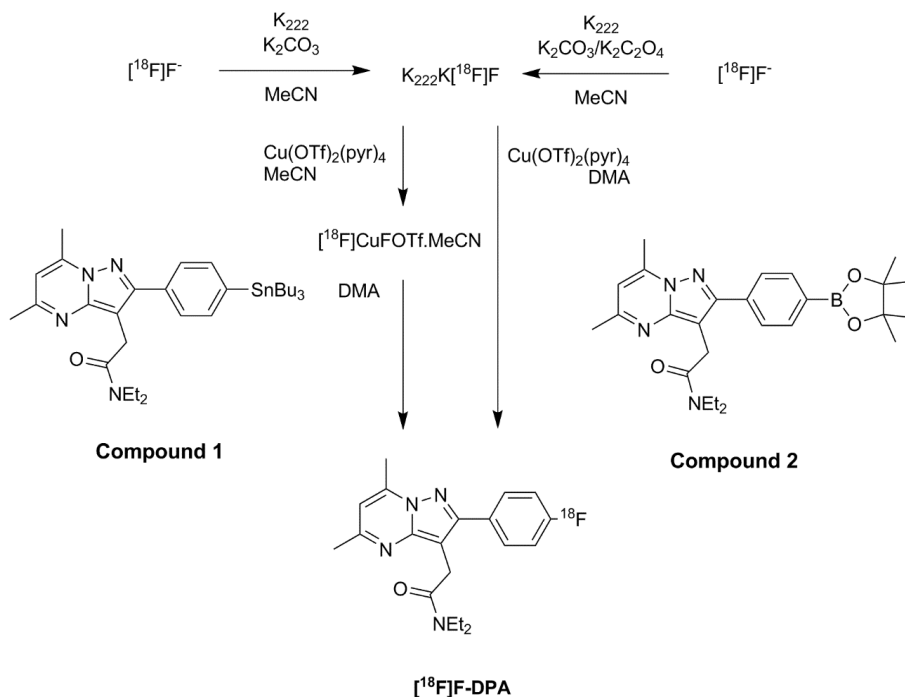


Figure 26: Nucleophilic Syntheses of $[^{18}\text{F}]\text{F-DPA}$ from Compounds 1 and 2

4.6.2 Copper-mediated ^{18}F -Fluorination of Compound 2 (Unpublished)

For the ^{18}F -fluorination of Compound 2, the procedure for the drying of the $[^{18}\text{F}]\text{fluoride}$ was carried out employing the 9:1 mixture of $\text{K}_2\text{CO}_3/\text{K}_2\text{C}_2\text{O}_4$ as the potassium source (Figure 26). Upon drying, Compound 2 and $\text{Cu}(\text{OTf})_2(\text{pyr})_4$ (1.2 eq) in DMA were added to the $\text{K}_{222}/\text{K}[^{18}\text{F}]\text{F}$ complex and the reaction was heated under reflux for 10 min.

4.6.3 HPLC purification, analysis and formulation for injection

The same procedure was employed for the purification of the products from either reaction (Table 8 Entry 2). Following the reaction, the solvent was evaporated to reduce the volume of the crude mixture by half, the remaining reaction mixture was diluted with the 1.5 mL of the aqueous phase of the preparative HPLC system (0.1 M aq. AcONH_4 pH 8.5) and injected onto the HPLC column for purification.

The product-containing fraction was collected and diluted with water and the radioligand was trapped on a Waters Sep-Pak Light tC18 cartridge. After the cartridge was washed with water, the $[^{18}\text{F}]\text{F-DPA}$ was eluted using ethanol which was then diluted with 0.1 M phosphate buffer, giving a 10% ethanolic solution that

was suitable for intravenous injection. The final product was analysed by radio-HPLC (Table 8 Entry 5) to determine non-isolated radiochemical yield, radiochemical purity and A_m (decay corrected to EOB).

4.7 Preclinical evaluations of [^{18}F]F-DPA and comparison with [^{18}F]DPA-714

The experimental animals used for the preclinical work in Studies I – III are outlined in Table 9. The ethical permissions for each study are outlined in the studies themselves (Studies I – III).

Table 9: A summary of the animals used in Studies I – III. SD = Sprague Dawley, TG = transgenic mouse model of Alzheimer's disease, APP/PS1-21, WT = wildtype,

Study	Species	Strain/ Genotype	n	Gender	Weight (g)	Age (months)
I	Rats	SD	36	m	290 ± 30	2
II	Mice	TG	31	16 f, 15 m	29.5 ± 5.7	4.5 – 19
		WT	19	9 f, 10 m	29.0 ± 6.8	4.5 – 24
III	Mice	TG	3	1 f, 2 m	26.5 ± 3.1	9
		WT	3	2 f, 1 m	38.1 ± 1.7	

Initially [^{18}F]F-DPA was evaluated in healthy Sprague Dawley rats, to determine its metabolic profile *in vivo* and blood-brain barrier penetration (Study I). Subsequently, this led to Studies II and III where the [^{18}F]F-DPA was evaluated in a transgenic (TG) APP/PS1-21 mouse model of AD. APP/PS1-21 mice were originally purchased from Koesler (Rottenburg, Germany) and further bred with C57BL/6Cn mice in the Central Animal Laboratory of University of Turku. Wildtype (WT) mice from the same litter were used as control animals.

4.7.1 *In vivo* PET imaging and tracer kinetics

In vivo PET imaging for Studies I – III was carried out on the animals described in Table 9. After being anaesthetised with 2.5% isoflurane/oxygen gas, the animals underwent a 10-minute computed tomography (CT) scan for attenuation correction and anatomical reference. Following this, a 60 min dynamic PET scan was started and the radiotracer was administered intravenously. The scanning was carried out using an Inveon Multimodality PET/CT tomograph (Siemens Medical Solutions, Knoxville, TN, USA).

Table 10: Summary of details of *in vivo* imaging from Studies I–III. Molar activity (A_m) is given for the time of injection. Volumes of interest (VOIs) were: WB (whole brain), FC (frontal cortex), CTX (neocortex), HIPP (hippocampus), cerebellar cortex (CB), parietotemporal cortex (PTC), STR (striatum), THA (thalamus) and HYP (hypothalamus)

Study	Route of Tracer production	Injected activity (MBq)	Injected mass ($\mu\text{g/kg}$)	A_m (GBq/ μmol)	VOIs
I	Electrophilic	31.4 ± 2.1	10 ± 2	4.1 ± 0.4	WB, heart, lungs, liver, kidneys
II	Electrophilic	6.9 ± 0.6	50 ± 30	2.4 ± 1.2	WB, FC, CTX, HIPP, CB
III	Electrophilic	6.8 ± 0.1	38 ± 15	2.3 ± 1.0	PTC, HIPP, WB
	Nucleophilic	7.0 ± 0.2	0.34 ± 0.13	260 ± 110	

The PET scan took 51 frames at the following intervals: 30 x 10 s, 15 x 60 s, 4 x 300 s and 2 x 600 s. For the image analysis, the dynamic PET images were first co-registered with corresponding CT image and subsequently the PET/CT images were aligned with an averaged mouse MRI template. Volumes of interest (VOIs) were drawn over the regions specified in Table 10. Time–activity curves (TACs) and standardised uptake values (SUVs) were obtained from the VOIs. SUVs were calculated from the concentration of radioactivity signal in a certain tissue, expressed as a percentage of the total injected dose per gram of tissue, by dividing by the total body weight of the imaging subject.

4.7.2 *Ex vivo brain autoradiography (II & III)*

Since Studies II and III involved the use of animal models of AD disease, the radioactivity accumulation in the brain was studied *ex vivo* as well as *in vivo*. After the *in vivo* studies the mice were sacrificed by cardiac puncture. For Study III this was carried out after imaging with the high A_m [^{18}F]F-DPA. After the animal was dissected, the whole brain (WB) was weighed and the radioactivity was measured, the brain was then frozen and sliced using a cryomicrotome. The brain slices, mounted on glass slides, were exposed onto an imaging plate for around 4 hours.

The exposed imaging plates were scanned using Fuji BAS-5000 reader and the resulting images were analysed. Regions-of-interest (ROIs) were drawn in the frontal cortex (FC), hippocampus (HIPP), cerebellar cortex (CB), lateral ventricle

(LV) and hypothalamus (HYP) (Study II) and FC, parietotemporal cortex (PTC), striatum (STR), HIPp, thalamus (THL) and HYP (Study III). The data was presented as region-of-interest to hypothalamus ratios.

4.7.3 *Ex vivo biodistribution (I & II)*

Biodistribution studies were carried out with [^{18}F]DPA-714 (Study I) and [^{18}F]F-DPA (Studies I and II). The animals were injected with tracer and sacrificed at different time-points (described in Table 11). In the case of the Study II 60-minute animals, $n > 3$ since these were some of the animals that had been used for *in vivo* PET studies. The sacrificed animals were dissected, the tissues collected were weighed and the radioactivity was measured and reported as the percentage of injected dose per gram of tissue (%ID/g).

Table 11: Summary of tracers, injected doses (IDs), time points and n's for the biodistribution studies of Studies I and II

Study	Tracer	ID (MBq)	Time points (min)	n per time point
I	[^{18}F]DPA-714	29.0 ± 2.1	5, 15, 30, 60, 90	3
	[^{18}F]F-DPA	30.7 ± 1.5		
II	[^{18}F]F-DPA	6.8 ± 0.6	5, 15, 30, 60	3 (5, 15, 30 min) 19 (60 min)

4.7.4 *Specificity (II)*

To demonstrate the specificity of [^{18}F]F-DPA for the TSPO, a blocking study was performed. This entailed pre-treating three 15 month-old transgenic APP/PS1-21 mice with PK11195 (1 mg), a competitively binding TSPO ligand, 30 minutes before the tracer injection (Hardwick et al. 2005). These animals were scanned *in vivo* and *ex vivo* brain autoradiography was carried out. The data was compared with that of 15-month-old TG animals that had not been pre-treated.

4.7.5 *Radio-TLC analysis (I – III)*

To assess the stabilities of the tracers with respect to *in vivo* metabolism, the amount of the unchanged tracer and its radioactive metabolites from plasma and brain homogenate were analysed by radio-TLC. These samples were taken from the animals used for the *ex vivo* biodistribution studies and hence have the same time-points. The deproteinised samples were spotted onto a silica gel 60 TLC plate

and developed with DCM and MeOH (9:1 v/v). After this the plates were dried and exposed onto an imaging plate for approximately 4 hours. Following the exposure, the imaging plates were scanned and the digital images were analysed to generate radiochromatograms (Figure 27).

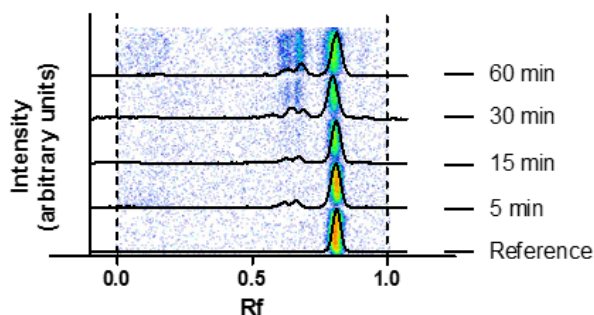


Figure 27: Example of radio-TLC analysis of mouse plasma with overlaid derived radiochromatograms

4.7.6 Immunohistochemical staining (II)

Immunohistochemical staining was performed using the ionised calcium binding adaptor molecule 1 (Iba1) to visualise the Iba1-immunoreactive microglia, this was carried out as described previously by Takkinen et al. (Takkinen et al. 2017).

4.8 Statistical methods (I – IV)

Statistical tests were performed on the data collected to determine the statistical significance of the differences between various groups. For Studies I and III, a two-tailed unpaired t-test was used to test the difference between the *ex vivo* blood activities for the two radiotracers (Study I), between SUVs and ratios calculated from autoradiographs of TG and WT animals when they were imaged with either high or low A_m [^{18}F]F-DPA.

Study II involved more detailed statistical analyses of the data. For this study, the ANOVA model was used to test the differences between TG and WT animals regarding the uptake of tracer in various brain regions, measured both *in vivo* and *ex vivo*, at different ages.

In Study IV the significance of differences between non-isolated radiochemical yields as well as A_m 's achieved with the different conditions was tested using the unpaired t-test.

In all the studies, differences were considered to be statistically significant when the p value was less than 0.05.

5 RESULTS

5.1 Electrophilic Syntheses of [^{18}F]F-DPA (I – III and unpublished)

The initial direct fluorination reactions attempted employing [^{18}F]F₂ and the stannylated precursor (Compound **1**) did not result in the synthesis of the desired [^{18}F]F-DPA product. Analysis of the crude reaction mixture revealed that radio-fluorination did indeed occur. However, the radiofluorinated products eluted at approximately the same time as the unreacted precursor. These fractions were analysed by mass spectroscopy (MS) revealing the presence of mono, di, tri, tetra and even penta-fluorinated species (Figure 28).

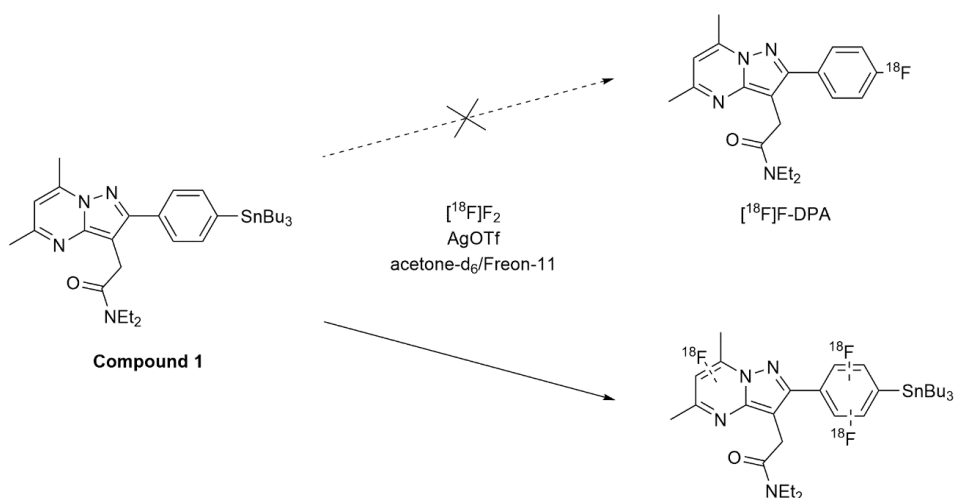


Figure 28: Attempted syntheses of [^{18}F]F-DPA from Compound **1**

Following the initial attempts to synthesise [^{18}F]F-DPA, the reaction was attempted using [^{18}F]Selectfluor *bis*(triflate) as the electrophilic source of fluorine-18. This approach yielded the desired [^{18}F]F-DPA. Optimisation of this reaction was carried out on a small scale, the different parameters studied were reaction volume and reaction time.

The optimised reaction conditions which were subsequently used for the synthesis of [^{18}F]F-DPA from Compound **1** for preclinical evaluation were; a 15-minute reaction time and a reaction volume of 100 μL . An analytical radio-HPLC chromatogram of the crude reaction mixture is presented in Figure 29.

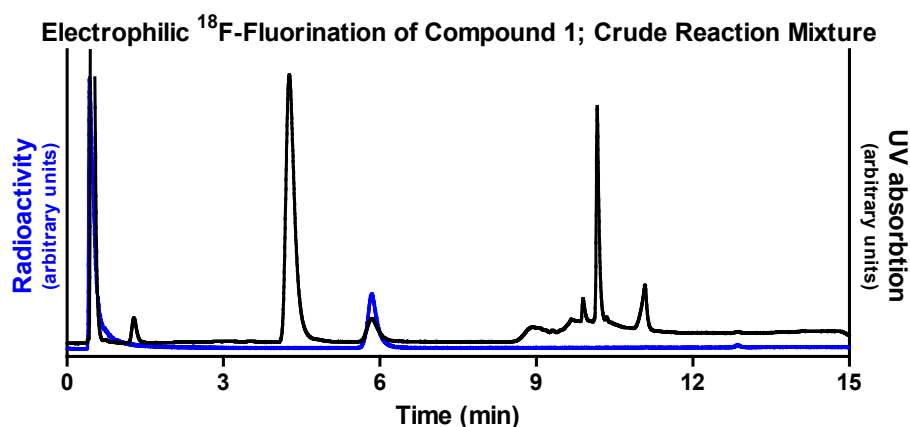


Figure 29: Example analytical radio-HPLC chromatogram of the crude product of the electrophilic ^{18}F -fluorination reaction carried out using the stannyl precursor (Compound 1). The $[^{18}\text{F}]\text{F-DPA}$ product has a retention time of 5.8 min. The UV active compound eluting at 4.2 min corresponds to the protonated analogue

The optimised reaction conditions which were subsequently used for the synthesis of $[^{18}\text{F}]\text{F-DPA}$ from Compound 1 for preclinical evaluation were; a 15-minute reaction time and a reaction volume of 100 μL . An analytical radio-HPLC chromatogram of the crude reaction mixture is presented in Figure 29.

Table 12: Summary of $[^{18}\text{F}]\text{F-DPA}$ syntheses for preclinical studies in Studies I – III. Radiochemical yield was calculated from the radioactivity of the product expressed as a percentage of the total radioactivity of $[^{18}\text{F}]\text{Selectfluor bis(triflate)}$ with both values being decay corrected to EOB. The A_m 's are decay corrected to the end of bombardment.

Study	$[^{18}\text{F}]\text{Selectfluor bis(triflate)}$ activity (GBq)	Radiochemical yield (%)	A_m (GBq/ μmol)	Radiochemical purity (%)
I	7.5 ± 0.8	15 ± 3	7.8 ± 0.5	> 99
II	7.5 ± 2.3	15 ± 3	7.5 ± 2.3	> 99
III	9.1 ± 2.0	16 ± 4	9.0 ± 2.9	> 99

The reaction conditions optimised in Study I were employed for the subsequent studies and the results from the electrophilic syntheses for the animal experiments are summarised by study in Table 12.

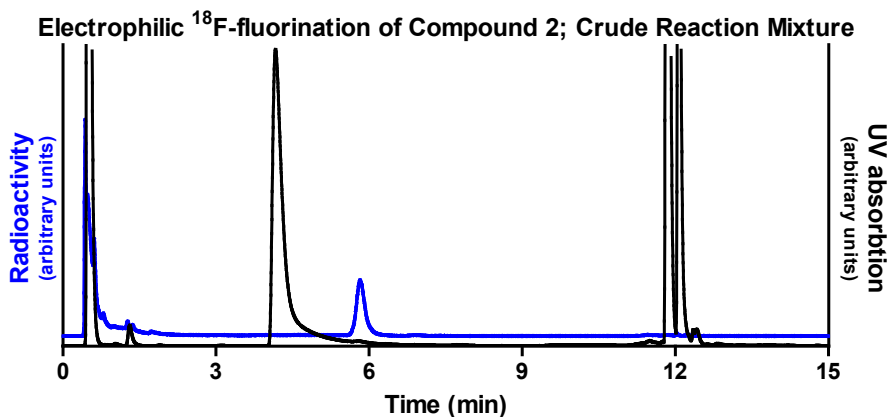


Figure 30: Example analytical radio-HPLC chromatogram of the crude product of the electrophilic ^{18}F -fluorination reaction carried out using the boronic ester precursor (Compound 2). The $[\text{}^{18}\text{F}]\text{F-DPA}$ product has a retention time of 5.8 min. The UV active compound eluting at 4.2 min corresponds to the protonated analogue.

The electrophilic ^{18}F -fluorination of Compound 2 (results unpublished) was carried out following a previously described procedure for the labelling of the boronic ester precursors (Stenhagen et al. 2013). The $[\text{}^{18}\text{F}]\text{F-DPA}$ product was obtained in $12.5 \pm 4.6\%$ non-isolated radiochemical yield, determined from analytical radio-HPLC (Figure 30), with an A_m of $10.4 \pm 3.1 \text{ GBq}/\mu\text{mol}$ (decay corrected to EOB). This yield and A_m obtained are on par with those of the electrophilic ^{18}F -fluorination reactions of Compound 1 (Study III, Table 12).

5.2 Synthesis of $[\text{}^{18}\text{F}]\text{F}_2$ by VUV-photon promoted isotopic exchange (IV)

The first parameters to be studied were the shape and coating of the illumination chamber. For this the reactions were carried out with relatively large amounts of carrier. The $[\text{}^{18}\text{F}]\text{F}_2$ produced in these reactions was used in the synthesis of $[\text{}^{18}\text{F}]\text{NFSi}$ which was subsequently analysed by radio-HPLC, results of these reactions are presented in Table 13. The $[\text{}^{18}\text{F}]\text{NFSi}$ radiochemical yields were calculated based on area of the $[\text{}^{18}\text{F}]\text{NFSi}$ peak in the analytical radio-HPLC radiochromatogram, expressed as a percentage of the total area under the chromatogram. The A_m 's determined for the $[\text{}^{18}\text{F}]\text{NFSi}$ product were decay corrected to the EOS.

Optimisation of the illumination times indicated that, with the conditions studied, increasing the number of pulses from 15000 to 30000 pulses resulted in an increase yield and A_m of the resulting $[\text{}^{18}\text{F}]\text{NFSi}$. However, no further increase could be

seen when 60000 pulses were used. Hence illuminations of 30000 pulses were employed in the remainder of the study.

Table 13: Optimisation of chamber shape and coating material. * based on radio-HPLC analysis of the crude product. A_m 's are decay corrected to EOS.

Chamber	Chamber details	Carrier F ₂ (nmol)	A_m (GBq/ μ mol)	Non-isolated [¹⁸ F]NFSi radiochemical yield *(%)
B	T-Shaped TiO ₂ coated end	1260	0.04 - 0.15	34 - 36
C	30 mm Spherical Al coated	1280	0.04 - 0.12	15
D	30 mm Spherical TiO ₂ coated	1280	0.04 - 0.10	5 - 9
E	20 mm Spherical Al coated	1090	0.04- 0.05	9 - 13

For the optimisation of the amount of carrier F₂ gas the reactions were carried out employing approximately 3 GBq of starting [¹⁸F]fluoride activity. Various quantities of carrier F₂ were assessed (Table 14), while the yield of the resulting [¹⁸F]NFSi decreased as the amount of F₂ was lowered, the A_m increased until 190 nmol after which it too decreased.

Table 14: Results from the reactions for the optimisation of carrier F₂ amounts. * based on radio-HPLC analysis of the crude product. A_m 's are decay corrected to EOS.

Carrier F ₂ (nmol)	A_m (GBq/ μ mol)	Non-isolated [¹⁸ F]NFSi radiochemical yield *(%)
1720	0.07 \pm 0.05	29 \pm 2
1180	0.16 \pm 0.07	31 \pm 3
380	0.66 \pm 0.41	23 \pm 5
190	0.93 \pm 0.43	13 \pm 6
95	0.57 \pm 0.37	5 \pm 2

Finally, the amount of starting activity was increased approximately ten-fold and the reaction was carried out using the optimised conditions. This reaction resulted in a non-isolated [^{18}F]NFSi yield of $13 \pm 3\%$ (based on radio-HPLC analysis of the crude product) and an A_m of $10.3 \pm 0.9 \text{ GBq}/\mu\text{mol}$ (decay corrected to EOS). These results are in line with those of the reactions performed using 190 nmol F_2 and the lower starting activity, the yield is the same, while the A_m , like the starting activity, is approximately ten-fold higher.

5.2.1 Synthesis of [^{18}F]F-DPA using VUV-photon promoted isotopic exchange produced [^{18}F]F $_2$ -derived [^{18}F]Selectfluor bis(triflate) (unpublished results)

The applicability of using [^{18}F]F $_2$ generated by VUV-photon illumination-promoted isotopic exchange to synthesise [^{18}F]Selectfluor bis(triflate) and subsequently [^{18}F]F-DPA was assessed. 1.7 μmol of carrier F $_2$ was used for the isotopic exchange reaction. [^{18}F]F-DPA was produced in 4 - 33% non-isolated yield (based on radio-HPLC analysis of the crude product) with an A_m of $0.071 \pm 0.017 \text{ GBq}/\mu\text{mol}$ (decay corrected to EOS). This A_m agrees with that which was previously achieved using this quantity of carrier (Table 14).

5.3 Copper-mediated nucleophilic ^{18}F -fluorination (III and unpublished)

The results of the nucleophilic ^{18}F -fluorination reactions using stannyl (Compound 1) and boronic ester (Compound 2) precursors are summarised in Table 15.

Table 15: Results of Cu-mediated nucleophilic ^{18}F -fluorinations of Compounds 1 and 2, the radiochemical yield (RCY) was calculated from the analytical radio-HPLC of crude reaction samples, A_m is decay corrected to EOB.

Study	Precursor	Non-isolated Radiochemical yield (%)	A_m (GBq/ μmol)
III	Compound 1	11.4 ± 1.0	990 ± 150
Unpublished	Compound 2	15.5 ± 10.5	27 - 2040

The copper-mediated ^{18}F -fluorination of the initially assessed boronic ester precursor did indeed yield the desired product in approximately 16% RCY (based on radio-HPLC analysis of the crude product). However, the chromatographic purification and analysis proved problematic. The difficulty of separating the UV peak corresponding to [^{18}F]F-DPA from a co-eluting UV active compound resulted in the wide range of apparent A_m 's determined.

The next copper-mediated ^{18}F -fluorination employed the stannylated precursor. This reaction was first attempted as a one-pot reaction with DMA or MeCN as the reaction solvent. However, neither of these reactions afforded the product. It was found that for this precursor, the dried ^{18}F fluoride complex needs to be pre-stirred with the copper (II) triflate in acetonitrile for 10 min prior to the labelling reaction, for which the solvent needs to be changed to DMA. The results of this reaction are presented in Table 15.

5.4 Preclinical evaluation (I – III)

^{18}F]-DPA synthesised from Compound 1 by electrophilic (Studies I – III) and nucleophilic (Study III) approaches underwent evaluation in a preclinical setting. In Study I, ^{18}F]-DPA was compared with the related tracer ^{18}F]-DPA-714 in healthy Sprague Dawley (SD) rats. For this study, ^{18}F]-DPA-714 was synthesised according to well described procedures in $43 \pm 7\%$ radiochemical yield (calculated from ^{18}F fluoride activity) and with an $A_m > 1$ TBq/ μmol (decay corrected to EOB).

5.4.1 *In vivo*

Initial *in vivo* PET imaging carried out in SD rats demonstrated that ^{18}F]-DPA quickly passes through the blood-brain barrier and subsequently quickly washes-out (Figure 31).

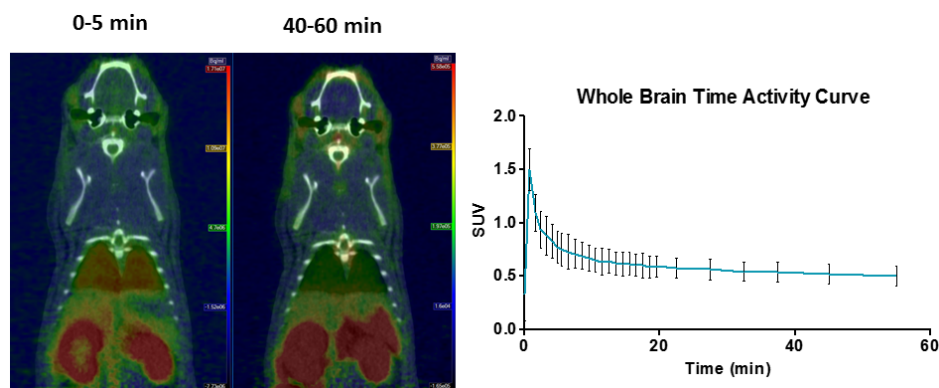


Figure 31: *In vivo* PET images of healthy Sprague Dawley rats summed over 0-5 and 40-60 min and the derived time activity curve for the whole brain. Acquired using ^{18}F]-DPA synthesised by the electrophilic route, A_m at time of injection: 4.1 ± 0.4 GBq/ μmol .

Cortical TACs from *in vivo* PET imaging of mice using ^{18}F]-DPA produced by an electrophilic route (Figure 32) demonstrated that in mice the kinetics follow

those observed previously in rats, a sharp initial uptake of radioactivity followed by rapid wash-out and an equilibrium that was reached at about 20 to 40 min after tracer-injection.

In transgenic APP/PS1-21 mice, the shapes of how cortical SUVs (Figure 32) vary with time depends on the age of the animal. Between 4.5 to 6 months the curves for TG mice strongly resemble the TACs of the age-matched WT animals. The level at which the curve plateaus, between 20 and 40 min, increases with age until 12 months and does not increase further to 15 months. At 19 months the plateau level and the height of the graph in general decrease relative to 15 months and are about the same as those of 12 - 24 month old WT animals.

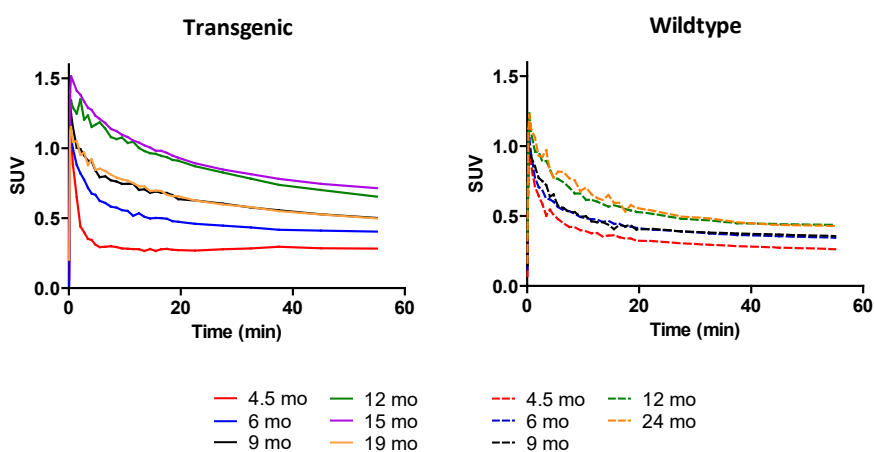


Figure 32: Graphs showing the variation of cortical standardised uptake values (SUVs) with time in transgenic APP/PS1-21 and wildtype animals at different ages. The curves are means without standard deviations for clarity. Acquired using [^{18}F]F-DPA synthesised by the electrophilic route, A_m at time of injection: $2.4 \pm 1.2 \text{ GBq}/\mu\text{mol}$.

The study of [^{18}F]F-DPA SUVs averaged over 20-40 min (Figure 33) shows that at the early ages studied (4.5 – 9 months) the uptake of [^{18}F]F-DPA in the brains of TG and WT animals does not differ significantly. The first significant increase can be seen at 9 months, the SUVs of TG animals then plateau between 12 and 15 months and a distinct drop can be seen at 19 months.

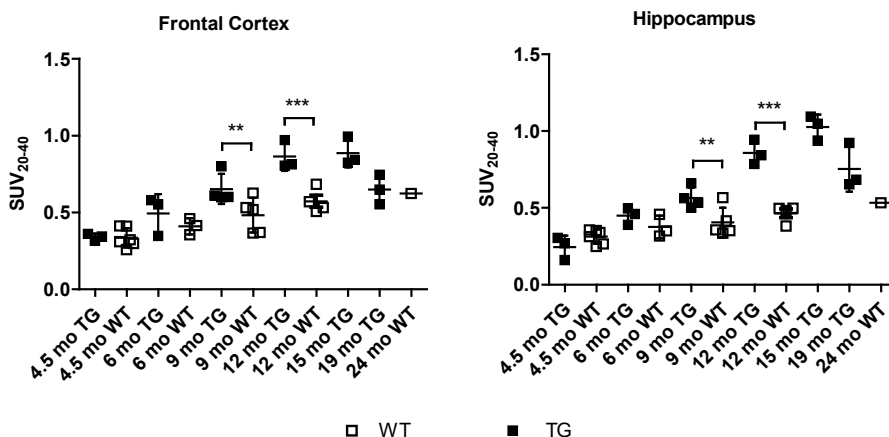


Figure 33: Frontal cortex (A) and hippocampus (B) standardised uptake values (SUVs) of transgenic APP/PS1-21 (TG) and wildtype (WT) mice at different ages averaged over 20-40 min. (** $p < 0.01$, *** $p < 0.001$). Acquired using [^{18}F]F-DPA synthesised by the electrophilic route, A_m at time of injection: 2.4 ± 1.2 GBq/ μmol .

The use of [^{18}F]F-DPA with different A_m 's for imaging was performed in Study III. The *in vivo* results from this, shown in Figure 34, demonstrate that while the [^{18}F]F-DPA produced by an electrophilic route has a high initial uptake and fast washout, the higher A_m [^{18}F]F-DPA, produced by the nucleophilic route, has a lower initial uptake and slower washout. This slower washout also means that the TACs do not reach a plateau even by the end of the 60 min scan.

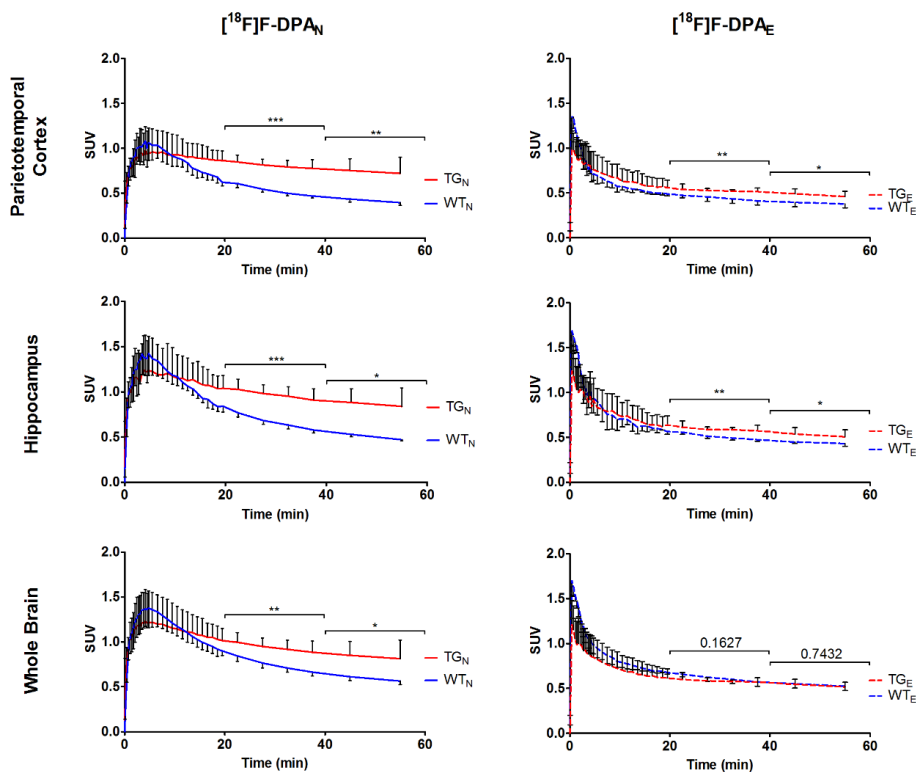


Figure 34: Standardised uptake values (SUVs) over 0-60 min for the parietotemporal cortices, hippocampi and whole brains of transgenic APP/PS1-21 (TG) and wildtype (WT) animals imaged with either high A_m [^{18}F]F-DPA_N or low A_m [^{18}F]F-DPA_E. Values are means \pm SD, $n=3$ per group. Statistical analyses were carried out to determine the significance of differences between the SUVs of TG and WT mice averaged over the 20-40 and 40-60 min periods. (* $p < 0.05$, ** $p < 0.01$, *** $p < 0.001$). A_m at time of injection: 260 ± 110 GBq/ μmol and 2.3 ± 1.0 GBq/ μmol for [^{18}F]F-DPA_N and [^{18}F]F-DPA_E respectively.

Comparison of averaged SUVs over 20-40 and 40-60 min for [^{18}F]F-DPA produced by electrophilic or nucleophilic routes, indicated by brackets and asterisks to denote the level of significance, (Figure 34) reveals that imaging with high A_m [^{18}F]F-DPA results in higher statistically significant difference between the SUVs of WT and TG animals during both intervals. Regardless of whether the imaging was carried out with high or low A_m [^{18}F]F-DPA, the differences between SUVs always have higher statistical significance during the 20-40 min interval.

5.4.2 *Ex vivo* brain autoradiography (II & III)

The *ex vivo* imaging of brain slices obtained after sacrifice showed that this higher resolution imaging modality allows significant differences between WT and TG

animals to be observed already at 4.5 months in the FC. The ROI/HYP ratios follow a similar trend to that already described for SUVs, increasing until 15 months and dropping at 19 months (Figure 35).

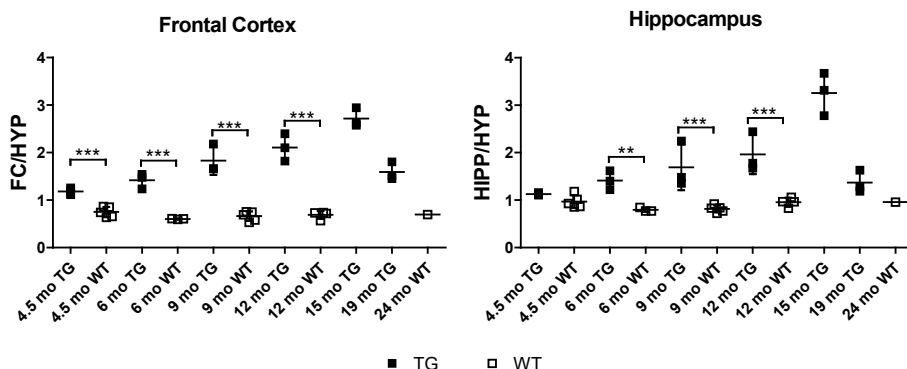


Figure 35: *Ex vivo* autoradiography results showing frontal cortex (FC) and hippocampus (HIPP) to hypothalamus (HYP) ratios determined from autoradiography of brain slices from transgenic APP/PS1-21 (TG) and wildtype (WT) animals at different ages. Shown are the individual values as well as the means \pm SD when $n \geq 3$. (** $p < 0.01$, *** $p < 0.001$). Acquired using [^{18}F]F-DPA synthesised by the electrophilic route, A_m at time of injection: 2.4 ± 1.2 GBq/ μmol .

The use of higher A_m [^{18}F]F-DPA (Study III), showed an increased separation between the ROI/HYP ratios of TG and WT in regions such as FC and CTX compared to the low A_m [^{18}F]F-DPA (Figure 36). Only in the FC, the FC/HYP ratio obtained using high A_m [^{18}F]F-DPA is significantly higher than that acquired using low A_m [^{18}F]F-DPA. No significant differences can be observed between the WT ROI/HYP ratios acquired with either high or low A_m [^{18}F]F-DPA.

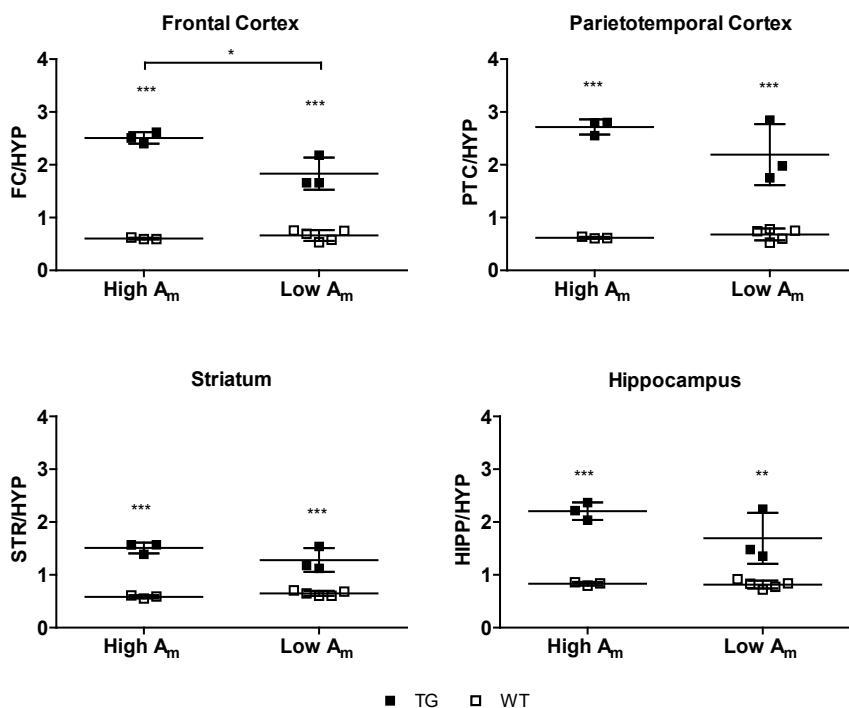


Figure 36: *Ex vivo* brain autoradiography results showing frontal cortex (FC), parietotemporal cortex (PTC), striatum (STR) and hippocampus (HIP) to hypothalamus (HYP) ratios of 9 month WT and TG animals injected with either high or low molar activity (A_m) [^{18}F]F-DPA. Shown are the individual values as well as the means \pm SD ($n = 3 - 5$). (** $p < 0.01$, *** $p < 0.001$). Acquired using [^{18}F]F-DPA synthesised by both nucleophilic (high A_m) and electrophilic (low A_m) routes. A_m at time of injection: 260 ± 110 GBq/ μmol and 2.6 ± 1.6 GBq/ μmol .

5.4.3 *Ex vivo* biodistribution

Comparison of the biodistribution of [^{18}F]DPA-714 and [^{18}F]F-DPA was carried out in healthy SD rats (Figure 37). This data shows that the radioactivity from these two tracers accumulates similarly in various tissues, particularly in TSPO rich organs such as the heart, lungs and kidneys as well as in steroid-producing organs such as the liver and adrenals.

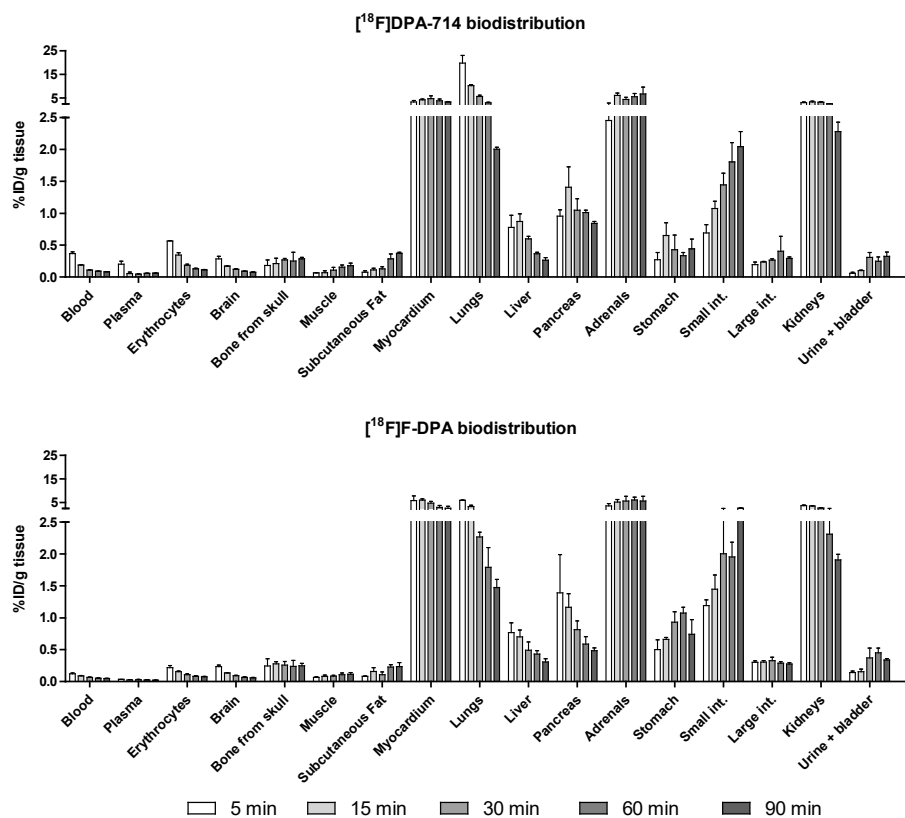


Figure 37: Comparison of [¹⁸F]DPA-714 and [¹⁸F]F-DPA (synthesised by the electrophilic route) distribution in healthy Sprague Dawley rats. The values presented are means \pm SD of the percentage of injected dose per gram (%ID/g) of tissue (n=3 per time point).

The plasma from animals that had been administered with either tracer was analysed to determine the fraction of radioactivity that is not bound to plasma proteins. [¹⁸F]DPA-714 showed a relatively high $33 \pm 9\%$ of free radioactivity in the plasma at 15 minutes after injection. However, at the same time point, only $7 \pm 3\%$ of the radioactivity from [¹⁸F]F-DPA was unbound to plasma proteins.

5.4.4 Specificity study in mice

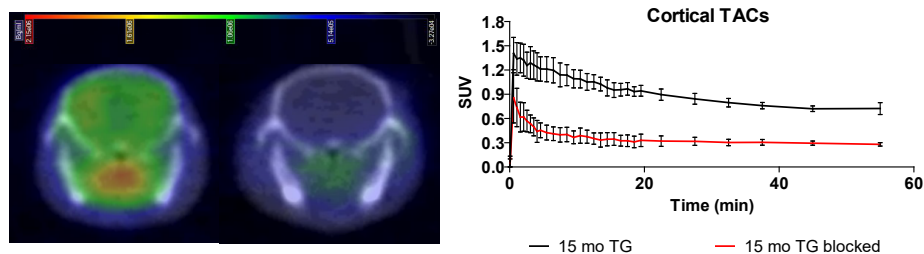


Figure 38: *In vivo* images of the brains of 15-month APP/PS1-21 (TG) and 15-month TG blocked mice (left and right respectively) and the derived cortical Standardised uptake values (SUV) time-activity curves (TACs). Mean \pm SD, $n = 3/\text{group}$. Acquired using [^{18}F]F-DPA synthesised by the electrophilic route. A_m at time of injection: $2.5 \pm 0.6 \text{ GBq}/\mu\text{mol}$.

Pre-treatment with the TSPO-specific ligand PK11195 before tracer administration resulted in a significant drop in the radioactivity uptake in the brains of the 15-month TG studied relative to the non-pretreated 15-month TG animals. This can be seen in both the *in vivo* data (Figure 38) as well as the *ex vivo* autoradiography images (Figure 39) and the derived data (Figure 40).

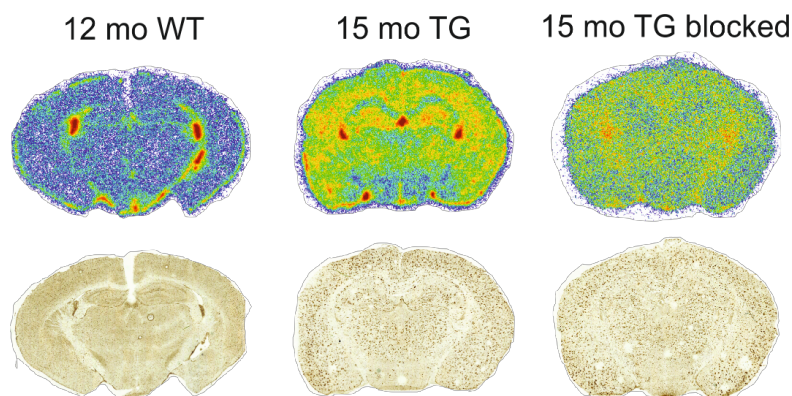


Figure 39: 12-month wildtype (WT) and 15-month transgenic APP/PS1-21 (TG) blocked and not blocked *ex vivo* mouse brain autoradiography images acquired using [^{18}F]F-DPA synthesised by the electrophilic route (top row) and corresponding Iba1-stained slices (bottom row)

The data collected by *ex vivo* autoradiography corroborates the *in vivo* observations and a significant difference can be seen between the 15-month TG animals and the pre-treated counterparts in all the brain regions studied.

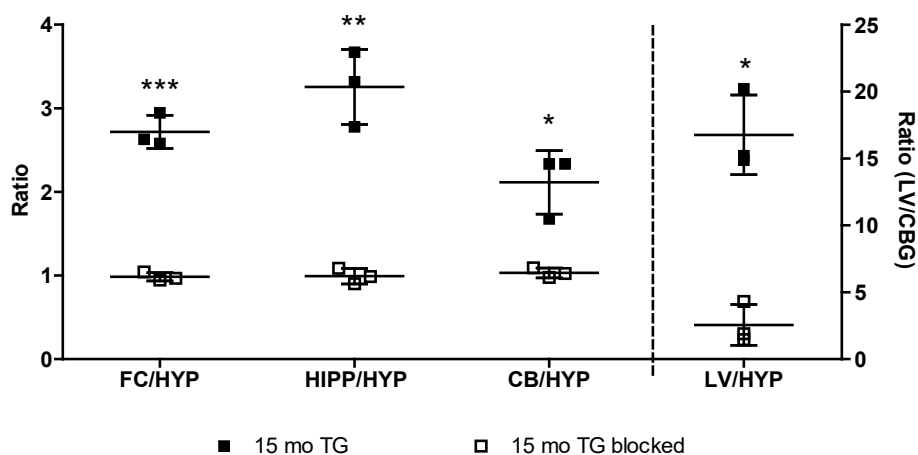


Figure 40: Derived, frontal cortex (FC), hippocampus (HIPP), cerebellar cortex (CB) and lateral ventricle (LV) to hypothalamus (HYP) ratios calculated from autoradiographs for 15-month transgenic APP/PS1-21 (TG) blocked and non-blocked mice. (* $p < 0.05$, ** $p < 0.01$, *** $p < 0.001$). Acquired using [^{18}F]F-DPA synthesised by the electrophilic route. A_m at time of injection: $2.5 \pm 0.6 \text{ GBq}/\mu\text{mol}$.

5.4.5 Radio-TLC analysis of radiometabolites

In Study I, analysis of the radiometabolic profile of [^{18}F]F-DPA was performed to discern whether the positioning of the fluorine-18 label directly on the aromatic ring conferred greater stability with respect to metabolic cleavage of the radiolabel compared to [^{18}F]DPA-714.

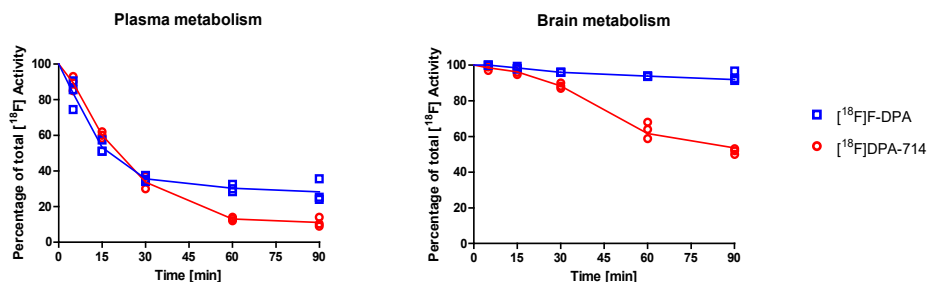


Figure 41: Graphs showing extent of [^{18}F]F-DPA and [^{18}F]DPA-714 metabolism in plasma and brain of Sprague Dawley rats. [^{18}F]F-DPA was synthesised by the electrophilic route.

The results from SD rats (Figure 41) demonstrated that in the plasma [^{18}F]F-DPA and [^{18}F]DPA-714 metabolise quickly and after 90 min the unchanged tracers account for approximately 30% and 10% of the remaining radioactivity

respectively. However, in the brain there is a much more apparent difference between the two tracers. In the case of [^{18}F]DPA-714, the unchanged tracer accounts for approximately 50% of the remaining activity 90 min after tracer injection. While more than 90% of the remaining radioactivity can be attributed to the unchanged [^{18}F]F-DPA at the same time point.

When the radiometabolic profile of [^{18}F]F-DPA was studied in mice, it was found that after 60 min more than 70% of the remaining radioactivity in the plasma comes from the unchanged [^{18}F]F-DPA. Furthermore, no radiometabolites can be observed in the brain and the unmetabolised [^{18}F]F-DPA accounts for more than 99% of the remaining radioactivity.

6 DISCUSSION

The work presented in this thesis addresses the issue of A_m in the synthesis of PET tracers by different approaches and the use of tracers with different A_m 's for PET imaging.

It is well known that a high A_m is generally favourable for PET imaging, this together with the relative ease of the nucleophilic ^{18}F -fluorination methodology means that the majority of ^{18}F -labelled tracers are made by the nucleophilic approach. Nevertheless the complementary electrophilic ^{18}F -fluorination methodology can provide an alternative synthetic route, which can, depending on the compound of interest, be synthetically simpler than the nucleophilic approach.

$[^{18}\text{F}]\text{F}_2$ which is used for the electrophilic ^{18}F -fluorination approach is a very reactive, corrosive and toxic species which requires specialised equipment to handle properly. This is not available at many PET centres and is one of the contributing factors to the limited use of electrophilic ^{18}F -fluorination for PET tracer synthesis. Another shortcoming of the use of electrophilic ^{18}F -fluorination for the labelling of PET tracers is the relatively low A_m that can be achieved by this approach. Even the post-target production approach, which was developed by Bergman and Solin to increase the A_m , and was employed throughout this thesis can, at best, achieve A_m 's of around 55 GBq/ μmol .

It has been shown in this work that a high proportion of non-radioactive compound affects the washout profile of the tracer and decreases the difference between the SUVs of TG and WT animals. However, the issue of A_m plays a more critical role in the imaging of small animals, where there is a tendency to push the limits of the injected dose. Hence, in preclinical work, minimising the proportion of the non-radioactive, competitively binding, analogue is favourable, particularly in the case of small-animal imaging and when there is low target abundance. In a clinical setting, although high A_m is favourable, in certain instances it is not crucial, as is demonstrated by the continued use of numerous PET tracers, such as 6- $[^{18}\text{F}]$ fluoro-L-DOPA, $[^{18}\text{F}]\text{CFT}$ and $[^{18}\text{F}]\text{EF5}$, synthesised by the electrophilic route.

Despite the downsides associated with electrophilic ^{18}F -fluorination, it is a useful tool in the initial development of PET tracers, when A_m is not crucial, particularly when the alternative nucleophilic method proves troublesome.

6.1 Electrophilic ^{18}F -fluorination reactions for the production of $[\text{}^{18}\text{F}]\text{F-DPA}$ (I – IV and unpublished)

Despite the testing of several reaction conditions, including the use of silver as an additive, as well as the high reactivity of F_2 and usual effectiveness of the organotin as a leaving group, none of the $[\text{}^{18}\text{F}]\text{F-DPA}$ was observed, when the direct ^{18}F -fluorination of the stannyl precursor was attempted with $[\text{}^{18}\text{F}]\text{F}_2$.

The development of a new HPLC purification method, employing mobile phases suitable for mass spectroscopy (MS), allowed investigation into the identity of these ^{18}F -fluorinated species. MS was carried out on these fractions and it was found that the masses corresponded to mono, di, tri, tetra and even penta-fluorinated species.

The element tin has several stable isotopes with varying abundancies, with ^{116}Sn , ^{118}Sn and ^{120}Sn being the most abundant. These, together with the less abundant isotopes, result in characteristic tin lines which are observed in the mass spectra of tin-containing compounds. Figure 42 shows the 605 – 755 m/z region of the mass spectrum obtained for the late-eluting ^{18}F -fluorinated species.

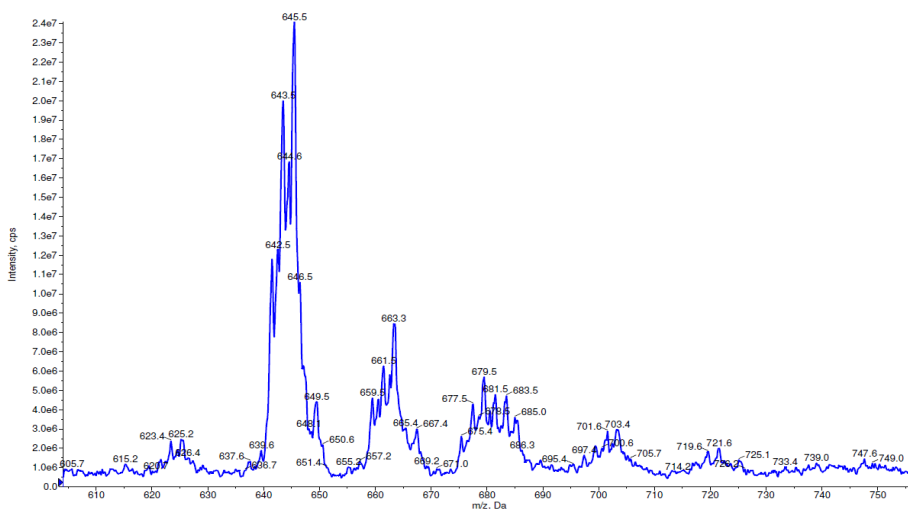


Figure 42: Mass spectrum for the late-eluting ^{18}F -fluorinated species (605 – 755 m/z region)

The molecular weight of the stannylated precursor of F-DPA is 625.5, the peaks corresponding to this can be seen in the 620 – 630 range of the spectrum. The subsequent group of peaks has a mass that is approximately 19 higher and this trend follow for each on the subsequent peaks shown. This, together with the characteristic tin-lines confirmed that there were poly-fluorinated tin containing

species. The specific fluorination positions were not identified, however shown in Figure 43 are some of the possible locations of the labels.

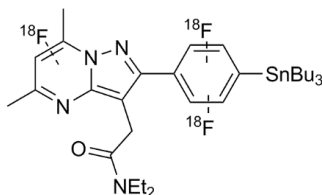


Figure 43 : Possible sites of ^{18}F -fluorination in the perfluorinated tin-containing species

To avoid the unwanted ^{18}F -polyfluorination reactions, $[^{18}\text{F}]$ Selectfluor *bis*(triflate) was employed for the next reactions attempted. $[^{18}\text{F}]$ Selectfluor *bis*(triflate) which can be made from $[^{18}\text{F}]\text{F}_2$ gas with relative ease, is a milder ^{18}F -fluorination reagent, which, once produced can be stored as a stock solution and used for multiple reactions. Furthermore since the $[^{18}\text{F}]$ Selectfluor *bis*(triflate) is dissolved in solution this can allow for longer reaction times as well as heating and stirring if necessary.

Table 16: Comparison of the use of VUV-illumination and HV discharge for the synthesis of $[^{18}\text{F}]\text{F}_2$ in the production of $[^{18}\text{F}]\text{F-DPA}$. A_m 's are decay corrected to EOS. * based on radio-HPLC analysis of the crude product

Carrier F_2 amount (μmol)	Excitation method	$[^{18}\text{F}]$ Selectfluor <i>bis</i> (triflate) Activity (MBq)	$[^{18}\text{F}]\text{F-DPA}$	
			A_m (GBq/ μmol)	non-isolated radiochemical yield (%) *
1.7	VUV- illumination	347 ± 49	0.07 ± 0.02	16 ± 15
1.7	HV discharge	500 ± 13	0.90 ± 0.11	33 ± 3.6

The synthesis of $[^{18}\text{F}]\text{F-DPA}$ using $[^{18}\text{F}]$ Selectfluor *bis*(triflate) derived from $[^{18}\text{F}]\text{F}_2$ made by various post-target production routes has also been studied. Employing VUV-illumination for the generation of $[^{18}\text{F}]\text{F}_2$ gave the $[^{18}\text{F}]\text{F-DPA}$ product in appreciable yield and with an A_m that is on the same level as those reported for the $[^{18}\text{F}]\text{NFSi}$ production carried out using that level of carrier. However, both the RCY and A_m obtained by this route are significantly lower than those achieved when using the HV discharge to promote the isotopic exchange reaction (Table 16).

When using SF_6 derived $[^{18}\text{F}]\text{F}_2$ to produce $[^{18}\text{F}]$ Selectfluor *bis*(triflate) and subsequently $[^{18}\text{F}]\text{F-DPA}$, the final product was obtained in 1.3 GBq/ μmol A_m but

in quite low 2% RCY (determined by radio-HPLC analysis of the crude product) (Krzyszmonik et al. 2017).

6.2 Nucleophilic ^{18}F -fluorination reactions for the production of ^{18}F]-DPA (III and unpublished)

During Study III, different labelling approaches were studied for the synthesis of ^{18}F]-DPA. It was found that when employing Compound **1** as the precursor for the copper-mediated nucleophilic ^{18}F -fluorination reaction, it was favourable to pre-stir the copper triflate with the ^{18}F]fluoride in acetonitrile prior to the labelling reaction. However, in those cases when Compound **2** was used, such a pre-stir was not necessary.

It has previously been hypothesised that acetonitrile has a crucial stabilising role on an intermediate $\text{Cu}[^{18}\text{F}]\text{FOTf}$ complex in copper-mediated nucleophilic fluorinations of aryl-stannanes (Gamache et al. 2016). In these fluorination reactions of tin containing precursors (Gamache et al. 2016, Makaravage et al. 2016) the only species that can act as a stabilising ligand is acetonitrile. In contrast, the reaction for the labelling of Compound **2** proceeds despite the absence of acetonitrile. This may be due to the fact that the labelling protocol for boronic esters which was applied for this reaction (Preshlock et al. 2016a, 2016b, Tredwell et al. 2014) employs a mixture of potassium oxalate and carbonate as the potassium source for the formation of the $\text{K}_{222}/\text{K}[^{18}\text{F}]\text{F}$ complex. The oxalate can potentially act as a stabilising ligand for the intermediate $\text{Cu}[^{18}\text{F}]\text{FOTf}$ complex.

The hypothesis that the intermediate $\text{Cu}[^{18}\text{F}]\text{FOTf}$ complex requires a stabilising ligand is supported by numerous recently reported studies on the Cu-mediated radiofluorination of aryl pinacol boronates carried out in tandem with the work reported in this thesis. Antuganov et al. found that the addition of pyridine can significantly improve the radiofluorination yield of when using cesium carbonate and kryptofix as solubilising agents for the ^{18}F]fluoride (Antuganov et al. 2017).

Zichler et al. applied the Cu-mediated radiofluorination methodology to the synthesis of ^{18}F]-DPA (Zischler et al. 2017) and showed that the presence of various alcohols can enhance the radiofluorination yield. For that study Et_4NHCO_3 was used in place of $\text{K}_2\text{CO}_3/\text{K}_{222}/\text{KOTf}/\text{Py}$ for elution of the ^{18}F]fluoride. Since Et_4NHCO_3 cannot act as a stabilising ligand for the hypothesised intermediate species the reaction would not proceed without the addition of an alcohol. No A_m was reported for ^{18}F]-DPA synthesised by this approach, however the model molecules 6- ^{18}F]FDA and 6- ^{18}F]Fluoro-L-DOPA also synthesised during the course of the study were obtained in 39 and 37 GBq/ μmol respectively.

Although Compound **2** was successfully used as a precursor for the synthesis of [^{18}F]F-DPA by a nucleophilic route, the preparative HPLC purification as well as radio-HPLC analysis of the crude and final products proved to be troublesome. This problem has also been reported in a recent study by Mossine et al. employing the Cu-mediated ^{18}F -fluorodeboronation reaction for the synthesis of PET tracers (Mossine et al. 2018). Mossine et al. explored alternative reaction conditions to minimise the formation of the unwanted co-eluting impurity. However together with decreasing the concentration of the by-product these resulted in a decrease in radiochemical yield, hence alternative HPLC methods were developed.

The ^{18}F -fluorination reaction of Compound **1** yielded [^{18}F]F-DPA with a high molar activity, ten-fold higher than that reported by Wang et al. (Wang et al. 2017). Due to the relative ease of the reactions, HPLC-purification and radio-HPLC analysis employing Compound **1** as a precursor compared to those reactions using Compound **2**, only the products from the labelling reactions performed using the stannylated precursor, Compound **1**, were used for preclinical evaluation.

6.3 Metabolism of [^{18}F]F-DPA (I & II)

Increased stability with respect to metabolism, compared to [^{18}F]DPA-714, was observed when the metabolic profile of [^{18}F]F-DPA was studied in rats. This demonstrated that, as postulated, the fluorine-18 label is more stable on the aromatic position compared to the terminal position of the alkoxy chain in [^{18}F]DPA-714. The metabolism of [^{18}F]DPA-714 has been studied in detail by Peyronneau et al. (Peyronneau et al. 2013) and various fragments were identified by mass spectrometry. A variation could be observed between the metabolism of [^{18}F]DPA-714 between rats and baboons. However, in each species defluorination of [^{18}F]DPA-714 by *O*-deethylation did occur. In Study I, metabolism of both [^{18}F]DPA-714 and [^{18}F]F-DPA was observed. However, in the case of [^{18}F]F-DPA, due to the location of the ^{18}F -fluorine on the aromatic ring, the tracer was found to metabolise to a lower extent.

Unexpectedly, despite the generally faster metabolism of mice, compared to rats, no metabolism of [^{18}F]F-DPA could be observed when mouse brain homogenate was analysed by radio-TLC (Study II and III). This difference may either arise from interspecies variation of metabolic pathways, alternatively the mice may have a faster rate of excretion of radioactive metabolites from the brain.

6.4 Preclinical evaluation of [^{18}F]F-DPA

The preclinical evaluation carried out in healthy SD rats during Study I, proved that [^{18}F]F-DPA, like [^{18}F]DPA-714, can easily pass the blood-brain barrier and enter the brain. The evaluation during Study II further demonstrated that [^{18}F]F-DPA accumulates more in the brains of TG animals compared to the age-matched WT counterparts. While this only represents a significant difference for *in vivo* imaging at 12 months, the *ex vivo* results exhibit a significant difference as early as 4.5 months.

Whereas the cerebellum had been previously used, with [^{18}F]DPA-714, as a reference region for the calculation of ratios from SUVs and autoradiographs (Takkinen et al. 2017) during Study II it was found that when using [^{18}F]F-DPA, the cerebellum does not represent a valid region to be used as a reference.

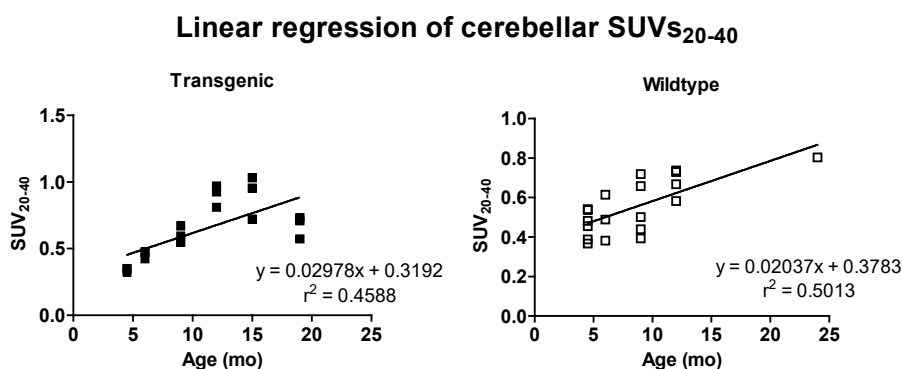


Figure 44: Linear regression analysis of transgenic APP/PS1-21 and wildtype cerebellum standardised uptake values (SUV_{s20-40}). Acquired using [^{18}F]F-DPA synthesised by the electrophilic route, A_m at time of injection: 2.4 ± 1.2 GBq/ μmol .

Although there is no significant increase in cerebellar [^{18}F]F-DPA uptake between successive age groups, it was observed that there is an overall increase in both TG as well as WT animals over the entire age periods studied (Figure 44). Immunohistochemical staining of brain slices using Iba1 (Figure 45) demonstrated that the hypothalamus is a region that remain relatively clear of neuroinflammation and the accompanying microglial activation and hence this was used as the reference region for the calculation of ratios from autoradiographs.

However, during *in vivo* imaging a high uptake of radioactivity can be observed in the pituitary gland (Figure 38). Due to the proximity of the hypothalamus to the pituitary gland, the hypothalamus could not however be used as a reference region for calculating SUV ratios.

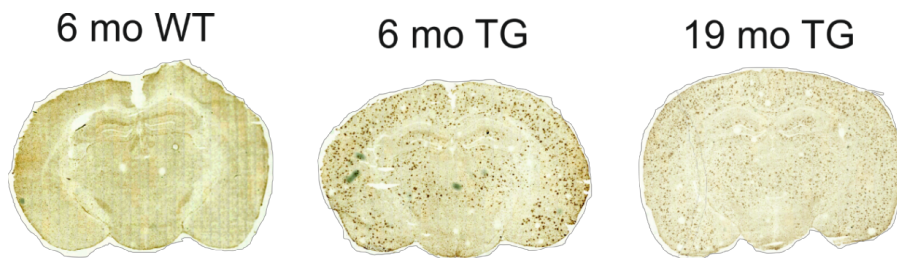


Figure 45: Immunohistochemical staining using Iba1 of brain slices from 6-month wildtype (WT) and transgenic APP/PS1-21 (TG) and 19-month TG mice.

Pre-treatment of 15-month TG animals with PK11195 was performed to assess the specificity of [^{18}F]F-DPA for the TSPO target. Significantly higher tracer uptake was seen in all brain regions of age-matched mice which had not undergone pre-treatment. These findings were in line with concurrent work where the blocking of [^{18}F]F-DPA with PK11195 was studied in a rat model of ischemic stroke (Wang et al. 2017).

As expected, the ROI/HYP ratios for the FC, HIPPO and CB for the blocked animals were approximately 1, thereby proving that, due to the blocking, the radioactivity was equally distributed in the brain. While not complete, a blocking effect was also seen in the LV where vast amounts of TSPO are present.

Since A_m is an oft-addressed subject with regards to PET tracers, a comparison of *in vivo* data collected from the same animals with high and low A_m batches of the same tracer is important for the development of this novel tracer and for the future development of ^{18}F -fluorination methodologies. The A_m 's obtained from the two different labelling strategies employed varied by a factor of approximately 100, since the injected dose was kept approximately equal, the injected mass of tracer hence also varied 100-fold.

A greater difference could be observed between the *in vivo* data of TG and WT when they were imaged with high A_m [^{18}F]F-DPA compared to when they were imaged using the low A_m tracer. The high A_m [^{18}F]F-DPA showed significantly higher uptake in TG versus WT animals in all the brain regions studied *in vivo*. Furthermore, apart from the striatum, the TG animals showed a significantly higher uptake when they were imaged with high A_m versus low A_m tracer. The SUVs for this comparison were averaged over different time intervals depending on the A_m of the [^{18}F]F-DPA employed. The analysis was carried out thus since the low A_m tracer showed the greatest difference between WT and TG animals already at 20-40 min post-injection, while the high A_m tracer gave the best separation in the 40-60 min interval.

Naturally, *ex vivo* comparison could not be performed in the same animals. However when the *ex vivo* data from different animals were compared, a trend similar to that described earlier for *in vivo* data was seen.

The varying A_m had a pronounced effect on the shapes of the TACs (Figure 34) due to the relatively high proportion of non-radioactive F-DPA in the low A_m tracer. The shape of those TACs resembles similar graphs for animals that have been pre-treated or co-injected with a competitively binding ligand (Delforge et al. 1993, Eberl et al. 2017, James et al. 2008, Samson et al. 1985), a sharp initial uptake followed by a relatively fast clearance. The time-activity curves for [^{18}F]F-DPA distribution in APP-PS1 mice were reported by Wang et al. (Wang et al. 2017). Although these are reported in a different model of AD, they nevertheless provide a valuable comparison. The A_m of [^{18}F]F-DPA obtained by Wang et al. ($96 \pm 22 \text{ GBq}/\mu\text{mol}$) is conveniently between those achieved by the electrophilic and nucleophilic ^{18}F -fluorination approaches employed in Study III. Visual inspection of the shapes of the TACs confirmed that as expected the shape is approximately in between those of [^{18}F]F-DPA_E and [^{18}F]F-DPA_N (Figure 34). The initial uptake is not as sudden as that seen for [^{18}F]F-DPA_E but faster than for [^{18}F]F-DPA_N. Similarly the subsequent washout of radioactivity is faster than [^{18}F]F-DPA_N but not as fast as [^{18}F]F-DPA_E.

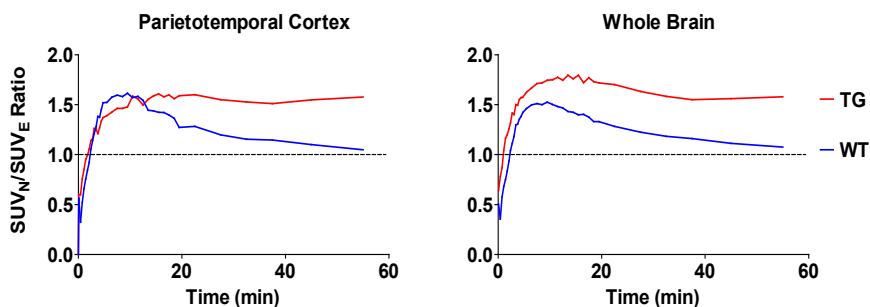


Figure 46: Ratio of standardised uptake value (SUV) time-activity curves (TACs) obtained from the PTC and WB of APP/PS-1-21 and WT mice using high and low molar activity (A_m) [^{18}F]F-DPA

Ratios of the high A_m and low A_m cortical TACs was calculated for PTC and WB of TG and WT animals (Figure 46). The differing kinetics observed for the two different A_m 's (Figure 34) result in the steep initial increase in the shape of the SUV_N/SUV_E ratio graphs, peaking at approximately 1.5, subsequently the TG and WT graphs vary from one another. In the case of the TG graphs, the presence specific binding and respective A_m 's of the tracer used for imaging cause an approximately one and a half times higher uptake of radioactivity in not only the PTC but the entire brain when the animals are imaged with high A_m [^{18}F]F-DPA.

The SUV_N/SUV_E ratio graph for WT animals shows that following the initial peak which is a result of the varying kinetics, the curve gradually decreases to approximately 1 (indicated by the dashed line). This suggests that due to the lack of specific binding there is very little difference between the uptake of radioactivity in the brains of WT animals when they are imaged with high or low A_m [^{18}F]F-DPA. This is in line with the results seen from the ratios calculated from autoradiographs (Figure 36).

6.5 Study limitations

The studies presented herein have expanded on numerous aspects of the radiochemistry of fluorine-18 for the synthesis of PET tracers as well as on the use of the novel TSPO-specific radioligand [^{18}F]F-DPA for the imaging of neuroinflammation in the APP-PS1-21 model of AD. Nevertheless there are certain limitations that can be associated with these studies. Some of these are addressed below.

The post-target production of [^{18}F]F₂ for electrophilic ^{18}F -fluorination requires specialised equipment which is not commonly available. This limits the applicability of electrophilic fluorination to the field of PET radiochemistry as a whole. Regardless, the development and use of electrophilic ^{18}F -fluorination methodologies for labelling is an important field, since it can allow access to some molecules that prove to be difficult to label by a nucleophilic approach.

Careful consideration needs to be made when planning preclinical studies, since the principles of the 3Rs (Replacement, Reduction and Refinement) should be adhered to whenever possible. However, minimising the numbers of experimental animals can affect the data, specifically it can limit the significance of statistical comparisons. Throughout the studies involving experimental animals, the 3Rs were adhered to whenever possible. Bar a few exceptions, the group size was $n = 3$ for all ages and time-points. While $n = 3$ is sufficient to perform statistical analysis, increasing group size can increase the significance of the data and lessen skew from outlying data.

It is well known that humans possess a single nucleotide polymorphism (rs6971) which separates individuals into 3 categories in terms of tracer binding to TSPO, high, mixed and low-affinity binders (Owen et al. 2012). The majority of TSPO-specific radiotracers are sensitive to this polymorphism, this includes [^{18}F]DPA-714 upon which [^{18}F]F-DPA is based. Hence, in order to make accurate conclusions from the PET data collected from humans, genotyping must be carried out. While this is not the case in rodents, it somewhat limits the potential of [^{18}F]F-

DPA translation into humans. Nevertheless [^{18}F]F-DPA can be used to study neuroinflammation models in animals.

There is some contention within the PET community as to the usefulness of TSPO as a target for imaging. This mainly arises due to the ubiquitous prevalence of TSPO throughout the body. It is difficult to find a suitable non-binding region that can be employed as a reference tissue in the brain. Although TSPO-specific radiotracers can be used for AD imaging, they do not image the disease pathology directly but rather visualise the resulting neuroinflammation. However, the over-expression of TSPO in a range of medical conditions means that TSPO-specific tracers can be used to study a range of diseases including numerous neurological conditions, cancers, and addiction (Kohn et al. 2019, Li et al. 2016).

7 CONCLUSIONS

Study I – An electrophilic route for the synthesis of [^{18}F]F-DPA was employed using [^{18}F]Selectfluor *bis*(triflate). The investigation of the alternative, more direct, electrophilic ^{18}F -fluorination employing [^{18}F]F₂ demonstrated that F₂ gas is too reactive for the precursor and results in the formation of perfluorinated products. The A_m of the resulting tracer (7.8 ± 0.5 GBq/ μmol) was enough for preclinical evaluation to show that the tracer crosses the blood-brain barrier into the brains of healthy rats and has more metabolic stability than [^{18}F]DPA-714.

Study II – The imaging of APP/PS1-21 mice at different ages using [^{18}F]F-DPA showed that it can be used to detect elevated TSPO in diseased animals. Whereas the *in vivo* PET data shows the first significant elevation in TSPO at 12 months of age, the higher resolution autoradiography imaging allows visualisation of the significant elevation already at 4.5 months. A blocking study involving pre-treatment of the animals with PK11195 resulted in a significantly reduced uptake of [^{18}F]F-DPA, indicating that [^{18}F]F-DPA and PK11195 have a common TSPO binding site.

Study III – Alternative electrophilic and nucleophilic syntheses were studied for the synthesis of [^{18}F]F-DPA. Nucleophilic ^{18}F -fluorination of a stannylated precursor by a copper-mediated reaction resulted in the desired product with very high A_m (0.99 ± 0.15 TBq/ μmol). Investigation of the effect a one-hundred-fold increased A_m has on preclinical imaging, revealed a change of the washout profile and a 1.5 fold increase of specific uptake in animals with elevated TSPO. Reactions employing a boronic ester precursor resulted in problematic purifications and very long reaction times.

Study IV – a) VUV-illumination can be used in place of high voltage discharge to promote the $^{18}\text{F}/^{19}\text{F}$ isotopic exchange reaction for the post-target synthesis of [^{18}F]F₂. The chamber shape, coating, and amount of carrier are all important parameters that must be considered since they can greatly affect the yields and A_m's obtained. The optimal conditions produced [^{18}F]F₂ that could be used for the labelling of model molecules with an A_m of 0.93 ± 0.43 GBq/ μmol , and when a ten-fold starting activity was used; 10.3 ± 0.9 GBq/ μmol .

b) [^{18}F]F₂ produced by VUV illumination of [^{18}F]MeF and F₂ mixture can be used for the synthesis [^{18}F]Selectfluor *bis*(triflate) which can further be used in the labelling of [^{18}F]F-DPA.

8 ACKNOWLEDGEMENTS

This work was carried out at the Radiopharmaceutical Chemistry Laboratory and at the MediCity Research Laboratory of the Turku PET Centre, University of Turku.

I would like to thank Professor Juhani Knuuti, Director of the Turku PET centre, Professor Jaakko Hartiala and Adjunct Professor Jukka Kemppainen, the former and current Heads of the Department of Clinical Physiology and Nuclear Medicine, the MediCity Research Laboratory and the Chemistry Department of the University of Turku, for granting me the opportunity and access to the facilities to carry out this work. I would also like to thank Professor Tapio Salakoski, Dean of the Faculty of Science and Engineering, and Professor Petriina Paturi and Professor Juri Poutanen, the former and current directors of the Doctoral Programme in physical and chemical sciences, for giving me the opportunity to complete this thesis.

I am deeply grateful to my supervisors Professor Olof Solin, Adjunct Professor Sarita Forsback and Adjunct Professor Merja Haaparanta-Solin for teaching me everything I know about radiochemistry and preclinical research, for their guidance during my studies as well as for always being available to answer my many questions.

I am thankful to Adjunct Professor Francisco López-Picón for advising me on numerous aspects of preclinical work and helping me to make heads or tails of the preclinical results.

I would like to offer special thanks to the Supervisors, Fellows and Advisory Board of the Radiomi Network. In particular, I wish to express my thanks to Professor Anthony Gee and Doctor Victor Pike for reviewing my thesis and offering constructive comments and criticism which significantly improved my thesis. I would also like to thank Professor Véronique Gouverneur for introducing me to the field of fluorine chemistry during my Masters and for her supervision during my secondment in her group.

I am grateful to my fellow researchers, Jörgen Bergman, Olli Eskola, Anna Kirjavainen, Salla Lahdenpohja, Paula Lehtiniemi and Cheng-Bin Yim for sharing their expertise with me. In particular, I would like to thank my colleague, Anna Krzyczmonik, for all the help with my reactions and for our lengthy discussions about the results and their interpretation.

I would like to thank Obada Alzghool, Aake Honkaniemi, Tove Grönroos, Elisa Riuttala, Annina Snellmann, Jatta Takkinen and Marko Vehmanen for their invaluable help with all the preclinical work.

I would like to thank Mikael Bergelin, Per-Olof Eeriksson, Stefan Johansson and Johan Rajander of the Accelerator Laboratory of the Åbo Akademi University, for the cyclotron operation and radionuclide production without which this work would not be possible. I am grateful to Esa Kokkomäki, Timo Saarinen and Simo Vauhkala for their technical support. I would also like to thank Riikka Kivelä, Nina Lauren, Miika Lehtinen, Marja-Liisa Pakkanen, Hanna Seikkula, Juha Seikkula, Jani Uotinen, Tapio Viljanen and Margit Åhman-Kantola for helping me with numerous lab-related issues.

I also wish to warmly acknowledge my collaborators from the CEA; Annelaure Damont, Fanny Cacheux and Doctor Frédéric Dollé. I would also like to acknowledge Professor Mathias Jucker who provided the animal model for Studies II and III.

I am grateful to my friends in Finland; Aleks, Eerik, Kamil and Suvi, Kumail and Amy, and Miikka for the countless sauna evenings and camping trips. I would especially like to thank Vilma for her support and for making me feel at home in Finland.

Last but not least, I would like to thank my family, my parents Jitka and Pablo, and my brother Jakob, for believing in me, supporting me and helping me during all my studies that have led me here.

This work was financially supported by the European Community's Seventh Framework Programs FP7-PEOPLE-2012-ITN-RADIOMI-316882 and HEALTH-F2-2011-278850 (INMiND), by a clinical grant from the Turku University Hospital Education and Research Foundation (EVO, grant number 13250) and by the Academy of Finland (grant numbers 266891 and 310962).

Turku, May 2019

Thomas Keller

9 REFERENCES

- Adam MJ, Pate BD, Ruth TJ, Berry JM and Hall LD. Cleavage of aryl-tin bonds with elemental fluorine: rapid synthesis of [^{18}F]fluorobenzene. *J Chem Soc, Chem Commun.* 1981; 15, 733–733.
- Adam MJ, Ruth TJ, Jivan S and Pate BD. Fluorination of aromatic compounds with F_2 and acetyl hypofluorite: synthesis of ^{18}F -aryl fluorides by cleavage of aryl-tin bonds. *J Fluor Chem.* 1984; 25, 3, 329–337.
- Al-Labadi A, Zeller KP and Machulla HJ. Synthesis of 6-[^{18}F]fluoroveratraldehyde by nucleophilic halogen exchange at electron-rich precursors. *J Radioanal Nucl Chem.* 2006; 270, 2, 313–318.
- Alva-Sánchez H, Quintana-Bautista C, Martínez-Dávalos A, Ávila-Rodríguez MÁ and Rodríguez-Villafuerte M. Positron range in tissue-equivalent materials: Experimental microPET studies. *Phys Med Biol.* 2016; 61, 17, 6307–6321.
- Anderson CD. The positive electron. *Phys Rev.* 1933; 43, 6, 491–494.
- Antuganov D, Zykov M, Timofeeva K, Antuganova Y, Orlovskaya V and Krasikova R. Effect of Pyridine Addition on the Efficiency of Copper-Mediated Radiofluorination of Aryl Pinacol Boronates. *ChemistrySelect.* 2017; 2, 26, 7909–7912.
- Antuganov D, Zykov M, Timofeev V, Timofeeva K, Antuganova Y, Orlovskaya V, Fedorova O and Krasikova R. Copper-Mediated Radiofluorination of Aryl Pinacolboronate Esters: A Straightforward Protocol by Using Pyridinium Sulfonates. *European J Org Chem.* 2019; 2019, 5, 918–922.
- Armendia PF and Schumacher HJ. The Kinetics and Mechanism of the Photochemical Reaction Between SF_4 and Fluorine at 365 nm. *J Photochem.* 1985; 28, 491–502.
- Banati RB. Visualising microglial activation in vivo. *Glia.* 2002; 40, 2, 206–217.
- Banister SD, Shen B, Chin FT and Kassiou M. Metabolically fortified DPA-714 analogs for improved PET imaging of translocator protein (TSPO). *Abstr Pap Am Chem Soc.* 2014; 248, 219.
- Banks RE, Mohaialdin-Khaffaf SN, Lal GS, Sharif I and Syvretb RG. 1-Alkyl-4-fluoro-1,4-diazoniabicyclo[2.2.2]octane Salts: a Novel Family of Electrophilic Fluorinating Agents. *Chem Commun.* 1992; 595–596.
- Barnhart TE, Converse AK, Dabbs KA, Schueller MJ, Stone CK, Nickles RJ and Roberts AD. Production of [^{17}F]CH $_3\text{F}$ ($t_{1/2} = 65$ s), an improved PET tracer for rCBF measurement. *Appl Radiat Isot.* 2005; 62, 4, 525–532.
- Bergman J and Solin O. Fluorine-18-labeled fluorine gas for synthesis of tracer molecules. *Nucl Med Biol.* 1997; 24, 7, 677–683.
- Bernstein RB and Katz JJ. Isotopic Exchange Reactions in Rate Theory. *J Phys Chem.* 1952; 56, 7, 885–888.
- Berridge MS, Apana SM and Hersha JM. Teflon radiolysis as the major source of carrier in fluorine-18. *J Label Compd Radiopharm.* 2009; 52, 13, 543–548.
- Best L, Ghadery C, Pavese N, Tai YF and Straffella AP. New and Old TSPO PET Radioligands for Imaging Brain Microglial Activation in Neurodegenerative Disease. 2019; 19, 5, 24.
- Bienvenu A, Barthelemy A, Boichut S, Marquet B, Billard T and Langlois BR. Synthesis of 4-Fluorophenols from 4-tert-Butylphenols and Fluoride Sources Under Oxidative Conditions. *Collect Czechoslov Chem Commun.* 2002; 67, 1467–1478.
- Blessing G, Coenen HH, Franken K and Qaim SM. Production of [^{18}F]F $_2$, H ^{18}F and $^{18}\text{F}_{\text{aq}}^-$ using the $^{20}\text{Ne}(\text{d},\alpha)^{18}\text{F}$ process. *Int J Radiat Appl Instrumentation Part A.* 1986; 37, 11, 1135–1139.
- Block D, Klatte B, Knochel A, Beckmann R and Holm U. N.C.A. [^{18}F]-Labelling of Aliphatic Compounds in High Yields via Aminopolyether - Supported Nucleophilic Substitution. *J Label Compd Radiopharm.* 1986; 23, 5, 467–477.
- Blom E, Karimi F and Långström B. [^{18}F]/ ^{19}F exchange in fluorine containing compounds for potential use in ^{18}F -labelling strategies. *J Label Compd Radiopharm.* 2009; 52, 12, 504–511.
- Van Der Born D, Pees A, Poot AJ, Orru RVA, Windhorst AD and Vugts DJ. Fluorine-18 labelled building blocks for PET tracer synthesis. *Chem Soc Rev.* 2017; 46, 15, 4709–4773.

- Bourdier T, Henderson D, Fookes CJR, Lam P, Mattner F, Fulham M and Katsifis A. Synthesis of [^{11}C]PBR170, a novel imidazopyridine, for imaging the translocator protein with PET. *Appl Radiat Isot.* 2014; 90, 46–52.
- Boutin H, Chauveau F, Thominiaux C, Kuhnast B, Gregoire M, Jan S, Trebossen R, Dollé F, Tavitian B, Mattner F, et al. In vivo imaging of brain lesions with [^{11}C]CLINME, a new PET radioligand of peripheral benzodiazepine receptors. *Glia.* 2007; 55, 1459–1468.
- Briard E and Pike VW. Substitution-reduction: An alternative process for the [^{18}F]N-(2-fluoroethylation) of anilines. *J Label Compd Radiopharm.* 2004; 47, 4, 217–232.
- Briard E, Hong J, Musachio JL, Zoghbi SS, Fujita M, Imaizumi M, Cropley V, Innis RB and Pike VW. Synthesis and evaluation of two candidate ^{11}C -labeled radioligands for brain peripheral benzodiazepine receptors. *J Label Compd Radiopharm.* 2005; 48, S71.
- Briard E, Zoghbi SS, Imaizumi M, Gourley JP, Shetty HU, Hong J, Cropley V, Fujita M, Innis RB and Pike VW. Synthesis and Evaluation in Monkey of Two Sensitive ^{11}C -Labeled Aryloxyanilide Ligands for Imaging Brain Peripheral Benzodiazepine Receptors In Vivo. *J Med Chem.* 2008; 51, 17–30.
- Brodack JW, Kilbourn MR, Welch MJ and Katzenellenbogen JA. NCA 16a-[^{18}F]Fluoroestradiol-17b: The Effect of Reaction Vessel on Fluorine-1 Product Yield, and Effective Specific Activity. *Int J Radiat Appl Instrumentation Part A.* 1986; 37, 3, 217–221.
- Brownell G. and Sweet W. Localization of brain tumors with positron emitters. *Nucleonics.* 1953; 11, 11, 40–45.
- Buckingham F, Calderwood S, Checa B, Keller T, Tredwell M, Collier TL, Newington IM, Bhalla R, Glaser M and Gouverneur V. Oxidative fluorination of N-arylsulfonamides. *J Fluor Chem.* 2015; 180, 33–39.
- Cacace F, Speranza M, Wolf AP and Fowler JS. Labelling of Fluorinated Aromatics by Isotopic Exchange with [^{18}F]Fluoride. *J Label Compd Radiopharm.* 1981; 18, 12, 1721–1730.
- Cacace F, Speranza M, Wolf AP and MacGregor RR. Nucleophilic Aromatic Substitution; Kinetics of Fluorine-18 substitution reactions in Polyfluorobenzenes. Isotopic exchange between ^{18}F - and polyfluorobenzenes in dimethylsulfoxide a kinetic study. *J Fluor Chem.* 1982; 21, 145–158.
- Calderwood S, Collier TL, Gouverneur V, Liang SH and Vasdev N. Synthesis of ^{18}F -arenes from spirocyclic iodonium(III) ylides via continuous-flow microfluidics. *J Fluor Chem.* 2015; 178, 249–253.
- Camsonne R, Crouzel C, Comar D, Mazière M, Prenant C, Sastre J, Moulin M and Syrota A. Synthesis of N-(^{11}C)methyl, N-(methyl-1 propyl), (chloro-2 phenyl)-1 isoquinoline carboxamide-3 (PK 11195): A new ligand for peripheral benzodiazepine receptors. *J Label Compd Radiopharm.* 1984; 21, 10, 985–991.
- Casella V, Wolf AP, Fowler JS, MacGregor RR and Ruth TJ. Anhydrous F-18 Labeled Elemental Fluorine for Radiopharmaceutical Preparation. *J Nucl Med.* 1980; 21, 8, 750–757.
- Chambers RD. Fluorine in Organic Chemistry. 2004, Blackwell Publishing Ltd., Oxford.
- Chirakal R, Firnau G, Schrobilgen GJ, McKay J and Garnett ES. The Synthesis of [^{18}F]Xenon Difluoride from [^{18}F]Fluorine Gas. *Int J Appl Radiat Isot.* 1984; 35, 5, 401–404.
- Choi SR, Golding G, Zhuang Z, Zhang W, Lim N, Hefti F, Benedum TE, Kilbourn MR, Skovronsky D and Kung HF. Preclinical Properties of ^{18}F -AV-45: A PET Agent for A β Plaques in the Brain. *J Nucl Med.* 2009; 50, 11, 1887–1894.
- Chun JH and Pike VW. Single-step syntheses of no-carrier-added functionalized [^{18}F]fluoroarenes as labeling synthons from diaryliodonium salts. *Org Biomol Chem.* 2013; 11, 37, 6300–6306.
- Clementi E, Raimondi D and Reinhardt W. Atomic Screening Constants from SCF Functions. II. Atoms with 37 to 86 Electrons. *J Chem Phys.* 1967; 47, 4, 1300.
- Coenen HH. Fluorine-18 labeling methods: Features and possibilities of basic reactions. *Ernst Scher Res Found Work.* 2007; 62, 15–50.
- Coenen HH and Ermert J. ^{18}F -labelling innovations and their potential for clinical application. *Clin Transl Imaging.* 2018; 6, 3, 169–193.
- Coenen HH and Moerlein SM. Regiospecific Aromatic Fluorodemetalation of Group IVb Metalloarenes using Elemental Fluorine of Acetyl Hypofluorite. *J Fluor Chem.* 1987; 36, 63–75.

- Coenen HH, Schuller M and Stocklin G. Optimization of n. c. a. ^{18}F -fluorination of aliphatic carboxylic acids via nucleophilic substitution. *J Label Compd Radiopharm.* 1981; 21, 11–12, 1197.
- Coenen HH, Gee AD, Adam M, Antoni G, Cutler CS, Fujibayashi Y, Jeong JM, Mach RH, Mindt TL, Pike VW, et al. Consensus nomenclature rules for radiopharmaceutical chemistry — Setting the record straight. *Nucl Med Biol.* 2017; 55, 5–9.
- Constantinou M, Aigbirio FI, Smith RG, Ramsden CA and Pike VW. Xenon difluoride exchanges fluoride under mild conditions: A simple preparation of ^{18}F xenon difluoride for PET and mechanistic studies. *J Am Chem Soc.* 2001; 123, 8, 1780–1781.
- Converse AK, Dabbs KA, Barnhart TE, Dick DW, Larson J, Nickles RJ, Schneider ML, Schueller MJ and Roberts AD. Modulated delivery of F-17-fluoromethane for PET measurement of regional cerebral blood flow. *J Nucl Med.* 2001; 42, 5, 218–219.
- Converse AK, Barnhart TE, Dabbs KA, DeJesus OT, Larson JA, Nickles RJ, Schneider ML and Roberts AD. PET Measurement of rCBF in the presence of a neurochemical tracer. *J Neurosci Methods.* 2004; 132, 2, 199–208.
- Cortés González MA, Nordeman P, Bermejo Gómez A, Meyer DN, Antoni G, Schou M and Szabó KJ. Fluoro-benziodoxole: A no-carrier-added electrophilic fluorinating reagent. Rapid, simple radiosynthesis, purification and application for fluorine-18 labelling. *Chem Commun.* 2018; 54, 34, 4286–4289.
- Curie I and Joliot F. Électrons de matérialisation et de transmutation. *J Phys Radium.* 1933a; 4, 8, 494–500.
- Curie I and Joliot F. Électrons positifs de transmutation. *C R Hebd Seances Acad Sci.* 1933b; 196, 1885–1887.
- Curie I and Joliot F. Un nouveau type de radioactivité. *C R Hebd Seances Acad Sci.* 1934a; 198, 254–256.
- Curie I and Joliot F. Separation chimique des nouveaux radioéléments émetteurs d'électrons positifs. *C R Hebd Seances Acad Sci.* 1934b; 198, 559–561.
- Dabbs KA, Converse AK, Barnhart TE, Dick DW, Larson J, Nickles RJ, Oakes TR, Schneider ML, Schueller MJ, Shelton SE, et al. Visual activation using F-17-fluoromethane in rhesus monkey. *J Nucl Med.* 2001; 42, 5, 219–220.
- Damont A, Roeda D and Dollé F. The potential of carbon-11 and fluorine-18 chemistry: Illustration through the development of positron emission tomography radioligands targeting the translocator protein 18 kDa. *J Label Compd Radiopharm.* 2013; 56, 3–4, 96–104.
- Damont A, Medran-Navarrete V, Cacheux F, Kuhnast B, Pottier G, Bernards N, Marguet F, Puech F, Boisgard R and Dollé F. Novel Pyrazolo[1,5-a]pyrimidines as Translocator Protein 18 kDa (TSPO) Ligands: synthesis, in vitro biological evaluation, ^{18}F -labeling, and in vivo neuroinflammation PET Images. *J Med Chem.* 2015a; 58, 7449–7464.
- Damont A, Caille F, Medran-Navarrete V, Cacheux F, Kuhnast B and Dollé F. The pyrazolo[1,5-a]pyrimidine F-DPA: synthesis, in vivo characterisation and radiolabelling with fluorine-18 using a nucleophilic approach. *J Label Compd Radiopharm.* 2015b; 58, S180.
- Delforge J, Syrota A, Bottlaender M, Varastet M, Loc'h C, Bendriem B, Crouzel C, Brouillet E and Maziere M. Modeling analysis of ^{11}C flumazenil kinetics studied by PET: Application to a critical study of the equilibrium approaches. *J Cereb Blood Flow Metab.* 1993; 13, 3, 454–468.
- Dirac PAM. The Quantum Theory of the Electron. *Proc R Soc London Ser A.* 1928; 117, 778, 610–624.
- Dirac PAM. A theory of electrons and protons. *Proc R Soc London Ser A.* 1930; 126, 801, 360–365.
- Dodgen HW and Libby WF. The Exchange Reaction between the Hydrogen Halides and the Halogens in the Gaseous State. *J Chem Phys.* 1949; 17, 10, 951–957.
- Duff K, Eckman C, Zehr C, Yu X, Prada CM, Perez-Tur J, Hutton M, Buee L, Harigaya Y, Yager D, et al. Increased amyloid- β 42(43) in brains of mice expressing mutant presenilin 1. *Nature.* 1996; 383, 6602, 710–713.
- Eberl S, Katsifis A, Peyronneau MA, Wen L, Henderson D, Loc'h C, Greguric I, Verschuer J, Pham T, Lam P, et al. Preclinical in vivo and in vitro comparison of the translocator protein PET ligands ^{18}F PBR102 and ^{18}F PBR111. *Eur J Nucl Med Mol Imaging.* 2017; 44, 2, 296–307.
- Elsinga PH. Radiopharmaceutical chemistry for positron emission tomography. *Methods.* 2002; 27, 208–217.

- Eskola O, Forsback S, Bergman J, Grönroos T and Solin O. Electrophilic Synthesis of [¹⁸F]EF5, a Radiotracer for Imaging of Tumor Hypoxia. *Eur J Nucl Med Mol Imaging*. 2005; 32, S53.
- Ferrarelli F, Haraldsson HM, Barnhart TE, Roberts AD, Oakes TR, Massimini M, Stone CK, Kalin NH and Tononi G. A [¹⁷F]-fluoromethane PET/TMS study of effective connectivity. *Brain Res Bull*. 2004; 64, 2, 103–113.
- Firna G, Garnett ES, Chirakal R, Sood S, Nahmias C and Schrobilgen G. [¹⁸F]Fluoro-L-dopa for the in vivo study of intracerebral dopamine. *Int J Radiat Appl Instrumentation Part A*. 1986; 37, 8, 669–675.
- Fookes CJR, Pham TQ, Mattner F, Greguric I, Loc C, Liu X, Berghofer P, Shepherd R, Gregoire M and Katsifis A. Synthesis and Biological Evaluation of Substituted [¹⁸F]Imidazo[1,2-a]pyridines and [¹⁸F]Pyrazolo[1,5-a]pyrimidines for the Study of the Peripheral Benzodiazepine Receptor Using Positron Emission Tomography. *J Med Chem*. 2008; 51, 3700–3712.
- Forsback S, Eskola O, Haaparanta M, Bergman J and Solin O. Electrophilic synthesis of 6-[¹⁸F]fluoro-L-DOPA using post-target produced [¹⁸F]F₂. *Radiochim Acta*. 2008; 96, 12, 845–848.
- Forsback S, Marjamäki P, Eskola O, Bergman J, Rokka J, Gronroos T, Haaparanta M and Solin O. [¹⁸F]CFT synthesis and binding to monoamine transporters in rat. *EJNMMI Res*. 2012; 2, 3, 1–12.
- Fujita M, Kobayashi M, Ikawa M, Gunn RN, Rabiner EA, Owen DR, Zoghbi SS, Haskali MB, Telu S, Pike VW, et al. Comparison of four ¹¹C-labeled PET ligands to quantify translocator protein 18 kDa (TSPO) in human brain: (R)-PK11195, PBR28, DPA-713, and ER176—based on recent publications that measured specific-to-non-displaceable ratios. *EJNMMI Res*. 2017; 7, 84, 1–5.
- Le Fur G, Guilloux F, Rufat P, Benavides J, Uzan A, Renault C, Dubroeuq MC and Guérémy C. Peripheral benzodiazepine binding sites: Effect of PK 11195, 1-(2-chlorophenyl)-n-methyl-(1-methylpropyl)-3-isoquinolinecarboxamide. II. In vivo studies. *Life Sci*. 1983a; 32, 16, 1849–1856.
- Le Fur G, Perrier ML, Vaucher N, Imbault F, Flamier A, Benavides J, Uzan A, Renault C, Dubroeuq MC and Guérémy C. Peripheral benzodiazepine binding sites: Effect of PK 11195, 1-(2-chlorophenyl)-n-methyl-(1-methylpropyl)-3-isoquinolinecarboxamide. I. In vitro studies. *Life Sci*. 1983b; 32, 16, 1839–1847.
- Gail R, Hocke C and Coenen HH. Direct N.C.A. ¹⁸F-fluorination of halo- and alkylarenes via corresponding diphenyliodonium salts. *J Label Compd Radiopharm*. 1997; 40, 50–52.
- Gamache RF, Waldmann C and Murphy JM. Copper-Mediated Oxidative Fluorination of Aryl Stannanes with Fluoride. *Org Lett*. 2016; 18, 18, 4522–4525.
- Gao Z, Lim YH, Tredwell M, Li L, Verhoog S, Hopkinson M, Kaluza W, Collier TL, Passchier J, Huiban M, et al. Metal-free oxidative fluorination of phenols with [¹⁸F]fluoride. *Angew Chemie - Int Ed*. 2012; 51, 27, 6733–6737.
- Giglio BC, Fei H, Wang M, Wang H, He L, Feng H, Wu Z, Lu H and Li Z. Synthesis of 5-[¹⁸F]fluoro- α -methyl tryptophan: New trp based PET agents. *Theranostics*. 2017; 7, 6, 1524–1530.
- Gill HS and Marik J. Preparation of ¹⁸F-labeled peptides using the copper(I)-catalyzed azide-alkyne 1,3-dipolar cycloaddition. *Nat Protoc*. 2011; 6, 11, 1718–1725.
- Gillis EP, Eastman KJ, Hill MD, Donnelly DJ and Meanwell NA. Applications of Fluorine in Medicinal Chemistry. *J Med Chem*. 2015; 58, 21, 8315–8359.
- Glaser M and Årstad E. “Click labeling” with 2-[¹⁸F]fluoroethylazide for positron emission tomography. *Bioconj Chem*. 2007; 18, 3, 989–993.
- Gnade BE, Schwaiger GP, Liotta CL and Fink RW. Preparation of Reactor-Produced Carrier-free ¹⁸F-fluoride as the Potassium 18-Crown-6 complex for Synthesis of Labelled Organic Compounds. *Int J Appl Radiat Isot*. 1981; 32, 2, 91–95.
- Gould GR. The LASER, Light Amplification by Stimulated Emission of Radiation, The Ann Arbor Conference on Optical Pumping: The University of Michigan, 1959, 128
- Gouverneur V, Szpera R, Moseley DFJ, Smith LB and Sterling AJ. The fluorination of C-H bonds: developments and perspectives. *Angew Chemie Int Ed*. 2019;

- Greenwood N and Earnshaw A. Chemistry of the Elements. (2nd ed.) 1997, Elsevier Butterworth-Heinemann, Oxford.
- Gu Y, Huang D, Liu Z, Huang J and Zeng W. Labeling Strategies with F-18 for Positron Emission Tomography Imaging. *Med Chem (Los Angeles)*. 2011; 7, 5, 334–344.
- Gulyás B, Halldin C, Karlsson P, Chou YH, Swahn CG, Bönöck P, Paróczai M and Farde L. Brain uptake and plasma metabolism of [^{11}C]vinpocetine: a preliminary PET study in a cynomolgus monkey. *J Neuroimaging*. 1999; 9, 4, 217–222.
- Hamacher K and Coenen HH. Efficient routine production of the ^{18}F -labelled amino acid O-(2- ^{18}F fluoroethyl)-L-tyrosine. *Appl Radiat Isot*. 2002; 57, 6, 853–856.
- Hamacher K, Coenen HH and Stöcklin G. Synthesis D-Glucose Using Aminopolyether Supported Nucleophilic Substitution. *J Nucl Med*. 1986; 27, 2, 235–238.
- Hardwick MJ, Chen MK, Baidoo K, Pomper MG and Guilarte TR. In vivo imaging of peripheral benzodiazepine receptors in mouse lungs: A biomarker of inflammation. *Mol Imaging*. 2005; 4, 4, 432–438.
- Henderson M, Livingston M and Lawrence EO. Artificial Radioactivity Produced by Deuteron Bombardment. *Phys Rev*. 1934; 45, 6, 428–429.
- Hess E, Blessing G, Coenen HH and Qaim SM. Improved target system for production of high purity ^{18}F fluorine via the $^{18}\text{O}(\text{p,n})^{18}\text{F}$ reaction. *Appl Radiat Isot*. 2000; 52, 6, 1431–1440.
- Hill DE and Holland JP. Computational studies on hypervalent iodonium(III) compounds as activated precursors for ^{18}F radiofluorination of electron-rich arenes. *Comput Theor Chem*. 2015; 1066, 34–46.
- Hollingworth C and Gouverneur V. Transition metal catalysis and nucleophilic fluorination. *Chem Commun*. 2012; 48, 24, 2929–2942.
- Holloway JH. The Photochemical Reaction of Xenon with Fluorine at Room Temperature. *J Chem Educ*. 1966; 43, 4, 202–203.
- Huheey J, Keiter E and Keiter R. Inorganic Chemistry: Principles of Structure and Reactivity. (4th ed.) 1993, HarperCollins College Publishers, New York.
- Ichiishi N, Brooks AF, Topczewski JJ, Rodnick ME, Sanford MS and Scott PJH. Copper-catalyzed ^{18}F fluorination of (Mesityl)(aryl)iodonium salts. *Org Lett*. 2014a; 16, 12, 3224–3227.
- Ichiishi N, Brooks AF, Topczewski JJ, Rodnick ME, Sanford MS and Scott PJH. Cu-catalyzed selective ^{18}F fluorination of (mesityl)(aryl)iodonium salts with $\text{K}[\text{F}-18]\text{F}$. *Abstr Pap Am Chem Soc*. 2014b; 248, 557.
- Ichiishi N, Canty AJ, Yates BF and Sanford MS. Copper-catalyzed fluorination of unsymmetrical diaryliodonium salts. *Abstr Pap Am Chem Soc*. 2014c; 248, 1032.
- Ido T, Wan C, Casella V, Fowler J, Wolf A, Reivich M and Kuhl D. Labeled 2-deoxy-D-glucose analogs: ^{18}F -labeled 2-deoxy-2-fluoro-D-glucose, 2-deoxy-2-fluoro-D-mannose and ^{14}C -2-deoxy-2-fluoro-D-glucose. *J Label Compd Radiopharm*. 1978; 14, 2, 175–183.
- Ikawa M, Lohith TG, Shrestha S, Telu S, Zoghbi SS, Castellano S, Taliani S, Da Settimo F, Fujita M, Pike VW, et al. ^{11}C -ER176, a Radioligand for 18-kDa Translocator Protein, Has Adequate Sensitivity to Robustly Image All Three Affinity Genotypes in Human Brain. *J Nucl Med*. 2017; 58, 2, 320–325.
- Imaizumi M, Briard E, Zoghbi SS, Gourley JP, Hong J, Fujimura Y, Pike VW, Innis RB and Fujita M. Brain and whole-body imaging in nonhuman primates of ^{11}C PBR28, a promising PET radioligand for peripheral benzodiazepine receptors. *Neuroimage*. 2008; 39, 3, 1289–1298.
- International Atomic Energy Agency; Nuclear Data Section; A-1400 Vienna; Austria. Live Chart of Nuclides. (<https://www-nds.iaea.org/relnsd/vcharthtml/VChartHTML.html>) accessed: January 2019.
- Jacobson O, Kiesewetter DO and Chen X. Fluorine-18 Radiochemistry, Labeling Strategies and Synthetic Routes. *Bioconjug Chem*. 2014; 26, 1–18.
- James ML, Fulton RR, Henderson DJ, Eberl S, Meikle SR, Thomson S, Allan RD, Dolle F, Fulham MJ and Kassiou M. Synthesis and in vivo evaluation of a novel peripheral benzodiazepine receptor PET radioligand. *Bioorg Med Chem*. 2005; 13, 22, 6188–6194.
- James ML, Fulton RR, Vercoullie J, Henderson DJ, Garreau L, Chalon S, Dolle F, Costa B, Guilloteau D, Kassiou M, et al. DPA-714, a new translocator protein-specific ligand: Synthesis, radiofluorination, and pharmacologic characterization. *J Nucl Med*. 2008; 49, 5, 814–822.

- Joliot F and Curie I. Artificial Production of a New Kind of Radio-Element. *Nature*. 1934; 133, 201–202.
- Katsifis A and Fookes C. Fluorinated ligands for targeting peripheral benzodiazepine receptors, WO/2008/022396, 2008.
- Kiesewetter DO, Jacobson O, Lang L and Chen X. Automated Radiochemical Synthesis of [^{18}F]FBEM: a Thiol Reactive Synthon for Radiofluorination of Peptides and Proteins. *Appl Radiat Isot*. 2011; 69, 2, 410–414.
- Kilbourn MR, Brodack JW, Chi DY, Dence CS, Jerabek PA, Katzenellenbogen JA, Patrick TB and Welch MJ. [^{18}F]Fluoride ion: a versatile reagent for radiopharmaceutical syntheses. *J Label Compd Radiopharm*. 1986; 23, 10–12, 1174.
- Kim DW, Jeong HJ, Lim ST, Sohn MH, Katzenellenbogen JA and Chi DY. Facile nucleophilic fluorination reactions using tert-alcohols as a reaction medium: Significantly enhanced reactivity of alkali metal fluorides and improved selectivity. *J Org Chem*. 2008; 73, 3, 957–962.
- Kohno M, Link J, Dennis LE, McCready H, Huckans M, Hoffman WF and Loftis JM. Neuroinflammation in addiction: A review of neuroimaging studies and potential immunotherapies. *Pharmacol Biochem Behav*. 2019; 179, June 2018, 34–42.
- Kreisl WC, Fujita M, Fujimura Y, Kimura N, Jenko KJ, Kannan P, Hong J, Morse CL, Zoghbi SS, Gladding RL, et al. Comparison of [^{11}C](R)-PK 11195 and [^{11}C]PBR28, Two Radioligands for Translocator Protein (18 kDa) in Human and Monkey: Implications for Positron Emission Tomographic Imaging of this Inflammation Biomarker. *Neuroimage*. 2010; 49, 2924–2932.
- Krzychmonik A, Keller T, Kirjavainen AK, Lahdenpohja S, Forsback S and Solin O. Use of SF_6 for the production of electrophilic ^{18}F -fluorination reagents. *J Fluor Chem*. 2017; 204, October, 90–97.
- Kwon Y Do, Son J, Yun M and Chun JH. Azeotropic drying-free aliphatic radiofluorination to produce PET radiotracers in a mixed organic solvent system. *Tetrahedron Lett*. 2018; 59, 29, 2848–2852.
- Kwon Y Do, Son J and Chun JH. Chemoselective Radiosyntheses of Electron-Rich [^{18}F]Fluoroarenes from Aryl(2,4,6-trimethoxyphenyl)iodonium Tosylates. *J Org Chem*. 2019; 84, 6, 3678–3686.
- Lacapère JJ and Papadopoulos V. Peripheral-type benzodiazepine receptor: Structure and function of a cholesterol-binding protein in steroid and bile acid biosynthesis. *Steroids*. 2003; 68, 7–8, 569–585.
- Landge KP, Jang KS, Lee SY and Chi DY. Approach to the synthesis of indoline derivatives from diaryliodonium salts. *J Org Chem*. 2012; 77, 13, 5705–5713.
- Lawrence EO. Radioactive sodium produced by deuteron bombardment. *Phys Rev*. 1934; 46, 8, 746.
- Lawrence EO. Transmutations of sodium by deuterons. *Phys Rev*. 1935; 47, 1, 17–27.
- Lawrence EO, McMillan E and Thornton R. The transmutation functions for some cases of deuteron-induced radioactivity. *Phys Rev*. 1935a; 48, 6, 493–499.
- Lawrence EO, McMillan E and Henderson M. Transmutations of nitrogen by deuterons. *Phys Rev*. 1935b; 47, 4, 273–277.
- Lee E, Kamlet AS, Powers DC, Neumann CN, Gregory B, Furuya T, Choi DC, Hooker JM and Ritter T. A Fluorine-Derived Electrophilic Late-Stage Fluorination Reagent for PET Imaging. *Science*. 2011; 334, 6056, 639–642.
- Lee E, Hooker JM and Ritter T. Nickel-mediated oxidative fluorination for PET with aqueous [^{18}F]fluoride. *J Am Chem Soc*. 2012; 134, 42, 17456–17458.
- Lee SJ, Makaravage KJ, Brooks AF, Scott PJH and Sanford MS. Copper-Mediated Aminoquinoline-Directed Radiofluorination of Aromatic C–H Bonds with K^{18}F . *Angew Chemie - Int Ed*. 2019; 58, 10, 3119–3122.
- Li F, Liu J, Liu N, Kuhn LA, Garavito RM and Ferguson-Miller S. Translocator Protein 18 kDa (TSPO): An Old Protein with New Functions?. *Biochemistry*. 2016; 55, 20, 2821–2831.
- Link JM, Shoner SC and Krohn KA. Sources of carrier F-19 in F-18 fluoride. *AIP Conf Proc*. 2012; 1509, 61–65.
- Lu S and Pike VW. Synthesis of [^{18}F]xenon difluoride as a radiolabeling reagent from [^{18}F]fluoride ion in a micro-reactor and at production scale. *J Fluor Chem*. 2010; 131, 10, 1032–1038.
- Lu S, Giamis AM and Pike VW. Synthesis of [^{18}F]fallypride in a micro-reactor: rapid optimization and multiple-production in small doses for micro-PET studies. *Curr Radiopharm*. 2009; 2, 1, 1–14.

- Lutar K, Slivnik J and Šmalc A. Some Photosynthesis with Elemental Fluorine. *J Fluor Chem.* 1980; 16, 6, 638.
- Makaravage KJ, Brooks AF, Mossine A V., Sanford MS and Scott PJH. Copper-Mediated Radiofluorination of Arylstannanes with [^{18}F]KF. *Org Lett.* 2016; 18, 20, 5440–5443.
- Marik J and Sutcliffe JL. Click for PET: rapid preparation of [^{18}F]fluoropeptides using CuI catalyzed 1,3-dipolar cycloaddition. *Tetrahedron Lett.* 2006; 47, 37, 6681–6684.
- Mattner F, Quinlivan M, Greguric I, Pham T, Liu X, Jackson T, Berghofer P, Fookes CJR, Dikic B, Gregoire MC, et al. Radiosynthesis, in Vivo Biological Evaluation, and Imaging of Brain Lesions with [^{123}I]-CLINME, a New SPECT Tracer for the Translocator Protein. *Dis Markers.* 2015; 2015.
- McCammant MS, Thompson S, Brooks AF, Krska SW, Scott PJH and Sanford MS. Cu-Mediated C-H ^{18}F -Fluorination of Electron-Rich (Hetero)arenes. *Org Lett.* 2017; 19, 14, 3939–3942.
- McMillan E and Lawrence EO. Transmutations of aluminum by deutons. *Phys Rev.* 1935; 47, 5, 343–348.
- Moehlmann T, Winkler E, Xia X, Edbauer D, Murrell J, Capell A, Kaether C, Zheng H, Ghetti B, Haass C, et al. Presenilin-1 mutations of leucine 166 equally affect the generation of the Notch and APP intracellular domains independent of their effect on A β 42 production. *Proc Natl Acad Sci.* 2002; 99, 12, 8025–8030.
- Moissan H. Action d'un courant électrique sur l'acide fluorhydrique anhydre. *C R Hebd Seances Acad Sci.* 1886; 102, 1543–1544.
- Mossine A V., Brooks AF, Makaravage KJ, Miller JM, Ichiishi N, Sanford MS and Scott PJH. Synthesis of [^{18}F]Arenes via the Copper-Mediated [^{18}F]Fluorination of Boronic Acids. *Org Lett.* 2015; 17, 23, 5780–5783.
- Mossine A V., Brooks AF, Ichiishi N, Makaravage KJ, Sanford MS and Scott PJH. Development of customized [^{18}F]fluoride elution techniques for the enhancement of copper-mediated late-stage radiofluorination. *Sci Rep.* 2017; 7, 1, 1–9.
- Mossine A V., Brooks AF, Bernard-Gauthier V, Bailey JJ, Ichiishi N, Schirmacher R, Sanford MS and Scott PJH. Automated synthesis of PET radiotracers by copper-mediated ^{18}F -fluorination of organoborons: Importance of the order of addition and competing protodeborylation. *J Label Compd Radiopharm.* 2018; 61, 3, 228–236.
- Mulholland G, Hutchins G, Toorongian S and Jewett D. Entry into F-17 ($T_{1/2} = 65$ sec) Radiopharmaceuticals - on line electrophilic synthesis of the blood-flow agent [^{18}F]-17]fluoromethane. *J Nucl Med.* 1987; 28, 6, 1082–1082.
- Mullan M, Crawford F, Axelman K, Houlden H, Lilius L, Winblad B and Lannfelt L. A pathogenic mutation for probable Alzheimer's disease in the APP gene at the N-terminus of β -amyloid. *Nat Genet.* 1992; 1, 5, 345–347.
- Namavari M, Bishop A, Satyamurthy N, Bida G and Barrio JR. Regioselective radiofluorodestannylation with [^{18}F]F $_2$ and [^{18}F]CH $_3$ COOF: A high yield synthesis of 6-[^{18}F]fluoro-L-dopa. *Int J Radiat Appl Instrumentation Part A.* 1992; 43, 8, 989–996.
- National Nuclear Data Center; Brookhaven National Laboratory; NY 11973-5000; Upton. NuDat 2.7. (<https://www.nndc.bnl.gov/nudat2/>) accessed: January 2019.
- Nickles RJ, Daube ME and Ruth TJ. An $^{18}\text{O}_2$ target for the production of [^{18}F]F $_2$. *Int J Appl Radiat Isot.* 1984; 35, 2, 117–122.
- Nickles RJ, Gatley SJ, Votaw JR and Kornuth ML. Production of reactive fluorine-18. *Int J Radiat Appl Instrumentation Part A.* 1986; 37, 8, 649–661.
- Nodwell MB, Yang H, Čolović M, Yuan Z, Merckens H, Martin RE, Bénard F, Schaffer P and Britton R. ^{18}F -Fluorination of Unactivated C-H Bonds in Branched Aliphatic Amino Acids: Direct Synthesis of Oncological Positron Emission Tomography Imaging Agents. *J Am Chem Soc.* 2017; 139, 10, 3595–3598.
- O'Hagan D. Understanding organofluorine chemistry. An introduction to the C–F bond. *Chem Soc Rev.* 2008; 37, 2, 308–319.
- Owen DR, Howell OW, Tang S-P, Wells LA, Bennacef I, Bergstrom M, Gunn RN, Rabiner EA, Wilkins MR, Reynolds R, et al. Two binding sites for [^3H]PBR28 in human brain: implications for TSPO PET imaging of neuroinflammation. *J Cereb Blood Flow Metab.* 2010; 30, 9, 1608–1618.

- Owen DR, Yeo AJ, Gunn RN, Song K, Wadsworth G, Lewis A, Rhodes C, Pulford DJ, Bennacef I, Parker CA, et al. An 18-kDa Translocator Protein (TSPO) polymorphism explains differences in binding affinity of the PET radioligand PBR28. *J Cereb Blood Flow Metab.* 2012; 32, 1, 1–5.
- Owen DRJ, Gunn RN, Rabiner EA, Bennacef I, Fujita M, Kreisl WC, Innis RB, Pike VW, Reynolds R, Matthews PM, et al. Mixed-Affinity Binding in Humans with 18-kDa Translocator Protein Ligands. *J Nucl Med.* 2011; 52, 1, 24–32.
- Papadopoulos V, Amri H, Boujrad N, Cascio C, Culty M, Garnier M, Hardwick M, Li H, Vidic B, Brown AS, et al. Peripheral benzodiazepine receptor in cholesterol transport and steroidogenesis. *Steroids.* 1997; 62, 1, 21–28.
- Perrone M, Moon BS, Park HS, Laquintana V, Jung JH, Cutrignelli A, Lopodota A, Franco M, Kim SE, Lee BC, et al. A Novel PET Imaging Probe for the Detection and Monitoring of Translocator Protein 18 kDa Expression in Pathological Disorders. *Sci Rep.* 2016; 6, 20422, 1–13.
- Petersen IN, Kristensen JL and Herth MM. Nucleophilic ^{18}F -Labeling of Spirocyclic Iodonium Ylide or Boronic Pinacol Ester Precursors: Advantages and Disadvantages. *European J Org Chem.* 2017; 2017, 3, 453–458.
- Peyronneau M-A, Loc'h C, Mattner F, Pham T, Jiang C, Pellegrini P, Greguric I, Gregoire M-C and Katsifis A. In vitro metabolism of [^{18}F]PBR102 and [^{18}F]PBR111 in rats and humans. *Eur J Nucl Med Mol Imaging.* 2011; 38, S231.
- Peyronneau M, Saba W, Goutal S, Damont A, Dollé F, Kassiou M, Bottlaender M, Valette H. Metabolism and Quantification of [^{18}F]DPA-714, a New TSPO Positron Emission Tomography Radioligand. *Drug Metab Dispos.* 2013; 41, 1, 122–131.
- Pike VW and Aigbirhio FI. Reactions of Cyclotron-produced [^{18}F]Fluoride with Diaryliodonium Salts—a Novel Single-step Route to No-carrier-added [^{18}F]Fluoroarenes. *J Chem Soc Chem Commun.* 1995; 21, 2215–2216.
- Preshlock S, Tredwell M and Gouverneur V. ^{18}F -Labeling of Arenes and Heteroarenes for Applications in Positron Emission. *Chem Rev.* 2016a; 116, 2, 719–766.
- Preshlock S, Calderwood S, Verhoog S, Tredwell M, Huiban M, Hienzsch A, Gruber S, Wilson TC, Taylor NJ, Cailly T, et al. Enhanced copper-mediated ^{18}F -fluorination of aryl boronic esters provides eight radiotracers for PET applications. *Chem Commun.* 2016b; 52, 54, 8361–8364.
- Radde R, Bolmont T, Kaeser SA, Coomaraswamy J, Lindau D, Stoltze L, Calhoun ME, Jäggi F, Wolburg H, Gengler S, et al. A β 42-driven cerebral amyloidosis in transgenic mice reveals early and robust pathology. *EMBO Rep.* 2006; 7, 9, 940–946.
- Di Raddo P, Diksic M and Jolly D. The ^{18}F Radiofluorination of Arylsilanes. *J Chem Soc Chem Commun.* 1984; 3, 159–160.
- Roberts A, Dabbs K, Schueller M and Nickles R. Production of the short-lived flow tracer fluorine-17 fluoromethane from proton irradiation of neon. *J Nucl Med.* 2000; 41, 5, 243.
- Rogers MT and Katz JJ. Fluorine Exchange Reactions between Hydrogen Fluoride and the Halogen Fluorides. *J Am Chem Soc.* 1952; 74, 6, 1375–1377.
- Rokka J, Federico C, Jurttila J, Snellman A, Haaparanta M, Rinne JO and Solin O. $^{19}\text{F}/^{18}\text{F}$ exchange synthesis for a novel [^{18}F]S1P $_3$ -radiopharmaceutical. *J Label Compd Radiopharm.* 2013; 56, 8, 385–391.
- Rotstein BH, Stephenson NA, Vasdev N and Liang SH. Spirocyclic hypervalent iodine(III)-mediated radiofluorination of non-activated and hindered aromatics. *Nat Commun.* 2014; 5, 1–7.
- Rotstein BH, Wang L, Liu RY, Patteson J, Kwan EE, Vasdev N and Liang SH. Mechanistic studies and radiofluorination of structurally diverse pharmaceuticals with spirocyclic iodonium(III) ylides. *Chem Sci.* 2016; 7, 7, 4407–4417.
- Ryzhikov N, Gomzina N, Fedorova O and Vasil'ev D. Preparation of Flumazenil, a Potential Radioligand for PET Imaging of Central Benzodiazepine Receptors, by Isotope Exchange. *Radiochemistry.* 2004; 46, 3, 290–294.
- Salvadori PA, Wolf AP, Fowler JS and Macgregor RR. A New Improved Synthesis of 2-Deoxy-2-[^{18}F]Fluoro-D-Glucose from ^{18}F -Labeled Acetyl Hypofluorite. *J Nucl Med.* 1982; 23, 10, 899–904.

- Samson Y, Hantraye P, Baron JC, Soussaline F, Comar D and Mazière M. Kinetics and Displacement of [^{11}C]RO15-1788, a Benzodiazepine Antagonist, Studied in Human Brain in vivo by Positron Tomography. *Eur J Pharmacol.* 1985; 110, 2, 247–251.
- Satyamurthy N, Bida GT, Phelps ME and Barrio JR. N-[^{18}F]fluoro-N-alkylsulfonamides: Novel reagents for mild and regioselective radiofluorination. *Int J Radiat Appl Instrumentation Part A.* 1990; 41, 8, 733–738.
- Satyamurthy N, Barrio JR and Ram MJ. No-Carrier-Added Nucleophilic [^{18}F] Fluorination of Aromatic Compounds, WO/2010/117435, 2010.
- Savisto N, Bergman J, Aromaa J, Forsback S, Eskola O, Viljanen T, Rajander J, Johansson S, Grigg J, Luthra S, et al. Influence of transport line material on the molar activity of cyclotron produced [^{18}F]fluoride. *Nucl Med Biol.* 2018; 64–65, 8–15.
- Schäfer D, Weiß P, Ermert J, Castillo Meleán J, Zarrad F and Neumaier B. Preparation of No-Carrier-Added 6-[^{18}F]Fluoro-L-tryptophan via Cu-Mediated Radiofluorination. *European J Org Chem.* 2016; 2016, 27, 4621–4628.
- Schirmmayer R, Wangler C and Schirmmayer E. Recent Developments and Trends in ^{18}F -Radiochemistry: Syntheses and Applications. *Mini Rev Org Chem.* 2007; 4, 4, 317–329.
- Schirmmayer R, Wängler B, Bailey J, Bernard-Gauthier V, Schirmmayer E and Wängler C. Small Prosthetic Groups in ^{18}F -Radiochemistry: Useful Auxiliaries for the Design of ^{18}F -PET Tracers. *Semin Nucl Med.* 2017; 47, 5, 474–492.
- Schrobligen GJ, Firnau G, Chirakal R and Garnett SE. Synthesis of [^{18}F]XeF₂, a Novel Agent for the Preparation of ^{18}F -Radiopharmaceuticals. *J Chem Soc Chem Commun.* 1981; 4, 198–199.
- Selleri S, Bruni F, Costagli C, Costanzo A, Guerrini G, Ciciani G, Costa B and Martini C. 2-Arylpyrazolo [1,5-a] pyrimidin-3-yl Acetamides. New Potent and Selective Peripheral Benzodiazepine Receptor Ligands. *Bioorg Med Chem.* 2001; 9, 10, 2661–2671.
- Shah P and Westwell AD. The Role of Fluorine in Medicinal Chemistry. *J Enzyme Inhib Med Chem.* 2007; 22, 5, 527–540.
- Skaff O, Jolliffe KA and Hutton CA. Synthesis of the side chain cross-linked tyrosine oligomers dityrosine, trityrosine, and pulcherosine. *J Org Chem.* 2005; 70, 18, 7353–7363.
- Slater J. Atomic Radii in Crystals. *J Chem Phys.* 1964; 41, 10, 3199–3205.
- Šmalc A, Lutar K and Slivnik J. Photosynthesis of xenon tetrafluoride. *J Fluor Chem.* 1976; 8, 1, 95–96.
- Solin O, Bergman J, Haaparanta M and Reissell A. Production of ^{18}F from Water Targets. Specific Radioactivity and Anionic Contaminants. *Int J Radiat Appl Instrumentation Part A.* 1988; 39, 10, 1065–1071.
- Sood S, Firnau G and Garnett ES. Radiofluorination with Xenon Difluoride: A New High Yield Synthesis of [^{18}F]2-Fluoro-2-deoxy-d-glucose. *Int J Appl Radiat Isot.* 1983; 34, 4, 743–745.
- Speranza M, Shiue CY, Wolf AP, Wilbur DS and Angelini G. Electrophilic radiofluorination of aryltrimethylsilanes as a general route to ^{18}F -labeled aryl fluorides. *J Fluor Chem.* 1985; 30, 1, 97–107.
- Stenhagen ISR, Kirjavainen AK, Forsback SJ, Jørgensen CG, Robins EG, Luthra SK, Solin O and Gouverneur V. [^{18}F]Fluorination of an arylboronic ester using [^{18}F]selectfluor bis(triflate): application to 6-[^{18}F]fluoro-L-DOPA. *Chem Commun.* 2013; 49, 14, 1386–1388.
- Streng L V. and Streng AG. Formation of Xenon Difluoride from Xenon and Oxygen Difluoride or Fluorine in Pyrex Glass at Room Temperature. *Inorg Chem.* 1965a; 4, 9, 1370–1371.
- Streng L V. and Streng AG. Photochemical Formation of Krypton Difluoride from Krypton and Fluorine or Oxygen Difluoride. *Inorg Chem.* 1965b; 5, 2, 328–329.
- Sutton LE (Ed). Tables of Interatomic Distances and Configuration in Molecules & Ions (Supplement 1956-1959) Special Publication No.18. 1965, The Chemical Society, London.
- Takkinen JS, López-Picón FR, Al Majidi R, Eskola O, Krzyczmonik A, Keller T, Löytyniemi E, Solin O, Rinne JO and Haaparanta-Solin M. Brain energy metabolism and neuroinflammation in ageing APP/PS1-21 mice using longitudinal ^{18}F -FDG and ^{18}F -DPA-714 PET imaging. *J Cereb Blood Flow Metab.* 2017; 37, 8, 2870–2882.

- Tang D, McKinley ET, Hight MR, Uddin MI, Harp JM, Fu A, Nickels ML, Buck JR and Manning HC. Synthesis and structure-activity relationships of 5,6,7-substituted pyrazolopyrimidines: Discovery of a novel TSPO PET ligand for cancer imaging. *J Med Chem.* 2013; 56, 8, 3429–3433.
- Tang D, Nickels ML, Tantawy MN, Buck JR and Manning HC. Preclinical Imaging Evaluation of Novel TSPO-PET Ligand 2-(5,7-Diethyl-2-(4-(2-[^{18}F]fluoroethoxy)phenyl)pyrazolo[1,5-a]pyrimidin-3-yl)-N,N-diethylacetamide ([^{18}F]VUIIS1008) in Glioma. *Mol Imaging Biol.* 2014; 16, 6, 813–820.
- Teare H, Robins EG, Arstad E, Luthra SK and Gouverneur V. Synthesis and reactivity of [^{18}F]-N-fluorobenzenesulfonimide. *Chem Commun.* 2007; 23, 2330–2332.
- Teare H, Robins EG, Kirjavainen A, Forsback S, Sandford G, Solin O, Luthra SK and Gouverneur V. Radiosynthesis and evaluation of [^{18}F]Selectfluor bis(triflate). *Angew Chemie - Int Ed.* 2010; 49, 38, 6821–6824.
- Thominiaux C, Mattner F, Greguric I, Boutin H, Chauveau F, Kuhnast B, Grégoire MC, Loc'h C, Valette H, Bottlaender M, et al. Radiosynthesis of 2-[6-chloro-2-(4-iodophenyl)imidazo [1,2-a]pyridin-3-yl]-N-ethyl-N-[^{11}C]methyl-acetamide, [^{11}C]CLINME, a novel radioligand for imaging the peripheral benzodiazepine receptors with PET. *J Label Compd Radiopharm.* 2007; 50, 4, 229–236.
- Thominiaux C, Damont A, Kuhnast B, Demphel S, Le Helleix S, Boissard S, Rivron L, Chauveau F, Boutin H, Van Camp N, et al. Radiosynthesis of 7-chloro-N,N-dimethyl-5-[^{11}C]methyl-4-oxo-3-phenyl-3,5-dihydro-4H-pyridazino[4,5-b]indole-1-acetamide, [^{11}C]SSR180575, a novel radioligand for imaging the TSPO (peripheral benzodiazepine receptor) with PET. *J Label Compd Radiopharm.* 2010; 53, 13, 767–773.
- Tian T, Zhong WH, Meng S, Meng XB and Li ZJ. Hypervalent iodine mediated para-selective fluorination of anilides. *J Org Chem.* 2013; 78, 2, 728–732.
- Tredwell M and Gouverneur V. ^{18}F labeling of arenes. *Angew Chemie - Int Ed.* 2012; 51, 46, 11426–11437.
- Tredwell M, Preshlock SM, Taylor NJ, Gruber S, Huiban M, Passchier J, Mercier J, Génicot C and Gouverneur V. A General Copper-Mediated Nucleophilic ^{18}F Fluorination of Arenes. *Angew Chemie - Int Ed.* 2014; 53, 30, 7751–7755.
- Vasdev N, Pointner BE, Chirakal R and Schrobilgen GJ. On the preparation of fluorine-18 labelled XeF_2 and chemical exchange between fluoride ion and XeF_2 . *J Am Chem Soc.* 2002; 124, 43, 12863–12868.
- Vincent MA and Hillier IH. The solvated fluoride anion can be a good nucleophile. *Chem Commun.* 2005; 47, 5902–5903.
- Vivash L and O'Brien TJ. Imaging Microglial Activation with TSPO PET: Lighting Up Neurologic Diseases?. *J Nucl Med.* 2015; 57, 2, 165–168.
- Vlasov VM. Fluoride ion as a nucleophile and a leaving group in aromatic nucleophilic substitution reactions. *J Fluor Chem.* 1993; 61, 3, 193–216.
- Wadsworth H, Jones PA, Chau WF, Durrant C, Fouladi N, Passmore J, O'Shea D, Wynn D, Morisson-Iveson V, Ewan A, et al. GE-180: A novel fluorine-18 labelled PET tracer for imaging Translocator protein 18 kDa (TSPO). *Bioorganic Med Chem Lett.* 2012; 22, 3, 1308–1313.
- Wagner FM, Ermert J and Coenen HH. Three-Step, “One-Pot” Radiosynthesis of 6-Fluoro-3,4-Dihydroxy-L-Phenylalanine by Isotopic Exchange. *J Nucl Med.* 2009; 50, 10, 1724–1729.
- Wang L, Cheng R, Fujinaga M, Yang J, Zhang Y, Hatori A, Kumata K, Yang J, Vasdev N, Du Y, et al. A Facile Radiolabeling of [^{18}F]FDPA via Spirocyclic Iodonium Ylides: Preliminary PET Imaging Studies in Preclinical Models of Neuroinflammation. *J Med Chem.* 2017; 60, 12, 5222–5227.
- Weeks JL, Chernick CL and Matheson MS. Photochemical Preparation of Xenon Difluoride. *J Am Chem Soc.* 1962; 84, 23, 4612–4613.
- Wester HJ, Herz M, Weber W, Heiss P, Senekowitsch-Schmidtke R, Schwaiger M and Stöcklin G. Synthesis and radiopharmacology of O-(2-[^{18}F]fluoroethyl)-L-tyrosine for tumor imaging. *J Nucl Med.* 1999; 40, 1, 205–212.
- Wilson AA, Garcia A, Parkes J, McCormick P, Stephenson KA, Houle S and Vasdev N. Radiosynthesis and initial evaluation of [^{18}F]-FEPPA for PET imaging of peripheral

- benzodiazepine receptors. *Nucl Med Biol.* 2008; 35, 3, 305–314.
- Wilson TC, Cailly T and Gouverneur V. Boron reagents for divergent radiochemistry. *Chem Soc Rev.* 2018; 47, 18, 6990–7005.
- Yusubov MS, Svitich DY, Larkina MS and Zhdankin V V. Applications of iodonium salts and iodonium ylides as precursors for nucleophilic fluorination in positron emission tomography. *Arkivoc.* 2013; 2013, 1, 364–395.
- Zarrad F, Zlatopolskiy BD, Krapf P, Zischler J and Neumaier B. A practical method for the preparation of ^{18}F -labeled aromatic amino acids from nucleophilic ^{18}F fluoride and stannyl precursors for electrophilic radiohalogenation. *Molecules.* 2017; 22, 2231–2256.
- Zhang M-R, Maeda J, Furutsuka K, Yoshida Y, Ogawa M, Suhara T and Suzuki K. ^{18}F FMDAA1106 and ^{18}F FEDAA1106: Two Positron-Emitter Labeled Ligands for Peripheral Benzodiazepine Receptor (PBR). *Bioorganic Med Chem Lett.* 2003; 13, 2, 201–204.
- Zhang M-R, Kumata K, Maeda J, Yanamoto K, Hatori A, Okada M, Higuchi M, Obayashi S, Suhara T and Suzuki K. ^{11}C -AC-5216: A Novel PET Ligand for Peripheral Benzodiazepine Receptors in the Primate Brain. *J Nucl Med.* 2007; 48, 11, 1853–1861.
- Zhang M-R, Yanamoto K, Kumata K, Yamasaki T, Yui J, Kawamura K, Hatori A and Suzuki K. Synthesis and Evaluation of ^{11}C DAC as a Novel Peripheral-Type Benzodiazepine Receptor PET Ligand in Kainic Acid-Lesioned Rat. *J Label Compd Radiopharm.* 2009; 52, S1, S123.
- Zhang W, Oya S, Kung MP, Hou C, Maier DL and Kung HF. F-18 Polyethyleneglycol stilbenes as PET imaging agents targeting A β aggregates in the brain. *Nucl Med Biol.* 2005; 32, 8, 799–809.
- Zischler J, Kolks N, Modemann D, Neumaier B and Zlatopolskiy BD. Alcohol-Enhanced Cu-Mediated Radiofluorination. *Chem - A Eur J.* 2017; 23, 14, 3251–3256.
- Zlatopolskiy BD, Zischler J, Krapf P, Zarrad F, Urusova EA, Kordys E, Endepols H and Neumaier B. Copper-mediated aromatic radiofluorination revisited: Efficient production of PET tracers on a preparative scale. *Chem - A Eur J.* 2015; 21, 15, 5972–5979.

Annales Universitatis Turkuensis



**UNIVERSITY
OF TURKU**

ISBN 978-951-29-7672-0 (PRINT)

ISBN 978-951-29-7673-7 (PDF)

ISSN 0082-7002 (Print) ISSN 2343-3175 (Online)